Structural Vibration damping using Lightweight, Low-wave-speed Media

by

Justin Matthew Verdirame

S.B., Mechanical Engineering
Massachusetts Institute of Technology (2000)
S.M., Mechanical Engineering
Massachusetts Institute of Technology (2003)

Submitted to the Department of Mechanical Engineering
in partial fulfillment of the requirements for the degree of

Doctor of Philosophy in Mechanical Engineering

at the

MASSACHUSETTS INSTITUTE OF TECHNOLOGY

February 2007

Author .....
Department of Mechanical Engineering
January 26, 2007

Certified by .....
Samir A. Nayfeh
Associate Professor
Thesis Supervisor

Accepted by .....
Lallit Anand
Chairman, Department Committee on Graduate Students

Structural Vibration damping using Lightweight, Low-wave-speed Media

by

Justin Matthew Verdirame

Submitted to the Department of Mechanical Engineering
on January 26, 2007, in partial fulfillment of the
requirements for the degree of
Doctor of Philosophy in Mechanical Engineering

Abstract

Incorporation of a low-density, low-wave-speed medium (LWSM) into a structure yields significant damping if the speed of wave propagation in the medium is low enough for standing waves to arise in it. In this thesis, we characterize wave propagation in low-density granular media and foams for use as structural damping treatments and develop analytical and numerical techniques for prediction of the damping attained in structures that incorporate LWSM.

Structural damping by incorporation of LWSM is attractive for hollow thin-walled structures. We develop analytical approximations for the loss-factor in the structural modes of cylindrical shells and Timoshenko beams and attain predictions in good agreement with measurements.

For more complicated geometries, it is often necessary to employ a finite element model to predict the dynamics of structures. But inclusion of LWSM into a finite element model significantly increases the size of the model, introduces frequency-dependent material properties, and introduces a large number of modes that are dominated by deformation of the LWSM. Hence, the eigenvalue problem becomes significantly more difficult by addition of the LWSM. We develop an iterative approach based on the eigensolution of a structure without LWSM and the forced response of the LWSM to obtain approximations for the complex eigensolution.

Damping by inclusion of LWSM is an attractive option for reduction of the sound radiated from vehicle driveshafts, which are typically thin-walled hollow cylinders with yokes welded at each end. The bending and ovaling modes of the driveshaft between 500 and 3000 Hz are efficient radiators of sound and are excited by gear transmission error in the rear differential. Filling the driveshaft with a lossy, low-density foam adds significant damping to these modes and thus reduces the radiated sound.

Thesis Supervisor: Samir A. Nayfeh
Title: Associate Professor

Acknowledgments

I've been at MIT a long time so I have built quite the list of people to thank, and at the top of that list is my advisor, Samir Nayfeh. He has been a better advisor than I ever could have dreamt. He never ceases to amaze with his depth of knowledge about seemingly everything. If I have absorbed ϵ of his knowledge, then I can consider grad school as a success.

I must also thank the other members of my thesis committee, Kim Vandiver and Warren Seering. I did not utilize their expertise as much as a should have, but I thank them for their insightful comments and particularly for keeping me focused on the objective, making a practical contribution to the field.

I cant forget my outstanding labmates. I sort of feel like "The Last of the Mohicans" since I'm the only one remaining after all this time. I'm not sure how Jon Rohrs lasted as long as he did sitting next to me, but I'm thankful to him for teaching me about a wide variety of subjects, such as machine design, weaving, Matlab, searching the internet, and wikipedia. It's certainly his "fault" that I listen to NPR now. Lei Zuo is an amazing resource and all-around nice person, once you can figure out what he is saying. Andrew Wilson was the loudest, tallest, and funniest guy in the lab. Joe Cattell, while technically not in the Nayfeh lab, was a good guy to have around. If he had actually been in our lab, neither of us would have ever gotten anything done. Kripa Varanasi did some early work on low-wave-speed media. Maggie Sullivan has been immensely helpful navigating MIT's bureaucracy.

I've made a lot of friends in my 3800+ days here at MIT, too many to mention every one here. I'm not quite sure what Rev. Dr. Max Berniker and I have in common that makes us friends, but he has been a great roommate for a number of years. The Neanderthals is a great group of friends and has been immense fun, although that hip pointer was pretty disgusting. Laxing with the "doctors" was an unforgettable experience. Oh yeah, Bico!

Finally, I want to express my gratitude to my family, Mom, Dad, Mike, and Claudia. If not for them, I would not be where I am today.

I would also like to acknowledge funding from the NDSEG Fellowship and Ford Motor Company.

Contents

List of Figures

List of Tables

Chapter 1

Introduction

1.1 Background

Vibration damping plays an important role in machines and structures by improving performance and stability, reducing noise, and increasing lifetime. Advances in and increased demands of motion control, vibration reduction, vibration isolation, and noise suppression require improvements in damping technology. Useful methods and accurate models are required to design, implement, and optimize damping treatments.

Vibration damping is often divided into two categories, active and passive. Active damping treatments utilize sensors to measure the performance of the machine or structure, and a control algorithm calculates a corrective action which is supplied by an actuator. Passive treatments typically involve converting kinetic or strain energy into heat through methods such as constrained-layer damping, tuned-mass dampers, viscous fluids, or passively-shunted piezoelectric materials. Active treatments are typically more complicated and more expensive than passive treatments.

1.1.1 Resonant damping

One common, typically passsive, damping treatment is a resonant damper, in which a sprung inertia reacts against the primary structure to reduce vibration. The simplest embodiment of a resonant damper is the tuned-mass damper, as illustrated Figure 1-1 [23]. Tuned-mass dampers are effective only in a narrow frequency band and are sensitive to frequency tuning. Previous researchers have explored methods to mitigate these problems. One of these methods includes using many resonant absorber as sketched in Figure 1-2. Zapfe and Lesieutre [75] showed that these types of absorbers but with a distribution of tuning frequencies can provide broadband damping. Some researchers have coined the term "fuzzy structures" for structures with many resonant subsystems.

During the study of viscoelastic free-layer damping treatments, Oberst [43] observed significant damping of flexural vibrations at frequencies corresponding to thickness resonances of the attached viscoelastic layer. Ungar and Kerwin [62] derived the first model for such systems and showed that significant damping can occur over a range of frequencies because an infinite number of through-the-thickness resonance

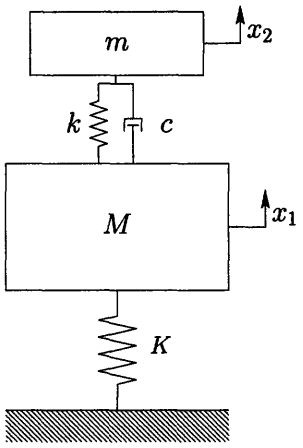

Figure 1-1: Single-degree-of-freedom tuned-mass damper

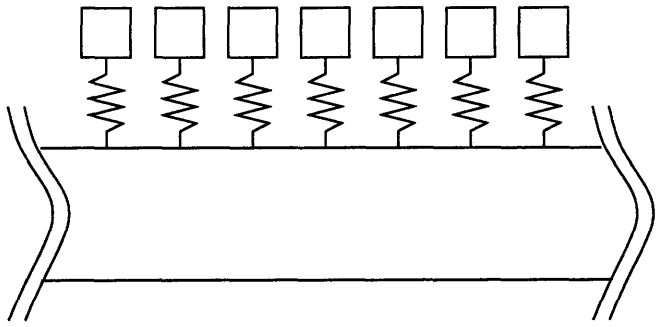

Figure 1-2: Vibrating structure with many resonant absorbers

can occur but that the amount of damping decreases after the first thickness resonance. This method of damping did not gain wide acceptance because of material limitations that existed at the time (1964). More specifically, the available viscoelastic materials were too dense and too stiff for it to be practical to add a thick layer of viscoelastic material because of the large associated weight penalty.

House *et al* [24, 45] recognized that damping using thickness resonances could be implemented using lightweight granular materials. Fricke [19] demonstrated applications where significant damping was attained using lightweight, low-wave-speed granular materials, but he did not use any quantitative models. Nayfeh and coworkers [41, 66, 65] developed detailed quantitative models and suggested the use of foams as a low-wave-speed damping material.

Damping using low-wave-speed media has many properties that make it suitable for a wide variety of applications. With proper material selection, it can be used at extreme temperatures. Foams, fibrous materials, and granular materials are durable and resilient making them well-suited for applications requiring long lifecycles and survival of large strains, impact, and shock. The damping is insensitive to frequency tuning and works over a broad frequency spectrum such that significant damping persists even with changes to the primary structure. LWSM damping does not introduce signficiant creep so it is attractive for precision applications. It is inexpensive and easy to package into a structure or machine, especially thin-walled tubing, making low-wave-speed media an attractive solution for mitigation of structure-borne sound. Figure 1-3 compares constrained-layer damping to LWSM damping for a hollow box beam for equal added mass. The LWSM treatment provides higher peak damping and equivalent performance at high frequencies. Additionally, the low-wave-speed damper is easier to manufacture.

1.1.2 Flexural Bearings

Flexural bearings are elastic elements that constrain an object in one or more directions. They play an important role in precision engineering because they allow for smooth motion. One drawback when designing using flexures is their susceptiblity to vibration. Varanasi [64] demonstrated that foam is well-suited to damping the vibratory modes of a planar flexure stage as shown in Figure 1-4. In such an application, performance is limited by the out-of-plane modes of the stage and modes dominated by deformation of the blades. A low-wave-speed foam is easily introducted into the gaps between the flexure blades and adds significant damping to these parasitic modes. Additionally, the introduction of the foam does not limit the range of the stage.

1.1.3 Drivetrain Noise

There are many sources of noise and vibrations in passenger vehicles, including interactions between the tires and the road, air flow around the vehicle, engine combustion and exhaust, and the drivetrain. In large rear-wheel-drive vehicles, the drivetrain can be a significant contributor of undesirable noise and vibration.

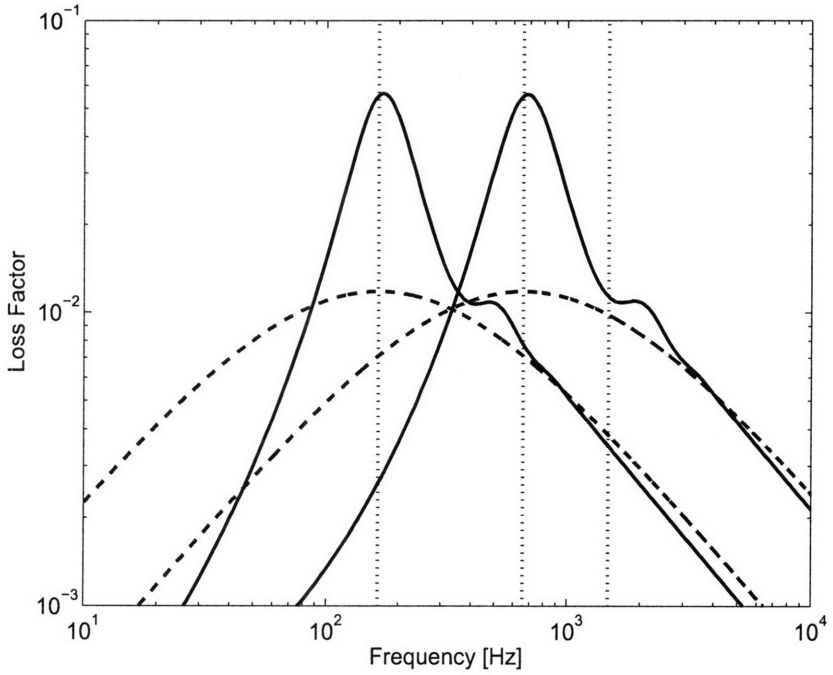

Figure 1-3: Comparison of optimized constrained-layer damping (CLD) treatment and low-wave-speed media damping treatments designed for the first and second bending modes of a simply-supported aluminum box beam (50 mm × 50 mm × 1 m, 5 mm wall thickness): LWSM (solid), CLD (dashed). Vertical dotted lines denote frequencies of Euler-Bernoulli vibration modes.

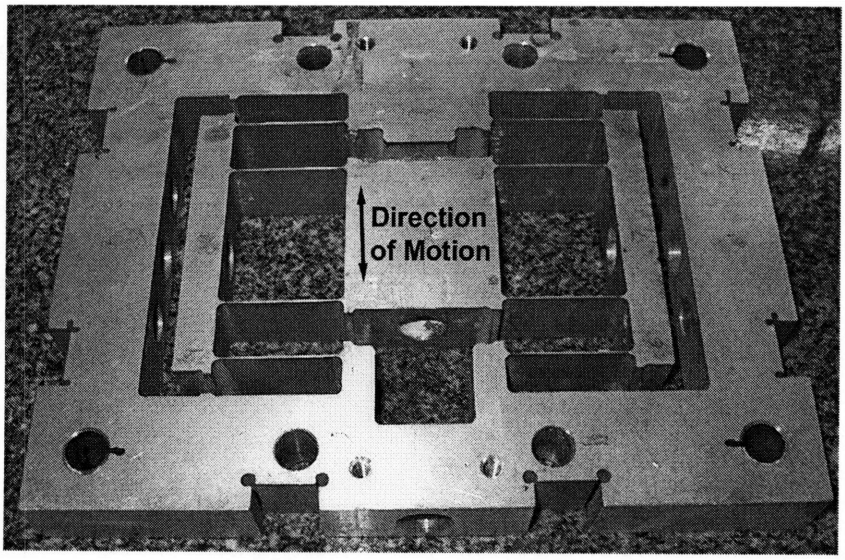

Figure 1-4: Planar flexure stage

A rear-wheel-drive vehicle's power train system consists of the engine, flywheel, clutch or torque converter, transmission, driveshaft, differential, and right and left axle half-shafts (see Figures 1-5 and 1-6). The transmission output is connected to the driveshaft which transmits the power to the rear differential. The driveshaft is typically a thin-walled tube (or pair of thin-walled tubes coupled at an intermediate bearing) connected to the transmission and differential by U-joints. The differential offers a further gear reduction and distributes power to the rear tires through the rear axle half-shafts.

Vibration sources for the drivetrain include meshing of gear teeth, gear transmission error, torque fluctuations from the engine, imbalance of rotating parts, and rapid acceleration or clutch engagement. Gear transmission error is considered by many researchers to be the largest contributor to drivetrain noise. Gear transmission error is the normalized velocity variation of the driven gear when the driving gear is rotating at a constant velocity (Smith [56]). The variations in velocity can result in large, impulsive forces that excite vibratory modes which create audible noise.

Various terminology exists to describe the vibration and noise phenomena that occur in vehicle drive-lines. Driveline shuffle, also known as shunt or tip-in and tip-out, is front to back oscillation of the entire drivetrain at 2-8 Hertz. Gear rattle is the noise produced by meshing of the unloaded transmission gears which occurs at frequencies less than 80 Hertz. Clutch judder is a vibratory phenomena in the 7-20 Hertz range caused by stick-slip during engagement of the clutch. While these lower frequency phenomena are largely "rigid body" motions, at frequencies above 500 Hertz the vibratory modes are dominated by deformation of the driveshaft. The modes, which are often excited by gear meshing, involve combinations of bending, torsion, and "ovaling" of the driveshaft. They are often referred to as whine or clonk [52].

System Modeling

One of the difficulties in understanding the behavior of vehicle drive-lines is development of accurate but manageable models. Many authors have used finite element models (e.g., Theodossiades *et al* [61]). Farshindianfar *et al* [15] used a distributed-lumped modelling technique in which some elements of the system are modelled as discrete and some as continuous and implemented it in Matlab and Simulink to study both clonk and shuffle. Couderc *et al* [9] used a discrete model to study low frequency (under 70 Hertz) vibrations and found that the model predicted the measured natural frequencies to within six percent. Because it is important to understand how the vibrations are excited initially, many papers have been written on modelling and dynamics of gears (e.g., Donley *et al* [13]) and on gear transmission error excitation (e.g., Kartik and Houser [31]). Previous researchers have also examined the noise/vibration paths that reach the passenger compartment (e.g., Wilson and Clapper [71]).

A vital portion of the modelling is determination of which vibration modes are responsible for the noise. Theodossiades *et al* [61] performed finite element analysis on a drivetrain test rig with a two-piece driveshaft to determine the dominant vibration modes. They conclude that clonk is dominated by the "ovaling" modes of the

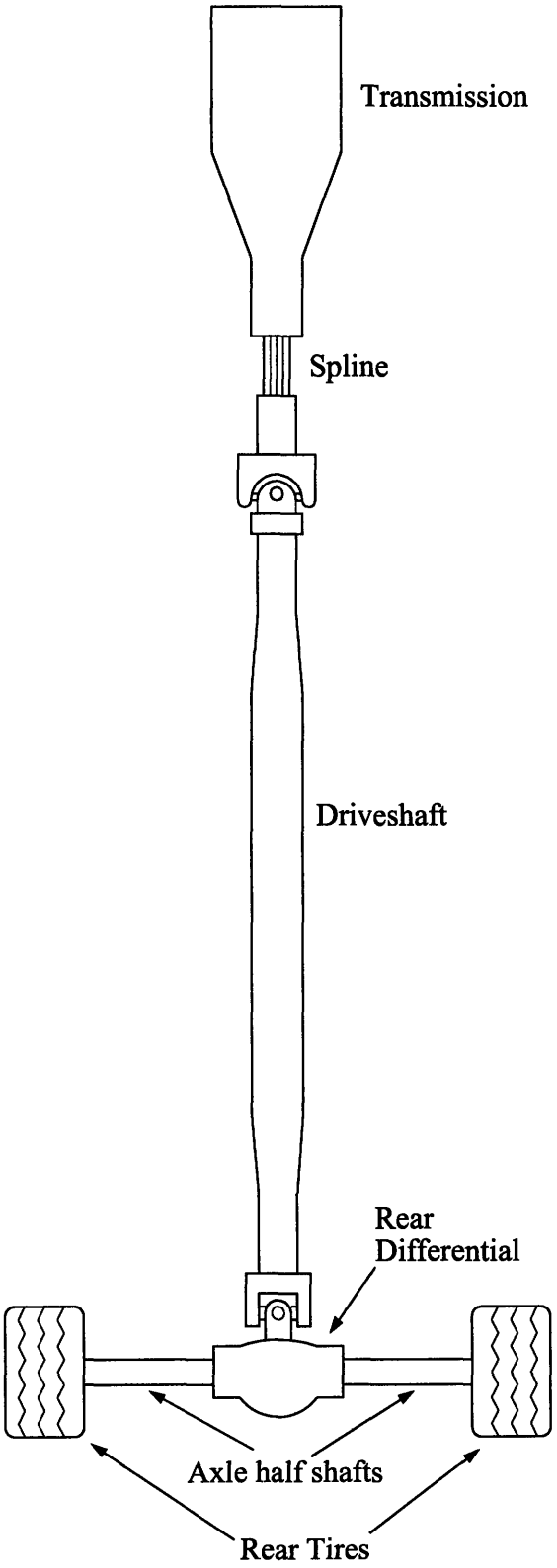

Figure 1-5: Schematic of drivetrain of rear-wheel-drive vehicle

Figure 1-6: Photograph of a driveshaft (shown next to a meter stick for scaling)

driveshaft. They identified ovaling modes between 1650 and 1750 Hertz for the rear driveshaft and above 3000 Hertz for the front driveshaft. Sun *et al* [60] identified the principle modes in the gear mesh frequency range, between 100 and 1000 Hertz. They identified the inertia of the differential's ring gear and the torsional stiffness at the pinion gear as the most sensitive parameters for noise reduction. Based on these findings they gave general rules for low-noise drivetrain design.

Approaches to Noise and Vibration Reduction

A variety of approaches have been proposed for reduction of high frequency noise. One common approach is to reduce the transmission error through better design or improved manufacturing tolerances. Chung *et al* [6] reduced noise levels by 10 dB by using finite element analysis of gear contact to design the gears to reduce transmission error. Another approach involves "tuning" components to reduce the noise. The components are selected such that the natural frequencies of the drive train which are lightly damped are not close to the mesh frequencies of the gears. Richards and Pines [53] used a periodic driveshaft to create stop bands such that the natural frequencies of the driveshaft would not be close to the mesh frequencies of the gears. Farshidianfar *et al* [15] used genetic algorithms to optimize the flywheel inertia, driveline backlash, and clutch spring stiffness to reduce the clonk noise. Miyauchi *et al* [39] modified the gear shapes and added a ring to the driven gear which is tuned to reduce

vibration. Noise may also be reduced by adding damping to the drive shaft by filling with foam or wrapping it with wire (see [63]). Active approaches have been studied but are not common, probably because they are too expensive to implement.

Automotive Gear Whine

The driveshaft is a lightly damped member of vehicle drivetrains and an efficient radiator of sound. Many vibration modes of the shaft lie within the gear mesh frequency ranges of the transmission and rear differential, 1–1.3 kHz and 300–800 Hz, respectively. Vibration modes of shell-type structures typically occur in clusters. For a complicated system such as this, the precise prediction of the natural frequencies is difficult because the boundary conditions are not exactly known and may vary. The mode shapes can be predicted with sufficient accuracy because they are not sensitive to small changes. Sound levels are observed to be highest when the shaft's shell modes are close in frequency to one or more of the bending modes [7]. The ideal solution must be robust to variations in frequency in addition to being cost-effective. Most of the previous work on this problem has dealt with improvements in modeling of the drivetrain, and the resulting approaches to reduce gear whine are design modifications which have resulted in only marginal improvement. However, Vafaei *et al* [63] filled the driveshaft with foam and wrapped it with wire but did not have a model to explain the results. A commercially available treatment is to apply cardboard liners with rubber spacers to the inside of driveshafts to damp the vibrations, but the results are limited [7]. Active damping methods have also been studied but are not common because they are too expensive. Low-wave-speed foams are an attractive solution because they are inexpensive, provide damping over a large frequency range, and are insensitive to changes in the natural frequencies of the driveshaft. Figure 1-7 shows the frequency response of a driveshaft that has been removed from the vehicle using an impact hammer and accelerometer for various damping treatments. The frequency response shows that a low-wave-speed foam adds significant damping even to the first bending mode. A moderately stiff foam does not perform as well. Analysis of foam-filled cylinder is presented in Chapter 6.

1.2 Overview

This thesis develops and demonstrates modelling and analysis tools to add damping to structures using low-wave-speed media.

Varanasi and Nayfeh [66] developed formulas for prediction of damping in Euler-Bernoulli beams coupled to lossy, lightweight granular materials. The Timoshenko beam model is more accurate than the Euler-Bernoulli model for thin-walled beams which one is likely to use if they are being filled with a granular material. Chapter 2 develops a method to predict the loss factor of Timoshenko beams coupled to a granular material and presents experimental verification. A similar procedure for Timoshenko beams coupled to a low-wave-speed foam is contained in the Chapter 3. Chapter 4 demonstrates a design approach for using foam to damp the bending modes

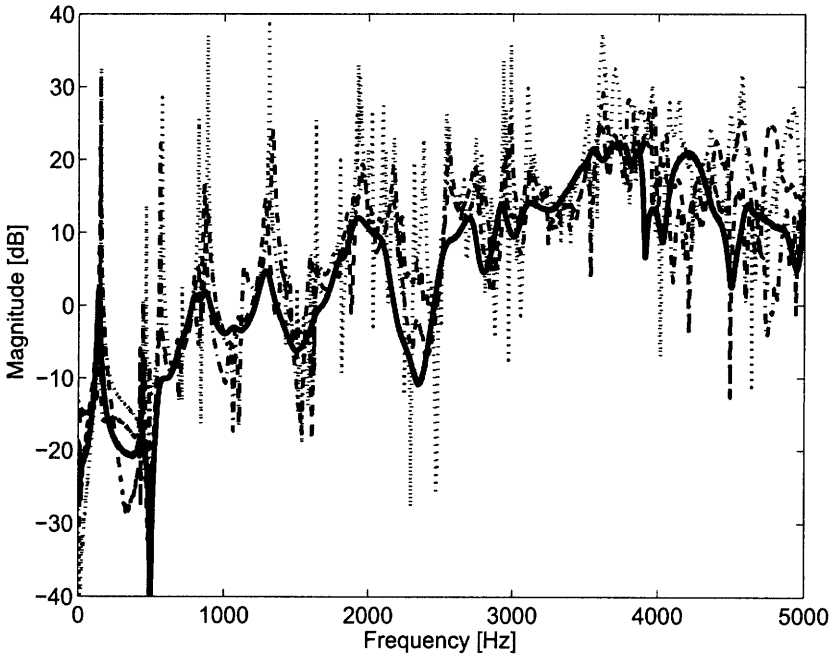

Figure 1-7: Frequency response of driveshaft removed from vehicle with various damping treatments: empty (dots), cardboard liner (dash-dot), moderately stiff foam (dashed), low-wave-speed foam (solid)

of solid and thin-walled beams and compares the results to those attainable with constrained-layer damping.

Thin-walled cylindrical shells are common structural element. Experimental results show that significant damping can be obtained in the beam bending and wall flexing modes when a cylindrical shell is filled with a lossy, low-wave-speed material. Chapter 5 presents an analytical method to predict the loss factor of cylindrical shells filled with a lightweight granular material. Chapter 6 presents an analytical method to predict the loss factor of cylindrical shells filled with lossy foams.

For large or complicated structures, the finite element method is commonly used to predict the vibratory response. The addition of a low-wave-speed material to the finite element model presents challenges such as frequency dependent properties, significant increase in number of degrees of freedom, and increase in number of vibratory modes. Chapter 7 develops and demonstrates an eigenvalue solver for structures coupled to low-wave-speed media (LWSM) that handles the problems created by the addition of the LWSM.

1.3 Summary of thesis contributions

- Vibration damping of Timoshenko beams filled with lightweight low-wave-speed media: We study an infinite length Timoshenko beam coupled to a low-wave-

speed granular material to obtain the loss factor as a function of frequency independent of boundary conditions. Comparison to the results using Euler-Bernoulli beam theory shows that the choice of beam model does not have a significant effect because the dynamics and model of the granular material is the dominant element in determining the loss factor.

- Comparison of low-wave-speed damping to constrained-layer damping: We compare the loss factors attainable using constrained-layer damping and low-wave-speed damping for a solid beam and for a thin-walled beam for a given amount of added mass and in the process present simple design formulas for the foam damping treatment. We show that LWSM can achieve higher peak loss factors and that LWSM provides better broadband performance for thin-walled tubes.

- Vibration damping of cylindrical shells filled with lightweight granular materials: We study vibrations in infinite length cylindrical shell filled with lightweight granular materials. We obtain the relation between loss factor and frequency independent of boundary conditions for beam bending and wall flexing mode shapes. Results are verified experimentally.

- Vibration damping of cylindrical shells filled with lightweight foams: We study vibrations in infinite length cylindrical shells filled with lightweight foams. We obtain the relation between loss factor and frequency independent of boundary conditions for axial, torsional, beam bending, and wall flexing mode shapes. Results are verified experimentally for the beam bending and wall flexing modes.

- Approximate eigenvalue solution of finite element formulation of structures coupled to lossy, low-wave-speed media: The eigenvalue problem for finite element models of structures coupled to low-wave-speed media is complicated by the frequency dependent nature of the LWSM, complex stiffness of the LWSM, and significant increase in the number of degrees of freedom of the model. An eigenvalue solution is developed that tailored to handle these complications.

- Characterization of material properties of low-wave-speed media: We use a non-resonant test to measure the shear and extensional moduli of foam samples for various initial strains. A resonant column test is used to measure the speed of sound and loss factor for a granular material.

Chapter 2

Vibration damping of Timoshenko beams coupled to lightweight, low-wave-speed granular materials

2.1 Introduction

The introduction of a granular material or foam into a structure or machine is a relatively simple and low-cost approach to attenuation of vibration. Oberst [43], Morris [40], and James [27] observed damping in structures consisting of metal and a soft, lossy laminate such as foam or rubber due to resonances through the thickness of the lossy material. Ungar and Kerwin [62] developed a model to estimate the loss factor of plates and beams with a viscoelastic layer due to resonances through the thickness and compared the model with experimental measurements. They modelled the viscoelastic material with a one-dimensional wave equation (through the thickness) and a complex Young's modulus. House [24] used a similar model to study damping in tubular beams filled with viscoelastic spheres with the idea that the small contact areas between the spheres results in an effectively softer viscoelastic material and hence the onset of damping occurs at a lower frequency than with a solid layer.

Traditionally, dense granular fills (such as sand, lead shot, or steel balls) have been selected for such applications in order to obtain strong coupling between the structure and the granular material. In general, damping with granular materials can be divided into two categories based on the dominant energy dissipation mechanism: continuum viscoelastic behavior such as demonstrated by House and co-workers above [24, 45] in which energy is dissipated through the hysteresis associated with elastic deformation of the particles and particle impact behavior in which energy is dissipated through impacts and sliding friction between particles. Particle impact dampers consist of a container partially filled with a relatively dense granular material such that the particles can more easily slide over one another or become "airborne" and impact the casing or another particle (e.g., [46, 35, 72, 47, 48, 18]). The particle impact damping mechanism is highly nonlinear. Accurate models do not exist for systems with particle impact dampers owing to the lack of a continuum type model for the granular medium.

The static, quasi-static, and dynamic behavior of granular materials include a variety of nonlinear phenomena that are the research focus of many physicists and applied mathematicians (e.g., [26]). The impact and frictional losses are negligible in the continuum mechanism because the particles are nearly locked together and only an insignificant fraction of particles is "airborne" at any instant.

Cremer and Heckl [10] noted that damping in sand-filled structures is caused by resonances through the thickness of the sand layer. Richards and Lenzi [54] performed a series of experiments on sand-filled tubes to determine the influence of parameters such as cavity shape, particle size, amount of granular material, and excitation amplitude and direction and concluded that damping attains a maximum at frequencies where resonances can be set up in the granular material and that damping is approximately proportional to the added mass. Bourinet and Le Houédec [4] expanded on the ideas of Cremer and Heckl. They modelled the sand-filled beams using Timoshenko beam theory with an added "apparent mass" to capture the behavior of the compression waves in the granular medium. Sun *et al* [59] modelled sand as a fluid while using statistical energy analysis to predict the damping in a sand-filled structure. Pamley *et al* [45] compared the use of viscoelastic spheres to constrained-layer and free-layer damping and concluded that the through-the-thickness damping is the most effective method for the same weight penalty. Rongong and Tomlinson [55] examined discrepancies between model and experiment caused by the idealization of the particles as a continuum and at relatively high levels of excitation. Experiments by Fricke [19] and Nayfeh *et.al.* [41] indicate that low-density particles can provide high damping of structural vibration if the speed of sound in the fill is sufficiently low. Varanasi and Nayfeh [65] showed that the dynamics of beams filled with such a low-density granular fill can be predicted by treating the fill as a compressible fluid with a complex speed of sound. Park [50, 49] studied properties of granular materials for application to vibration and noise reduction. Varanasi and Nayfeh [66] attained similar damping behavior using lossy, lightweight foams with a low speed of sound and modelled the foam using the two-dimensional equations of elasticity with complex moduli.

In this chapter, we consider the problem of damping vibration in beams coupled to lossy, lightweight granular materials. We present the results of experiments on powder-filled rectangular tubes and a powder-filled cylindrical tube. To model the damping phenomenon and obtain estimates for the damping, we consider steady harmonic wave propagation in the axial direction of an infinitely long beam and treat the powder as a compressible fluid with a complex speed of sound. We use both Euler-Bernoulli and Timoshenko beam models for comparison. Based on the spatial decay characterized by a complex wavenumber, we obtain an estimate of the loss factor associated with motion as a function of frequency.

2.2 Experiments

We conduct experiments on an aluminum rectangular tube, a steel square tube, and an aluminum circular tube. Frequency response functions of the empty and filled tubes

are measured using an impact hammer (PCB 086B03), accelerometer (PCB 356B21), and dynamic signal analyzer (Siglab 20-42). The excitation and acceleration measurements are at opposite ends of the beams. The beams are supported using elastic strings located 22% from each end to approximate free-free boundary conditions. The granular material for all experiments is 3M Glass K1 Microbubbles [1]. The ends of the beam were sealed with latex membranes when filled with powder.

2.2.1 Filled Box Beams

An aluminum rectangular tube of 1.83 m length, 25.4 mm width, 38.1 mm height, and 3.18 mm wall thickness was filled with a 67.6 kg/m^3 fill of glass microbubbles resulting in a 4.1% added mass to the beam. The noncollocated frequency response functions of the empty and filled beams are shown in Figure 2-1.

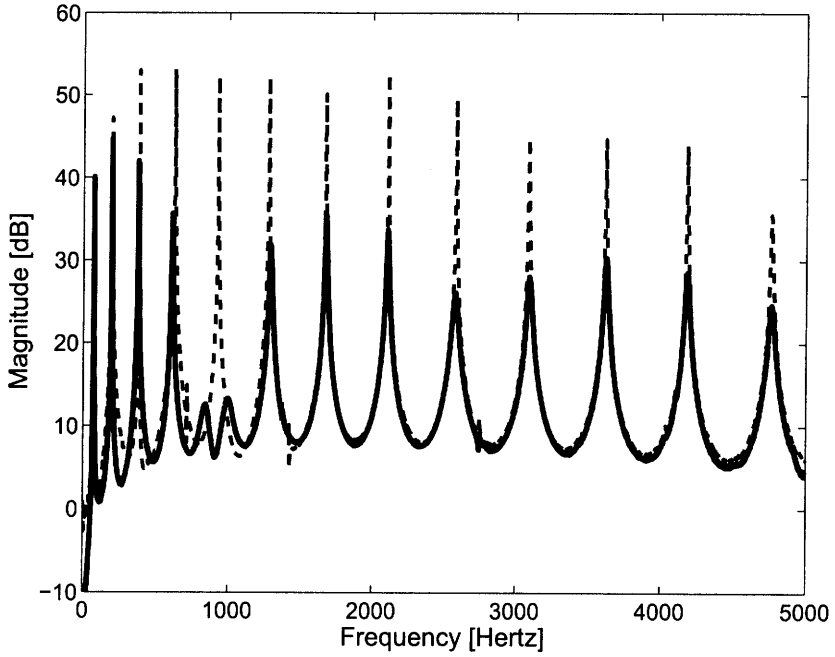

Figure 2-1: Measured noncollocated force-to-acceleration frequency response of rectangular aluminum tube (measurement and force at opposite ends of the beam): empty (dashed) and filled (solid)

A square steel box beam of length 2.04mm, width 19.1mm, and thickness 1.59mm was filled with 65.9 kg/m^3 of glass microbubbles resulting in an added mass of 1.9% to the beam. The noncollocated frequency response functions of the empty and filled beams are shown in Figure 2-2.

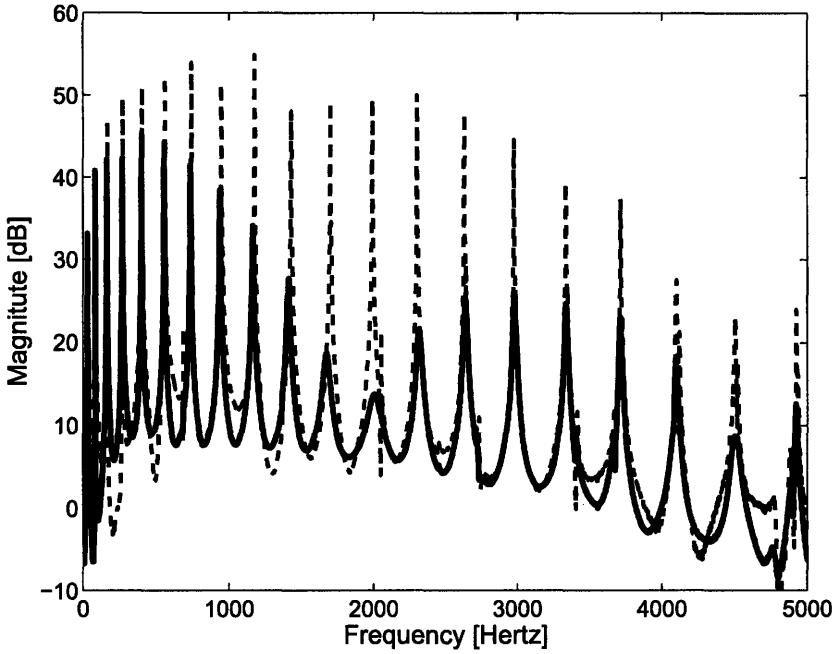

Figure 2-2: Measured noncollocated force-to-acceleration frequency response of square steel tube (measurement and force at opposite ends of the beam): empty (dashed) and filled (solid)

2.2.2 Filled Circular Tube

A circular aluminum tube of length 1.14m, outside diameter 42.2mm, and thickness 3.81mm was filled with 74.1 kg/m^3 of microbubbles resulting in an added mass of 6.0%. The empty and filled frequency response functions of the noncollocated measurements are shown in Figure 2-3.

2.2.3 Determination of Material Properties

Yanagida *et al* measured the stiffness and damping ratio of binary powder mixtures by measuring the resonance of a mass-loaded, powder-filled cup subject to harmonic excitation. Palumbo and Park [44] measured the speed of sound and loss factor of a uniform, granular fill using the same method.

Instead of using a mass-loaded sample, we measure the powder properties using a powder-filled tube with a fixed plunger at one end and a moveable piston at the other end (see Figures 2-4 and 2-5). The fixed plunger is connected to a high-sensitivity force sensor (PCB Piezotronics 208C01, 108.2 mV/lbf). The moveable piston is actuated using an electrodynamic shaker (Vibration Test Systems VG 100M-4). The acceleration of the piston is measured using PCB 356B21. Latex membranes are used to seal around the plunger and piston. The hardware setup for this method can be made more easily than the mass-loaded approach. By replacing the moving mass with

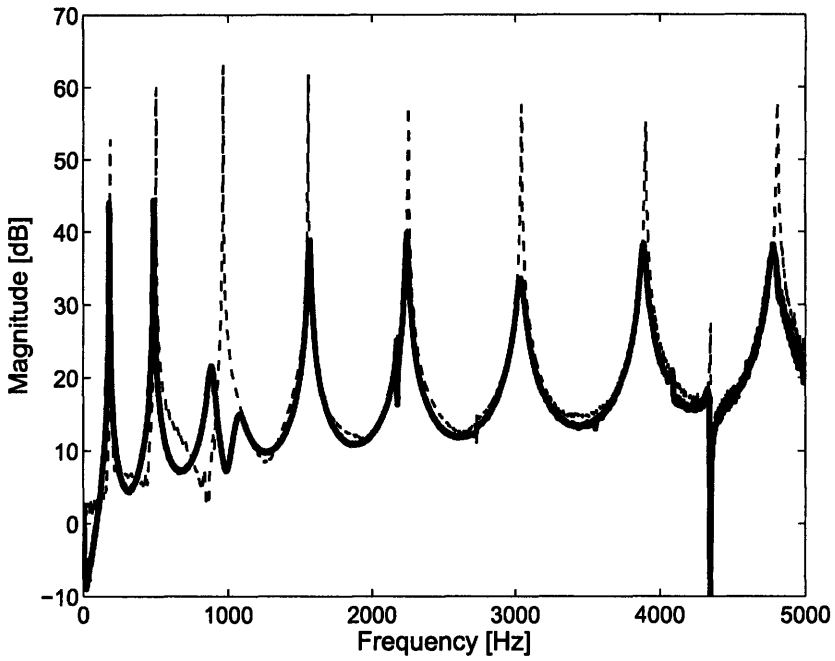

Figure 2-3: Measured noncollocated force-to-acceleration frequency response of circular aluminum tube (measurement and force at opposite ends of the beam): empty (dashed) and filled (solid)

a fixed wall, we reduce the load on the shaker and hence can test at higher frequencies for a given shaker.

A sine sweep is performed such that the sample is subject to compression while the force amplitude is kept approximately constant, and the acceleration-to-force transfer function is measured. The powder exhibits resonances at approximately integer intervals (see Figure 2-7). Based on this observation and the inability of the powder to support large shear stresses, we model the granular media as a compressible fluid. The energy dissipation is included through the imaginary part of the speed of sound. The speed of sound in the granular material is then given by

$$c = c_0(1 + j\eta) \tag{2.1}$$

where η is the loss factor and

$$c_0 = \frac{2\ell}{n} f_n \tag{2.2}$$

where ℓ is the depth of the sample, n is the number of vibration antinodes, and f_n is the natural frequency in Hertz of the acceleration-to-force transfer function. The loss factor is given by $\eta = 2\zeta$ where ζ is the damping ratio of the vibration mode.

We conduct a series of experiments using tubes of lengths 39.5 mm and 51.8 mm and diameter 34.5 mm with densities ranging from 69 kg/m^3 to 80 kg/m^3 at a force amplitude of 0.018 N. We use the smallest force amplitude possible to minimize

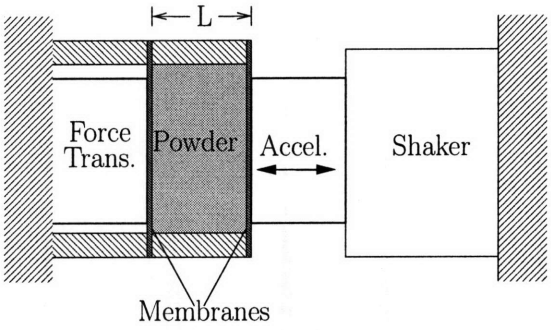

Figure 2-4: Schematic of powder property testing

nonlinear effects. Using the first three resonances of the 51.8 mm samples and the first two resonances of the 39.5 mm samples, we obtain the speed of sound and loss factors shown in Figure 2-6. This figure shows a softening trend with increasing frequency. The performance of the shaker limited the tests to below 2 kHz. Because we are interested in the properties of the granular material up to 5 kHz, we take the average speed of sound to be $c = 69(1 + 0.13j)$ meters per second.

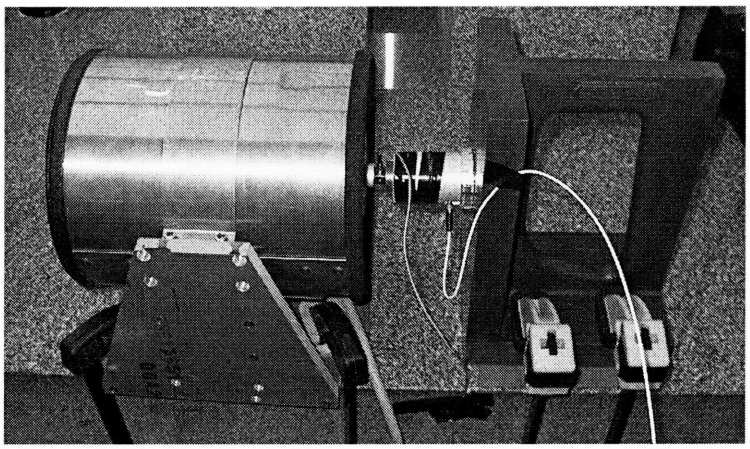

Figure 2-5: Photograph of apparatus for measuring the properties of the powder

2.3 Modelling

We develop an approach to obtaining estimates of the loss factor as a function of frequency based on a beam-fluid system of infinite length under steady harmonic vibration at frequency ω. We assume wave solutions ($Ae^{jk_x x}$) for the fluid pressure and beam displacements. Because the coupled equations are difficult to solve in closed form analytically and the density of the fluid is small compared to the mass of the beam, we use an iterative approach to solve. The results show that the scheme typically converges after just a few iterations. Using the estimated complex wavenumber

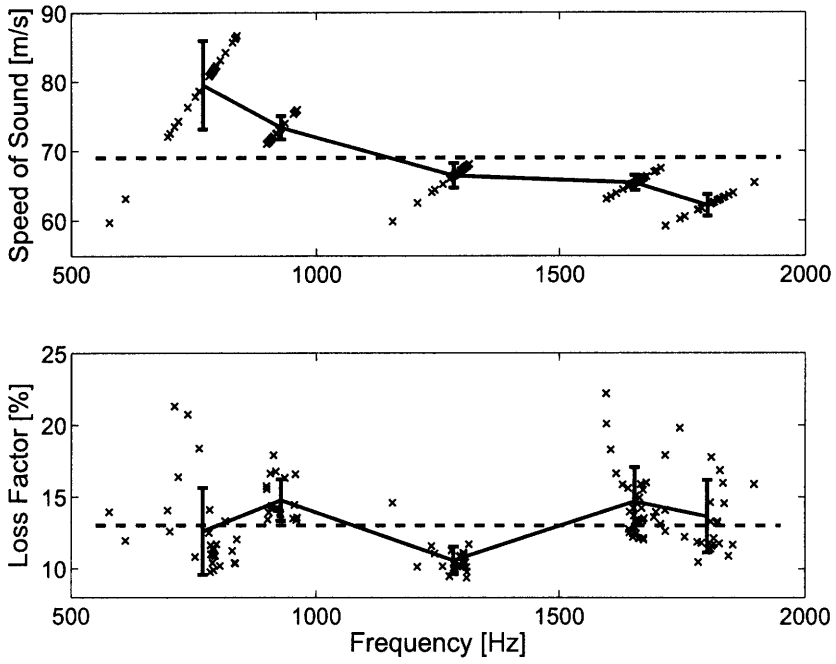

Figure 2-6: Measured speed of sound and loss factors (×), average speed of sound and loss factor (dashed)

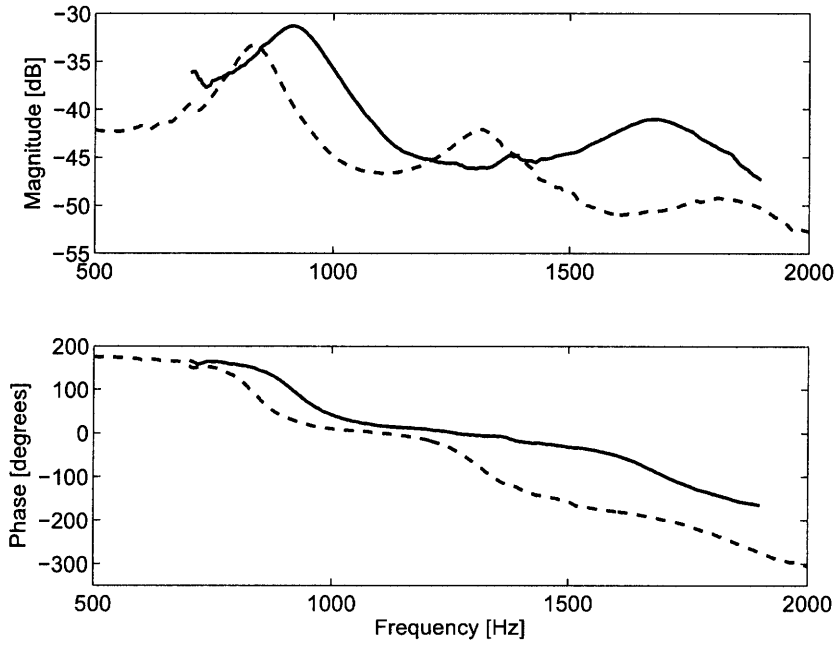

Figure 2-7: Typical measured acceleration-to-force frequency response functions for the 51.8 mm sample (dashed) and 39.5 mm sample (solid)

for each frequency, we compare the result to an equivalent beam with a complex Young's modulus to find the loss factor of the coupled beam-fluid system. Below, we consider three cases: a filled rectangular tube, a filled circular tube, and a solid bar with a free layer on top. We use both the Euler-Bernoulli and Timoshenko beam models for comparison because the Timoshenko model is known to be more accurate for thin-walled tubes and for higher mode shapes.

This approach offers many advantages over trying to solve for the loss factor of a finite length beam. This method is mathematically more simple because one does not need to impose boundary conditions at the ends of the beam. The result of this approach is a curve showing the loss factor as a function of frequency based on the material properties of the beam, granular medium, and cross-sectional geometry of the beam. It is independent of length and boundary conditions. This method could prove useful to the engineer designing a system or retrofitting a system to reduce vibration.

2.3.1 Euler-Bernoulli Beams

We model the structure as a Euler-Bernoulli beam. The nondimensional governing equation for the beam under harmonic motion where lengths and displacements have been nondimensionalized by the height of the powder layer h is

$$\frac{d^4w}{dx^4} - \Omega^2 w = \tilde{P}(x,\omega) \tag{2.3}$$

where

$$\Omega^2 = \frac{\rho A h^4}{EI}\omega^2 \tag{2.4}$$

ω is the frequency, w is the deflection, E is the Young's modulus, I is the moment of inertia of the beam, A is the cross sectional area of the beam, ρ is the volumetric density, and $\tilde{P}(x,\omega)$ is the loading from the pressure applied by the powder whose exact form depends on the cross sectional geometry of the beam.

The granular medium is modelled as a compressible fluid with a complex speed of sound $c = c_0(1 + j\eta)$ where η is the loss factor associated with the speed of sound. The speed of sound in terms of the material loss factor η_m is $c = c_0\sqrt{1 + j\eta_m}$ such that the material loss factor is approximately twice the speed of sound loss factor. It is governed by the wave equation

$$\frac{c^2}{\left(\frac{EI}{\rho A h^2}\right)}\nabla^2 p + \Omega^2 p = 0 \tag{2.5}$$

where c is the speed of sound in the fluid and p is the pressure in the fluid that has been nondimensionalized by $\frac{EI}{h^4}$. The boundary conditions of the powder depend on the geometry of the beam.

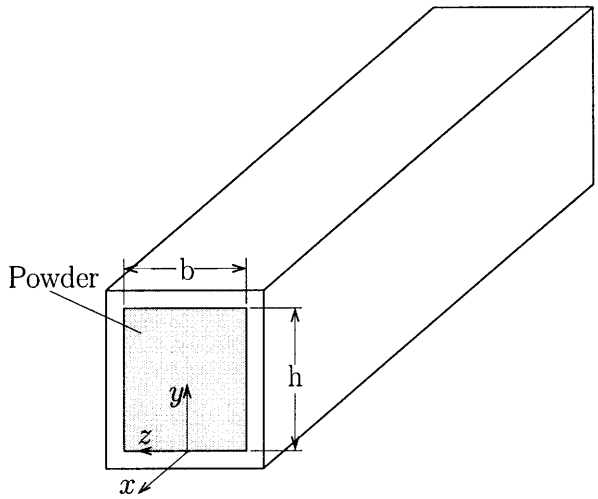

Figure 2-8: Sketch of a rectangular box beam

Filled rectangular beam

For a rectangular box beam of internal width b and height h where the powder has no free surface, we assume that the pressure in the granular medium is independent of the width-wise coordinate z; therefore, the force per unit length applied to the beam by the powder is

$$\tilde{P}(x,\Omega) = \frac{b}{h}\left(p(x,y=1,\Omega) - p(x,y=0,\Omega)\right) \tag{2.6}$$

The associated boundary conditions on the powder for steady harmonic motion are

$$\frac{\partial p(x,y=0,\Omega)}{\partial y} = \frac{\rho_f h^2}{\rho A}\Omega^2 w(x) \tag{2.7}$$

$$\frac{\partial p(x,y=1,\Omega)}{\partial y} = \frac{\rho_f h^2}{\rho A}\Omega^2 w(x) \tag{2.8}$$

where ρ_f is the density of the powder. We assume solutions of the form

$$w(x) = We^{jk_x x} \tag{2.9}$$

$$p(x,y) = \overline{p}(y)e^{jk_x x} \tag{2.10}$$

The governing equation for the beam becomes

$$(k_x^4 - \Omega^2)W = \frac{b}{h}(\overline{p}(y=1) - \overline{p}(y=0)) \tag{2.11}$$

The governing equation for the powder becomes

$$\frac{d^2\overline{p}}{dy^2} + \left(\frac{\Omega^2}{c^2}\frac{EI}{\rho A h^2} - k_x^2\right)\overline{p} = 0 \tag{2.12}$$

with boundary conditions

$$\frac{d\overline{p}(y=0)}{dy} = \frac{\rho_f h^2}{\rho A}\Omega^2 W \tag{2.13}$$

$$\frac{d\overline{p}(y=1)}{dy} = \frac{\rho_f h^2}{\rho A}\Omega^2 W \tag{2.14}$$

Solving the equation for the pressure, we obtain

$$\overline{p}(y) = c_1 \cos k_y y + c_2 \sin k_y y \tag{2.15}$$

where

$$k_y^2 = \frac{\Omega^2}{c^2}\frac{EI}{\rho A h^2} - k_x^2 \tag{2.16}$$

The boundary condition at $y = 0$ gives

$$c_2 = \frac{\rho_f h^2 \Omega^2}{\rho A k_y} W \tag{2.17}$$

and the boundary condition at $y = h$ gives

$$c_1 = \frac{\rho_f h^2 \Omega^2 W}{\rho A k_y \sin k_y}\left(\cos k_y - 1\right) \tag{2.18}$$

Therefore, the pressure in the fluid is

$$p(x, y, \omega) = \frac{\rho_f h^2 \Omega^2 W}{\rho A k_y}\left(\frac{\cos k_y - 1}{\sin k_y}\cos\left(k_y y\right) + \sin\left(k_y y\right)\right) \tag{2.19}$$

At the interface between the fluid and the beam ($y = 0, h$), we have

$$\overline{p}(y=0) = \frac{\rho_f h^2 \Omega^2 W}{\rho A k_y}\left(\frac{\cos k_y - 1}{\sin k_y}\right) = -\overline{p}(y=1) \tag{2.20}$$

The equations for the filled beam may be written using only a simple modification to the inertia term of the equations for the empty beam

$$\left(k_x^4 - \Omega^2\right) W = \Omega^2 W B \tag{2.21}$$

where

$$B = 2\frac{\rho_f b h}{k_y \rho A}\left(\frac{1 - \cos k_y}{\sin k_y}\right) \tag{2.22}$$

This quantity B is a mass ratio with a frequency dependent scale factor determined by the pressure at the interfaces between the fluid and the beam.

Next, we solve for the complex wavenumber as a function of frequency using an iterative approach. We use the dispersion relation for the empty beam as the initial guess for the wavenumber by setting $B = 0$. That is, we guess

$$k_x = \sqrt{\Omega} \tag{2.23}$$

This initial guess is real valued. Then, we calculate the corresponding value of B for each frequency. Then, we solve for the wavenumber using

$$k_x = \left(\Omega^2(1+B)\right)^{\frac{1}{4}} \tag{2.24}$$

The next iteration begins by recalculating the value of B from (2.22) at each frequency. We continue the iterations until they converge to within a desired error bound. For a one percent error, typically one or two iterations is sufficient.

To obtain the loss factor, we assume that there exists an equivalent empty beam with a modulus of $E = E_0(1 + j\eta)$. We solve for the modulus using the dispersion relation and then substitute the relation for the complex wavenumber (as a function of frequency) to obtain the complex modulus as a function of frequency. Then, the loss factor is given by

$$\eta = \frac{\operatorname{Im} E}{\operatorname{Re} E} \tag{2.25}$$

Making use of the dispersion relation for the empty beam (2.23) and recognizing that the modulus of the beam only appears in Ω, the loss factor is given by

$$\eta = \frac{\operatorname{Im} \frac{1}{k_x^4}}{\operatorname{Re} \frac{1}{k_x^4}} = \frac{\operatorname{Im} \frac{1}{\Omega^2}}{\operatorname{Re} \frac{1}{\Omega^2}} \tag{2.26}$$

Figure 2-9 compares the dimensionless dispersion relations for an empty and filled box beam. The nondimensinonal frequency

$$\Omega^* = \frac{4\pi}{c_0}\sqrt{\frac{EI}{\rho A h^2}}\Omega = \frac{4\pi\omega h}{c_0} \tag{2.27}$$

has been scaled such that resonances through the thickness of the powder occur at integer values. Comparing the real part of the dispersion curve of the filled beam with the dispersion curve of the empty beam, we find that the difference is small which confirms our assumption that the behavior (mode shapes and natural frequencies) of the beam is not significantly altered by the addition of the granular material. We notice that these two curves intersect when the nondimensional frequency is near 1, 2, 3, ... n, where n is an integer. These intersections correspond to resonances in the powder. The resonances occurring at odd n correspond to large increases in damping (see Figure 2-10)because the pressure distribution in the powder acts to significantly oppose the motion of the beam. The resonances occurring at even n do not give

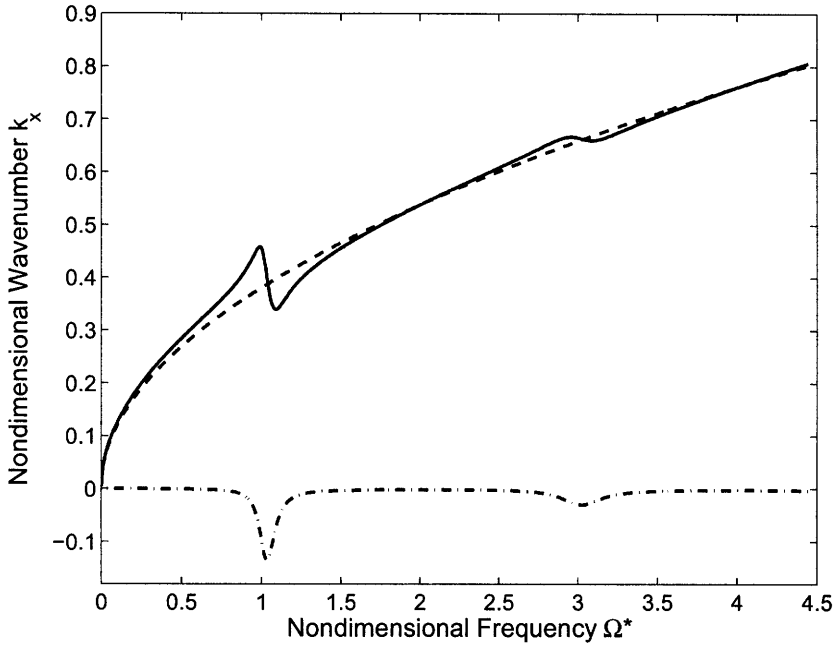

Figure 2-9: Typical dispersion curve for a rectangular tube with a loss factor of 0.05 and mass ratio of 20%: empty beam (dashed), real part (solid), imaginary part (dashdot).

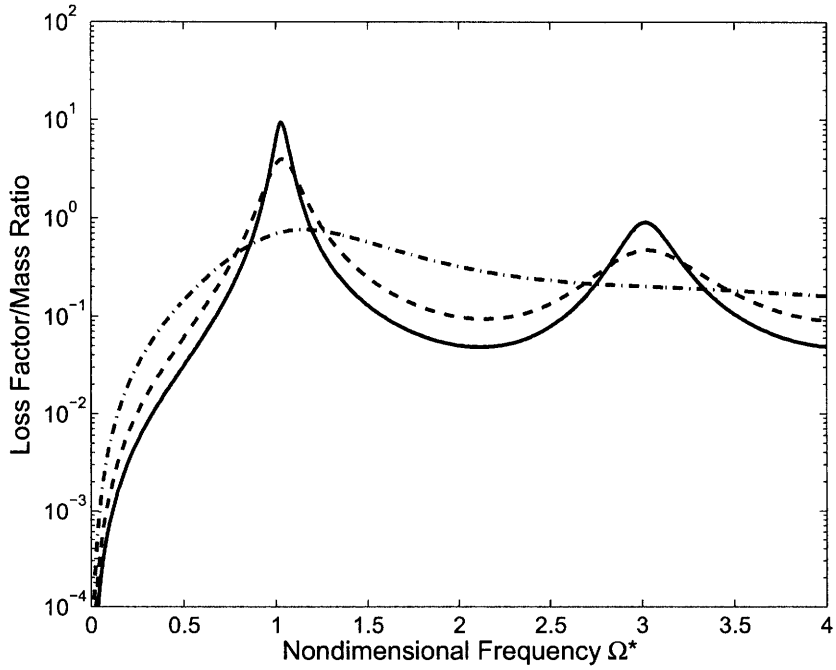

Figure 2-10: Typical curves of loss factor as a function of frequency for powder loss factors 0.05 (solid), 0.1 (dashed), 0.5 (dashdot)

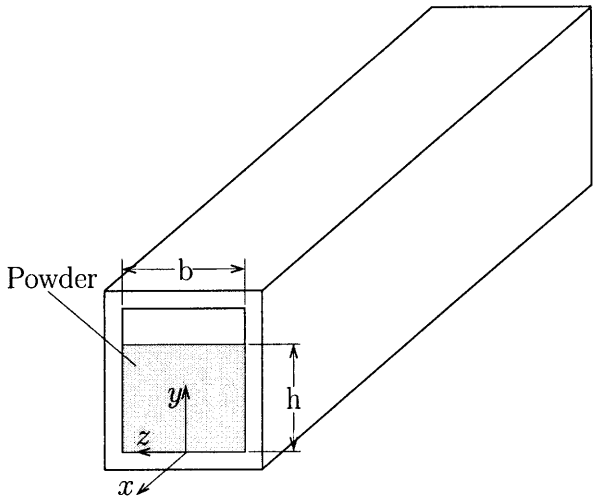

Figure 2-11: Sketch of box beam partially filled with powder

significant damping because the pressure at the top and bottom of the powder layer tend to cancel.

From the perspective of the beam, intersections of the real part of the dispersion curve for the filled beam and the dispersion curve of the empty beam correspond to changes in the perceived effect of the powder between added mass or added stiffness. For example, below a nondimensional frequency of 1 the powder acts primarily as an added mass, and the natural frequencies of the finite length beam are lower than the corresponding frequencies of the empty beam. Between a nondimensional frequency of 1 and 2, the powder acts as a spring to effectively stiffen the beam. The resulting natural frequencies of a finite length beam are higher than those of the empty beam. This transition from apparent added mass to added stiffness is similar to what occurs in a discrete tuned-mass damper system above and below the resonant frequency of the absorber subsystem.

Figure 2-10 plots the loss factor normalized by the mass ratio as a function of nondimensional frequency for various loss factors. The loss factor has local maxima near odd resonances of the powder and local minima near even resonances of the powder. The loss factor is normalized by the mass ratio because the loss factor is nearly linear with the added mass.

Free layer on beam

We now consider vibration a rectangular beam that is only partially filled with powder resulting in a free surface for powder (see Figure 2-11). The beam is again modelled by the Euler-Bernoulli model (2.3) and the granular medium by a compressible fluid (2.5).

The force per unit length applied to the beam by the powder is

$$\tilde{P}(x,\Omega) = -\frac{b}{h}p(x, y=0, \Omega) \tag{2.28}$$

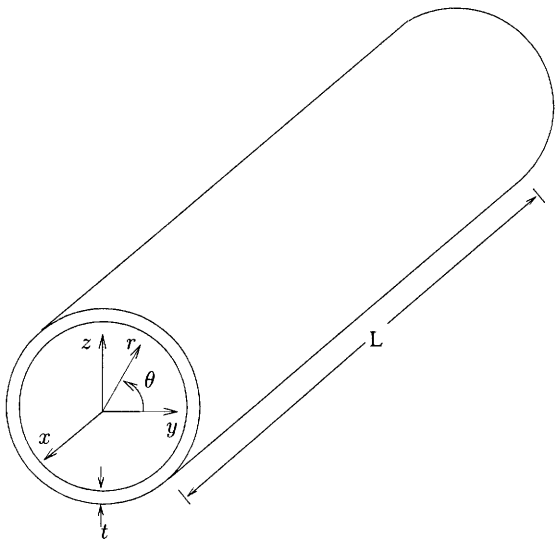

Figure 2-12: Sketch of circular tube geometry

The associated boundary conditions on the powder for steady harmonic motion are given by (2.7) and

$$p(x, y = 1, \Omega) = 0 \tag{2.29}$$

To obtain the loss factor for the partially filled beam, we follow the same procedure as for the filled beam. The correction term B given by (2.22) becomes

$$B = \frac{\rho_f bh}{\rho A k_y} \tan k_y \tag{2.30}$$

We again use the iterative procedure to find the complex wavenumber for each frequency of interest and then calculate the loss factor by finding an equivalent beam as described for the rectangular tube.

Filled circular beam

The circular beam (see Figure 2-12) filled with granular materials is modelled again using the Euler-Bernoulli beam (2.3) and a compressible fluid (2.5) where now we nondimensionalize lengths and displacements by the internal radius of the tube R and the pressure by $\frac{EI}{R^4}$ such that the nondimensional frequency is given by

$$\Omega^2 = \frac{\rho A R^4}{EI} \omega^2 \tag{2.31}$$

The force per unit length applied to the beam by the powder for a circular beam

of inner radius R is

$$\tilde{P}(x,\Omega) = \int_0^{2\pi} \sin\theta\, p(x, r=1, \theta, \Omega)\, d\theta \tag{2.32}$$

where θ is the angle relative to the horizontal as shown in Figure 2-12. The associated boundary conditions for steady harmonic motion on the powder are

$$p(x, r=0, \theta) < \infty \tag{2.33}$$

$$\frac{\partial p(x, r=1, \theta, \Omega)}{\partial r} = \frac{\rho_f R^2}{\rho A}\Omega^2 w \sin\theta \tag{2.34}$$

We assume the same solution for the beam as before

$$w(x) = We^{jk_x x} \tag{2.35}$$

For the fluid, we assume a solution of the form

$$p(x, r, \theta) = \overline{p}(r) \sin\theta\, e^{jk_x x} \tag{2.36}$$

Based on the form of the pressure, the force per unit length applied to the beam by the powder can be evaluated from

$$\tilde{P}(x,\Omega) = \int_0^{2\pi} \sin^2\theta\, \overline{p}(r=1) e^{jk_x x}\, d\theta = \pi \overline{p}(r=1) e^{jk_x x} \tag{2.37}$$

Making use of (2.36), the governing equation for the fluid (2.5) becomes a Bessel equation

$$r^2 \frac{d^2\overline{p}}{dr^2} + r\frac{d\overline{p}}{dr} + \left(r^2\left(\frac{\Omega^2}{c^2}\frac{EI}{\rho A R^2} - k_x^2\right) - 1\right)\overline{p} = 0 \tag{2.38}$$

with boundary conditions

$$\overline{p}(r=0) < \infty \tag{2.39}$$

$$\frac{d\overline{p}(r=1)}{dr} = \frac{\rho_f R^2}{\rho A}\Omega^2 W \tag{2.40}$$

The solution of (2.38) is

$$\overline{p}(r) = c_1 J_1(k_r r) + c_2 Y_1(k_r r) \tag{2.41}$$

where

$$k_r^2 = \frac{\omega^2}{c^2}\frac{EI}{\rho A h^2} - k_x^2 \tag{2.42}$$

J_1 is the Bessel function of the first kind of order one, and Y_1 is the Bessel function of the second kind of order one. Imposing the boundary conditions, we obtain

$$c_2 = 0 \tag{2.43}$$

$$c_1 = \frac{\rho_f R^2 \Omega^2 W}{\rho A J_1'(k_r)} \tag{2.44}$$

where J_1' is the derivative of the Bessel function of the first kind of order 1.

The resulting pressure distribution is

$$\overline{p}(r) = \frac{\rho_f R^2 \Omega^2 W}{\rho A J_1'(k_r)} J_1(k_r r) \tag{2.45}$$

Now the term B in (2.21) becomes

$$B = \frac{\pi \rho_f R^2}{\rho A J_1'(k_r)} J_1(k_r) \tag{2.46}$$

We solve (2.21) for the wavenumber using the same iterative procedure as for the rectangular tube. Then, we solve for the loss factor using the same procedure as before.

2.3.2 Timoshenko Beam

The Timoshenko beam model is an improvement over the Euler-Bernoulli model through inclusion of shear terms. The differences between the two models are most evident for thin-walled beams and for relatively high mode numbers. Below we develop the procedure to predict the loss factor as a function of frequency for Timoshenko beams coupled to lightweight, lossy granular materials and compare these results to the results obtained with the Euler-Bernoulli model.

The nondimensional governing equations for a uniform Timoshenko beam under steady, harmonic motion subjected to a force per unit length are

$$-\beta^2 \frac{\partial^2 \phi}{\partial x^2} + \phi - \frac{\partial w}{\partial x} - \Omega^2 \beta^2 \gamma^2 \phi = 0 \tag{2.47}$$

$$-\frac{\partial^2 w}{\partial x^2} + \frac{\partial \phi}{\partial x} - \beta^2 \Omega^2 w = \beta^2 \hat{P}(x, \Omega) \tag{2.48}$$

where ϕ is the rotation of the cross section, lengths and displacements are nondimensionalized by the height of the powder h, and

$$\beta^2 = \frac{EI}{kAGh^2} \tag{2.49}$$

$$\gamma^2 = \frac{I}{Ah^2} \tag{2.50}$$

$$\Omega^2 = \frac{\rho A h^4}{EI} \omega^2 \tag{2.51}$$

where k is the shear parameter determined by the geometry of the cross section and G is the shear modulus of the beam.

Filled rectangular beam

The rectangular box beam is sketched in Figure 2-8. The terms relating to the behavior of the powder do not change from the Euler-Bernoulli case because they are only dependent on the lateral deflection of the beam. The force per unit length applied to the beam by the powder is given by (2.6). The associated boundary conditions on the powder for steady harmonic motion are given by (2.7, 2.8).

We assume solutions of the form

$$\phi(x) = Ne^{jk_x x} \tag{2.52}$$

$$w(x) = We^{jk_x x} \tag{2.53}$$

$$p(x,y) = \overline{p}(y)e^{jk_x x} \tag{2.54}$$

The beam equation becomes

$$\begin{bmatrix} 1+\beta^2 k_x^2 - \beta^2\gamma^2\Omega^2 & -jk_x \\ jk_x & k_x^2 - \beta^2\Omega^2 \end{bmatrix} \begin{pmatrix} N \\ W \end{pmatrix} = \begin{pmatrix} 0 \\ \beta^2 \tilde{P}(x,\Omega) \end{pmatrix} \tag{2.55}$$

where

$$\tilde{P}(x,\Omega) = \frac{b}{h}(\overline{p}(y=1) - \overline{p}(y=0)) \tag{2.56}$$

The governing equation for the fluid becomes (2.12) with the associated boundary conditions given by (2.13) and (2.14). The solution for the pressure in the fluid is given by (2.19). At the interfaces between the fluid and the beam ($y = 0$ and $y = 1$), the pressure is given by (2.20). The equations for the filled beam may be written using only a modification to the inertia term of the equations for the empty beam in the form

$$\left(\begin{bmatrix} 1+\beta^2 k_x^2 & -jk_x \\ jk_x & k_x^2 \end{bmatrix} - \Omega^2 \begin{bmatrix} \beta^2\gamma^2 & 0 \\ 0 & \beta^2(1+B) \end{bmatrix} \right) \begin{pmatrix} N \\ W \end{pmatrix} = \begin{pmatrix} 0 \\ 0 \end{pmatrix} \tag{2.57}$$

where B is given by (2.22).

Next, we solve for the complex wavenumber as a function of frequency using an iterative approach. We use the dispersion relation for the empty Timoshenko beam as the initial guess for the wavenumber by setting the determinant of the matrix in (2.57) with $B = 0$ to zero. This initial guess will be real. Then, we calculate the corresponding value of B for each frequency. We substitute for B into (2.57) and solve for the wavenumber k_x by setting the determinant of the coefficient matrix to zero. The next iteration begins by recalculating the value of B at each frequency. We continue the iterations until they appear to converge, which has been after one or two iterations for most cases.

When solving for the wavenumber during each iteration, one obtains a quadratic equation in k_x^2 so there are four mathematically acceptable solutions for the wavenumber. The four solutions are really just two pairs of solutions for k_x^2, and within each pair the difference is a sign which indicates the direction of the wave. For convenience we choose the positive root. The difference between the two pairs of wavenumbers

is that only the spectrum derived from the positive root in the quadratic equation is valid [58].

To obtain the loss factor, we use the same method as with the Euler-Bernoulli beam. We assume that there exists an equivalent empty Timoshenko beam with a complex modulus $E = E_0(1 + j\eta)$. We solve for the modulus using the dispersion relation and then substitute the relation for the complex wavenumber (as a function of frequency) to obtain the complex modulus as a function of frequency. Then, the loss factor is given by (2.25).

The beam equations for an infinite beam under steady, harmonic motion may be written in nondimensional form [25]

$$\left(\begin{bmatrix} 1+\beta^2 k_x^2 & -jk_x \\ jk_x & k_x^2 \end{bmatrix} - \Omega^2 \begin{bmatrix} \beta^2\gamma^2 & 0 \\ 0 & \beta^2 \end{bmatrix} \right) \begin{pmatrix} N \\ W \end{pmatrix} = \begin{pmatrix} 0 \\ 0 \end{pmatrix} \tag{2.58}$$

Making use of

$$G = \frac{E}{2(1+\nu)} \tag{2.59}$$

we recognize that the modulus only shows up in Ω; therefore, if we solve for Ω^2, the loss factor is given by

$$\eta = \frac{\mathrm{Im}\,\frac{1}{\Omega^2}}{\mathrm{Re}\,\frac{1}{\Omega^2}} \tag{2.60}$$

The solution of Ω^2 is given by solving the eigenvalue problem (2.58). The proper value of the two solutions must be selected in keeping with the fact that there is only one valid spectrum of the Timoshenko beam model [58].

Figure 2-13 compares the loss factor curves found using the Euler-Bernoulli and Timoshenko beam theories for various values of the shear parameter k. From this figure, we conclude that the Euler-Bernoulli model is sufficient for calculating the loss factor (There are significant differences in the dispersion curves between the two models.). The physical reasoning behind this conclusion is that the behavior of granular material, specifically, the frequencies at which the powder resonances occur do not change.

Free layer on beam

The partially filled box beam (see Figure 2-11) is again modelled by the Timoshenko model (2.47, 2.48) and the granular medium by a compressible fluid (2.5). The force per unit length applied to the beam by the powder is given by (2.28). The associated boundary conditions on the powder for steady harmonic motion are given by (2.29) and (2.7).

We assume the same form of solutions as for the rectangular tube (2.52, 2.53, 2.54). After solving for the pressure at the beam-fluid interface, we again obtain the eigenvalue problem (2.57), but now the quantity B is given by (2.30).

We again use the iterative procedure to find the complex wavenumber for each frequency of interest and then calculate the loss factor by finding an equivalent beam

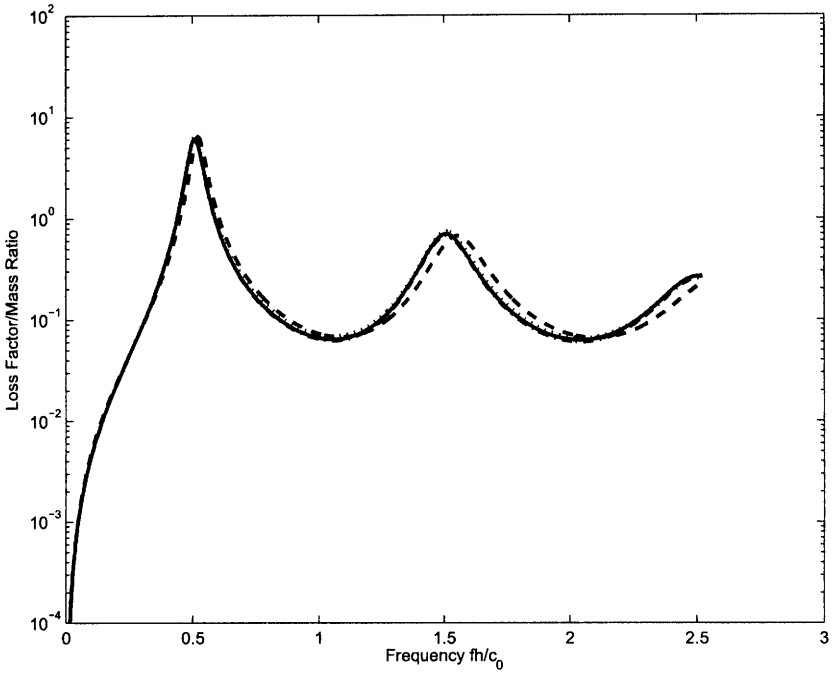

Figure 2-13: Comparison of the results using the Euler-Bernoulli and Timoshenko beam theories using different values of the shear parameter k: solid (Euler-Bernoulli), dashed ($k = 0.01$), dotted ($k = 0.1$), dashdot ($k = 1$). The beam is an aluminum rectangular tube with width 1", height 1.5", wall thickness 0.125". The actual value of the shear parameter for this beam is 0.53.

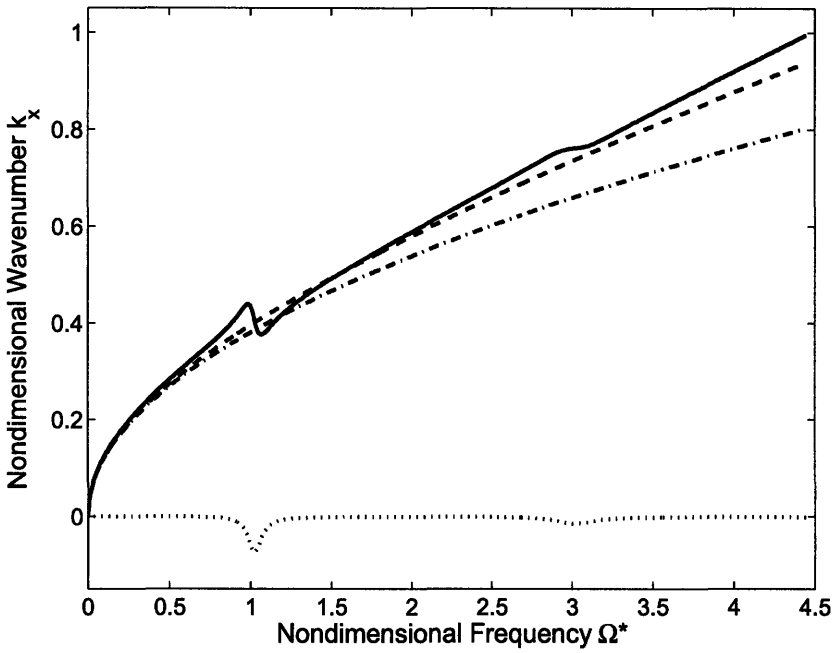

Figure 2-14: Comparison of dispersion relations for the Euler-Bernoulli and Timoshenko beam theories for a rectangular box beam with $k = 0.53$: imaginary part of Timoshenko dispersion relation for beam filled with powder (dotted), real part of Timoshenko dispersion relation for beam filled with powder (solid), Timoshenko dispersion relation for empty beam (dashed), Euler-Bernoulli dispersion relation for empty beam (dashdot)

as outlined for the rectangular tube.

Filled circular beam

The circular beam (see Figure 2-12) filled with granular materials is modelled again using the Timoshenko beam (2.47, 2.48) and a compressible fluid (2.5) where h is replaced by the internal radius of the cylinder R.

The force per unit length applied to the beam by the powder is given by (2.37). The associated boundary conditions for steady harmonic motion on the powder are given by (2.33) and (2.34).

We assume solutions (2.53), (2.52), and (2.36). The assumed solution for the pressure results in the beam loading $\tilde{P}(x,\omega)$ being given by (2.37). The governing equation for the fluid is then reduced to a Bessel equation (2.38). The resulting solution for the pressure after imposing the boundary conditions is (2.45), and the parameter B is given by (2.46). The resulting equation for the beam coupled to the powder is (2.57).

We proceed to solve for the wavenumber using the iterative procedure described above. After the wavenumber has been found, we can solve for the loss factor using (2.60).

2.4 Results

We compute the theoretical loss factor curves as a function of frequency using the methods outlined earlier. Figures 2-15, 2-16, and 2-17 show these curves along with the data for the beam experiments. Tables 2.1, 2.2, and 2.3 show the measured natural frequencies and loss factors of the filled beams and the predicted loss factors. For the predicted loss factors, the speed of sound in the powder is taken to be $c = 69(1 + 0.13j)$ m/s based on the series of measurements discussed earlier.

The mismatch between predicted and measured loss factor curves suggests that the real part of the speed of sound of the granular material is too large. Quantitative comparison suggests that the real part of the speed of sound (c_0) should be approximately 57 m/s. The errors obtained in measuring the properties of the granular material are likely due to a variety of factors including humidity and packing variations.

As can be seen in Figures 2-1 and 2-3 and in Tables 2.1 and 2.3, one of the modes of the undamped beam has "split" into two well-damped modes for the filled beam. This occurs near the first resonance of the powder. The addition of the powder creates an additional degree of freedom in the system. In this neighborhood, there is a mode in which the powder moves approximately in phase with the beam and one where the powder moves out of phase from the beam. As seen from the tabulated natural frequencies, this frequency is also the point at which powder transitions from acting as an added mass (filled beams have lower natural frequencies) to an added stiffness (filled beams have higher natural frequencies). In the steel beam experiments, the mode splitting is not visible because the new mode is well damped, but the added

Table 2.1: Natural frequencies and damping of aluminum box beam filled with powder

	Natural Frequency [Hz]		Loss Factor	
Mode	Empty	Filled	Measured	Predicted
1	71.8	70.5	1.7×10^{-3}	3.5×10^{-5}
2	197.5	193.6	2.9×10^{-3}	2.8×10^{-4}
3	384.3	375.8	3.9×10^{-3}	1.2×10^{-3}
4	628.8	610.2	9.0×10^{-3}	5.1×10^{-3}
		844.0	7.6×10^{-2}	2.3×10^{-2}
5	928.2	995.0	7.4×10^{-2}	7.3×10^{-2}
6	1277.2	1290.4	0.011	5.3×10^{-2}
7	1672.8	1674.8	0.0064	1.1×10^{-2}
8	2109.3	2105.0	6.8×10^{-3}	5.4×10^{-3}
9	2583.3	2577.3	1.4×10^{-2}	5.5×10^{-3}
10	3090.2	3094.9	9.5×10^{-3}	1.3×10^{-2}
11	3624.3	3635.0	6.0×10^{-3}	1.1×10^{-2}
12	4183.9	4183.2	0.0061	5.0×10^{-3}
13	4762.6	4762.7	0.0077	4.6×10^{-3}

Table 2.2: Natural frequencies and damping of powder-filled square steel box beam

	Natural Frequency [Hz]		Loss Factor	
Mode	Empty	Filled	Measured	Predicted
1	30.4	30.1	2.8×10^{-4}	7.4×10^{-7}
2	83.7	82.8	1.1×10^{-3}	5.6×10^{-6}
3	164.0	162.1	3.3×10^{-3}	2.2×10^{-5}
4	270.3	267.8	3.2×10^{-3}	6.0×10^{-5}
5	402.5	398.7	2.5×10^{-3}	1.3×10^{-4}
6	559.9	554.5	2.9×10^{-3}	2.8×10^{-4}
7	741.8	734.5	3.6×10^{-3}	5.5×10^{-4}
8	947.6	937.7	4.5×10^{-3}	1.0×10^{-3}
9	1176.2	1162.7	6.4×10^{-3}	2.0×10^{-3}
10	1427.4	1408.5	1.1×10^{-2}	4.2×10^{-3}
11	1699.4	1672.2	2.6×10^{-2}	1.0×10^{-2}
12	1991.3	2003.2	4.3×10^{-2}	3.7×10^{-2}
13	2302.0	2315.0	1.5×10^{-2}	5.2×10^{-2}
14	2631.1	2638.1	7.6×10^{-3}	2.0×10^{-2}
15	2976.2	2979.1	5.7×10^{-3}	9.2×10^{-3}
16	3336.8	3337.3	5.2×10^{-3}	5.2×10^{-3}
17	3714.9	3712.0	4.6×10^{-3}	3.5×10^{-3}
18	4100.1	4092.8	4.5×10^{-3}	2.6×10^{-3}
19	4503.6	4514.5	4.5×10^{-3}	2.3×10^{-3}
20	4925.5	4922.4	3.7×10^{-3}	2.3×10^{-3}

Table 2.3: Natural frequencies and damping of aluminum circular tube filled with powder

	Natural Frequency [Hz]		Loss Factor	
Mode	Empty	Filled	Measured	Predicted
1	184.4	179.4	0.0054	0.00027
2	501.8	486.6	0.0076	0.0026
3	964.4	883.2	0.060	0.025
		1045.1	0.12	0.094
4	1554.4	1567.2	0.0094	0.032
5	2253.8	2248.9	0.0086	0.0072
6	3042.3	3051.6	0.016	0.0094
7	3900.3	3903.8	0.0073	0.0082
8	4807.8	4819.9	0.0075	0.0039

mass to added stiffness transition still occurs.

2.5 Conclusions

Significant damping can be introduced to a structure by filling it with a lossy, lightweight, low-wave-speed granular material. Strong coupling between the vibration of the structure and motion of the granular material occurs at and above frequencies which support wave propagation through the thickness of the granular material results in significant damping.

This damping mechanism has many advantages. It introduces very little creep into the structure because the stresses in the granular material are small. Provided that the proper granular material is chosen, this method can be used at extreme temperatures. Many granular materials are inexpensive.

We have demonstrated an analytical, iterative approach to calculate the loss factor as a function of frequency of beams filled with granular materials. This approach calculates the loss factor using the spatial decay of an infinite-length beam under steady harmonic motion. As a result, the loss factor estimates are independent of the beam's boundary conditions or length. We have shown that the added complications of using Timoshenko beam theory instead of Euler-Bernoulli beam theory are unnecessary even at high frequencies because the powder behavior does not change significantly from one to the other and the powder behavior the dominant factor in determining the loss factor.

There exists numerous suitable granular materials besides glass microbubbles. Some materials that do not provide good damping in solid form may perform well if they are ground into a granular state.

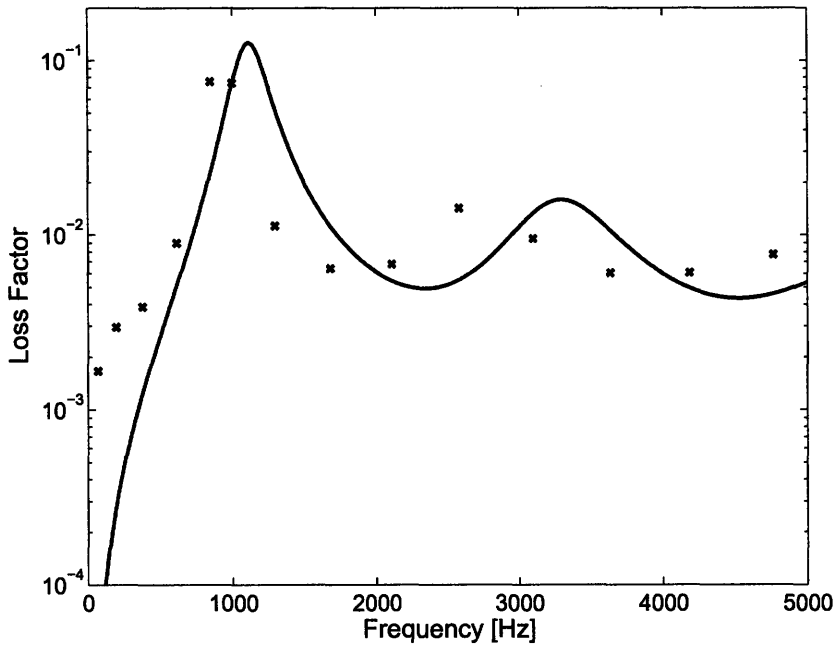

Figure 2-15: Loss factor for rectangular aluminum tube, theory (solid) and measurement (×)

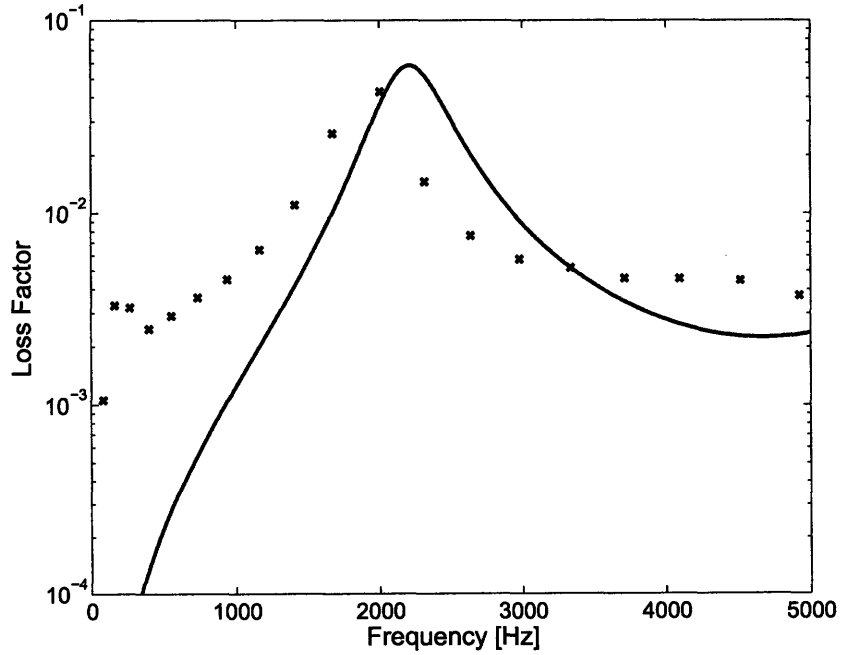

Figure 2-16: Loss factor for square steel tube, theory (solid) and measurement (×)

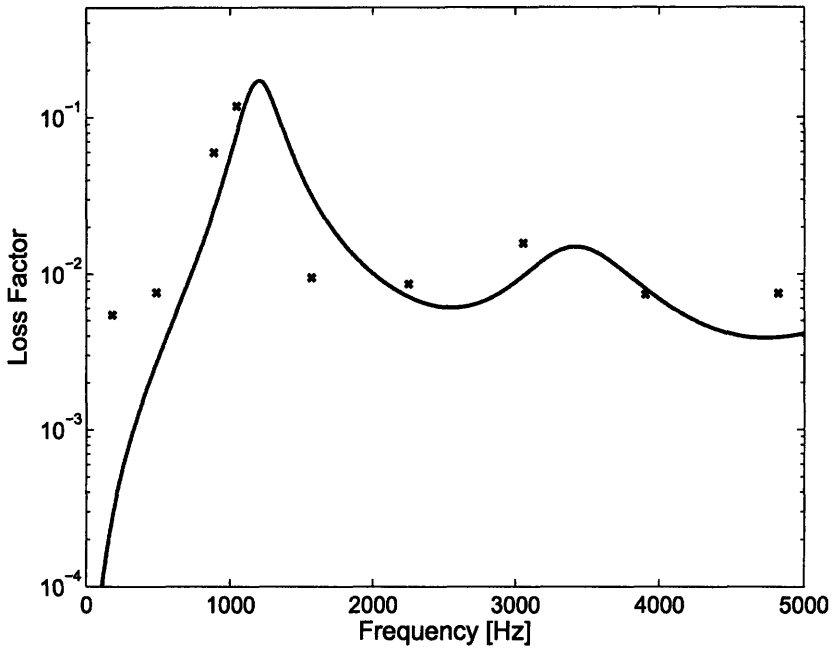

Figure 2-17: Loss factor for circular aluminum tube, theory (solid) and measurement (×)

Chapter 3

Vibration damping of beams coupled to lightweight, low-wave-speed media

3.1 Introduction

We consider the vibration of uniform beams coupled to lightweight, lossy foams. To model the damping phenomenon and obtain estimates for the damping, we consider steady harmonic wave propagation in the axial direction of an infinitely long beam and treat the foam as an elastic continuum with a complex modulus of elasticity. We use both Euler-Bernoulli and Timoshenko beam models for comparison. Based on the spatial decay characterized by a complex wavenumber, we obtain an estimate of the loss factor associated with motion as a function of frequency.

3.2 Euler-Bernoulli beam with a layer of foam

The governing differential equation for the Euler-Bernoulli beam under steady harmonic motion is

$$EI\frac{d^4\hat{w}}{d\hat{x}^4} - \rho A\omega^2\hat{w} - b\sigma_{\hat{y}}(\hat{x},\hat{y}=0,\omega) - \frac{bh}{2}\frac{\partial\tau_{\hat{x}\hat{y}}}{\partial\hat{x}}(\hat{x},\hat{y}=0,\omega) = 0 \tag{3.1}$$

where $\tau_{\hat{x}\hat{y}}(\hat{x},\hat{y}=0,\omega)$ and $\sigma_{\hat{y}}(\hat{x},\hat{y}=0,\omega)$ are the shear and normal stress in the foam at the beam-foam interface. Assuming a wave solution for the beam $\hat{w} = hWe^{jK_x x}$, the governing equation in dimensionless form becomes

$$K_x^4 W - \Omega^2 W - S_y(x,y=0,\Omega) - T_{xy}(x,y=0,\Omega) = 0 \tag{3.2}$$

where lengths, displacements, and the wavenumber K_x are nondimensionalized with the height of the beam h. The dimensionless frequency is given by

$$\Omega^2 = \frac{\rho A h^4}{EI}\omega^2 \tag{3.3}$$

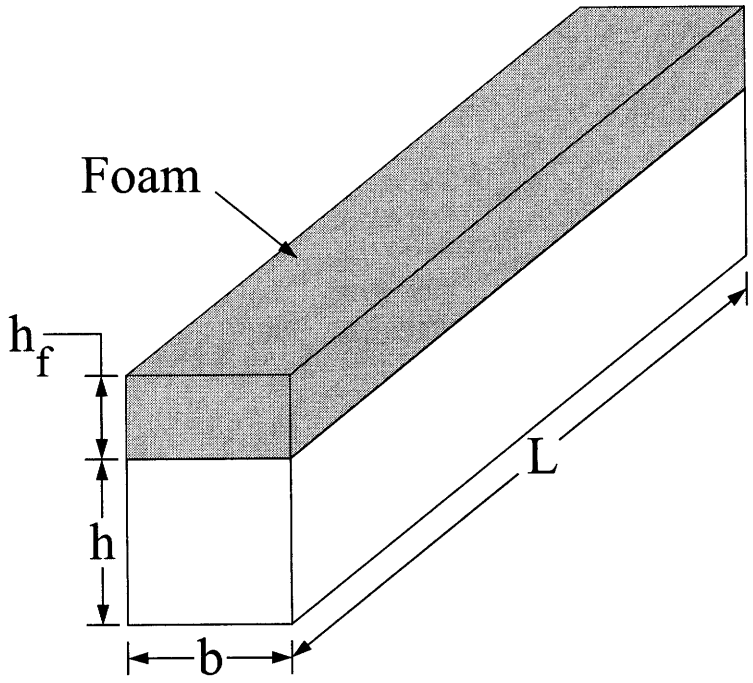

Figure 3-1: Sketch of solid beam with low-wave-speed damping treatment

The normal stress loading term S_y is

$$S_y = \frac{bh^3}{EI}\sigma_y(x, y = 0, \Omega) \tag{3.4}$$

The shear loading term T_{xy} is given by

$$T_{xy} = \frac{bh^3}{2EI}\frac{\partial \tau_{xy}}{\partial x}(x, y = 0, \Omega) \tag{3.5}$$

The governing equations for the foam in dimensionless form under steady harmnic motion assuming the same x dependence as the beam and exponential dependence in the y direction ($\hat{u} = hUe^{jK_x x + sy}$, $\hat{v} = hVe^{jK_x x + sy}$) are

$$\begin{bmatrix} \Omega_f^2 - K_x^2 + s^2\frac{G_f}{\lambda_f+2G_f} & jsK_x\frac{\lambda_f+G_f}{\lambda_f+2G_f} \\ jsK_k\frac{\lambda_f+G_f}{\lambda_f+2G_f} & \Omega_f^2 - \frac{G_f}{\lambda_f+2G_f}K_x^2 + s^2 \end{bmatrix} \begin{pmatrix} U \\ V \end{pmatrix} = \begin{pmatrix} 0 \\ 0 \end{pmatrix} \tag{3.6}$$

where G_f is the shear modulus of the foam, λ_f the Lamé parameter of the foam given by

$$\lambda_f = \frac{\nu_f E_f}{(1+\nu_f)(1-2\nu_f)} \tag{3.7}$$

where ν_f is the Poisson ratio of the foam, E_f is the Young's modulus of the foam,

and the dimensionless frequency is

$$\Omega_f^2 = \frac{\rho_f h^2}{\lambda_f + 2G_f}\omega^2 = \Omega^2 \frac{\rho_f}{\lambda_f + 2G_f}\frac{E}{\rho}\frac{I}{Ah^2} \tag{3.8}$$

The shear stress in the foam is

$$\tau_{xy} = G_f\left(\frac{\partial u}{\partial y} + \frac{\partial v}{\partial x}\right) \tag{3.9}$$

The normal stress in the foam is

$$\sigma_y = \lambda_f \frac{\partial u}{\partial x} + (\lambda_f + 2G_f)\frac{\partial v}{\partial y} \tag{3.10}$$

The first step is to obtain the dispersion relation for the beam without the foam. This dispersion relation is given by

$$K_x^4 = \Omega^2 \tag{3.11}$$

Then for each frequency of interest Ω, we solve for the displacements in the foam due to the deformation of the beam. The homogeneous equation for the foam can be solved by solving at each value of Ω the polynomial eigenvalue problem

$$\left(A_2 s^2 + A_1 s + A_0\right)\begin{pmatrix} U \\ V \end{pmatrix} = \begin{pmatrix} 0 \\ 0 \end{pmatrix} \tag{3.12}$$

where

$$A_2 = \begin{bmatrix} \frac{G_f}{\lambda_f + 2G_f} & 0 \\ 0 & 1 \end{bmatrix} \tag{3.13}$$

$$A_1 = jK_x \frac{\lambda_f + G_f}{\lambda_f + 2G_f}\begin{bmatrix} 0 & 1 \\ 1 & 0 \end{bmatrix} \tag{3.14}$$

$$A_0 = \begin{bmatrix} \Omega_f^2 - K_x^2 & 0 \\ 0 & \Omega_f^2 - \frac{G_f}{\lambda_f + 2G_f}K_x^2 \end{bmatrix} \tag{3.15}$$

The foam displacements are given by

$$\begin{pmatrix} u(x,y) \\ v(x,y) \end{pmatrix} = \sum_{i=1}^{4} c_i \begin{pmatrix} U_i \\ V_i \end{pmatrix} e^{jK_x x + s_i y} \tag{3.16}$$

where c_i are constants to be determined through imposition of the boundary conditions, s_i are the eigenvalues, and $(U_i\, V_i)^T$ are the eigenvectors. The boundary conditions on the foam are that the shear and normal stress must vanish at the free surface $y = h_f/h$ and that there is no slip at the beam-foam interface $y = 0$. The

boundary conditions are obtained by solving

$$B\begin{pmatrix} c_1 \\ c_2 \\ c_3 \\ c_4 \end{pmatrix} = \begin{pmatrix} -\frac{jK_x}{2}W \\ W \\ 0 \\ 0 \end{pmatrix} \tag{3.17}$$

where B is a square matrix whose i-th column is given by

$$\begin{bmatrix} U_i \\ V_i \\ \lambda_f jK_x U_i e^{s_i \frac{h_f}{h}} + (\lambda_f + 2G_f) s_i V_i e^{s_i \frac{h_f}{h}} \\ G_f \left(s_i U_i e^{s_i \frac{h_f}{h}} + jK_x V_i e^{s_i \frac{h_f}{h}} \right) \end{bmatrix} \tag{3.18}$$

Instead of solving for a particular value of W, we normalize the constants c_i by writing $c_{i_W} W = c_i$ to obtain the equation

$$B\begin{pmatrix} c_{1,W} \\ c_{2,W} \\ c_{3,W} \\ c_{4,W} \end{pmatrix} = \begin{pmatrix} -\frac{jK_x}{2} \\ 1 \\ 0 \\ 0 \end{pmatrix} \tag{3.19}$$

Then, we return to the relation for the coupled beam foam system. Substituting the results for the foam, we obtain the dispersion relation for the full system

$$K_x^4 = \Omega^2 + \frac{bh^3}{EI}\left(\sum_{i=1}^{4} \lambda_f jK_x c_{i,W} U_i + (\lambda_f + 2G_f) c_{i,W} s_i V_i \right) + \frac{bh^3}{2EI} G_f \left(\sum_{i=1}^{4} s_i c_{i,W} U_i + jK_x c_{i,W} V_i \right) \tag{3.20}$$

To solve this equation for the wavenumber K_x, we solve iteratively at each frequency of interest. First, we consider the beam decoupled from foam to obtain the original dispersion relation. Then, we use that value of the wavenumber on the right hand side and to solve for the deformation of the foam. Then we solve again for K_x and repeat the iterations until the error between successive estimates of the wavenumber is small enough.

To obtain the loss factor, we assume that there exists an equivalent empty beam with a modulus of $E = E_0(1 + j\eta)$. We solve for the modulus using the dispersion relation and then substitute the relation for the complex wavenumber (as a function of frequency) to obtain the complex modulus as a function of frequency. Then, the loss factor is given by

$$\eta = \frac{\operatorname{Im} E}{\operatorname{Re} E} \tag{3.21}$$

Making use of the dispersion relation for the empty beam (3.11) and recognizing that

the modulus of the beam only appears in Ω, the loss factor is given by

$$\eta = \frac{\text{Im}\,\frac{1}{k_x^4}}{\text{Re}\,\frac{1}{k_x^4}} = \frac{\text{Im}\,\frac{1}{\Omega^2}}{\text{Re}\,\frac{1}{\Omega^2}} \tag{3.22}$$

3.2.1 Results

Figure 3-2 shows the real part of the dispersion curve for a beam with a layer of foam with $\eta_f = 0.3$ and 5% added mass. The dispersion curve for the undamped beam is indistinguishable from the real part of the dispersion curve for the damped beam becuase the LWSM is a small perturbation to the system but does not significantly alter it's properties. Figure 3-3 shows the imaginary part of the dispersion relation. The local minima correspond to resonances in the LWSM and local maxima in the loss factor of the beam-foam system. The local maxima correspond to zeros of the foam and local minima of the beam-foam system. Figure 3-4 shows the loss factor as a function of nondimensional frequency.

Figure 3-5 shows the results of an experiment by Varanasi and Nayfeh [66]. Varanasi performed two methods of analysis, a complicated modal expansion and complex wavenumber approach similar to that given above. Both methods agree well with the experimental results.

3.3 Euler-Bernoulli beam filled with foam

The procedure to obtain the loss factor for an Euler-Bernoulli beam filled with foam is identical to that of the beam with a layer of foam except some of the equations differ because of the different geometry.

The governing equation becomes

$$EI\frac{d^4\hat{w}}{d\hat{x}^4} - \rho A\omega^2\hat{w} - b\sigma_{\hat{y}}(\hat{x}, \hat{y} = -h/2, \omega) + b\sigma_{\hat{y}}(\hat{x}, \hat{y} = h/2, \omega) + \frac{bh}{2}\left(\frac{\partial \tau_{\hat{x}\hat{y}}}{\partial \hat{x}}(\hat{x}, -h/2, \omega) + \frac{\partial \tau_{\hat{x}\hat{y}}}{\partial \hat{x}}(\hat{x}, h/2, \omega)\right) = 0 \tag{3.23}$$

where h is the height of the foam. Assuming a travelling wave solution for $\hat{w}$, the dimensionless equation (3.2) becomes

$$K_x^4 W - \Omega^2 W - \frac{bh^3}{EI}\left(\sigma_y(x, -1/2, \Omega) - \sigma_y(x, 1/2, \Omega)\right) + \frac{bh^3}{2EI}\left(\frac{\partial \tau_{xy}}{\partial x}(x, -1/2, \Omega) + \frac{\partial \tau_{xy}}{\partial x}(x, 1/2, \Omega)\right) = 0 \tag{3.24}$$

The governing equations for the foam (3.6) remain unchanged. The boundary conditions for the foam are no slip at the two beam-foam interfaces $y = \pm 1/2$. Therefore

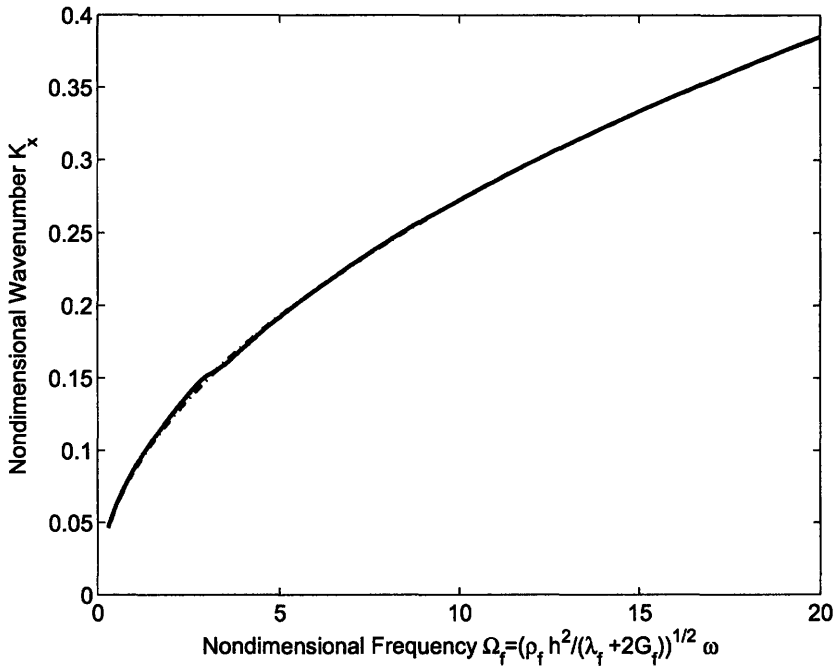

Figure 3-2: Real part of the dispersion curve for an Euler-Bernoulli beam with a layer of foam with loss factor $\eta_f = 0.3$ and 5% added mass. The dispersion curve of the undamped beam is indistinguishable from the real part of the dispersion curve of the damped beam.

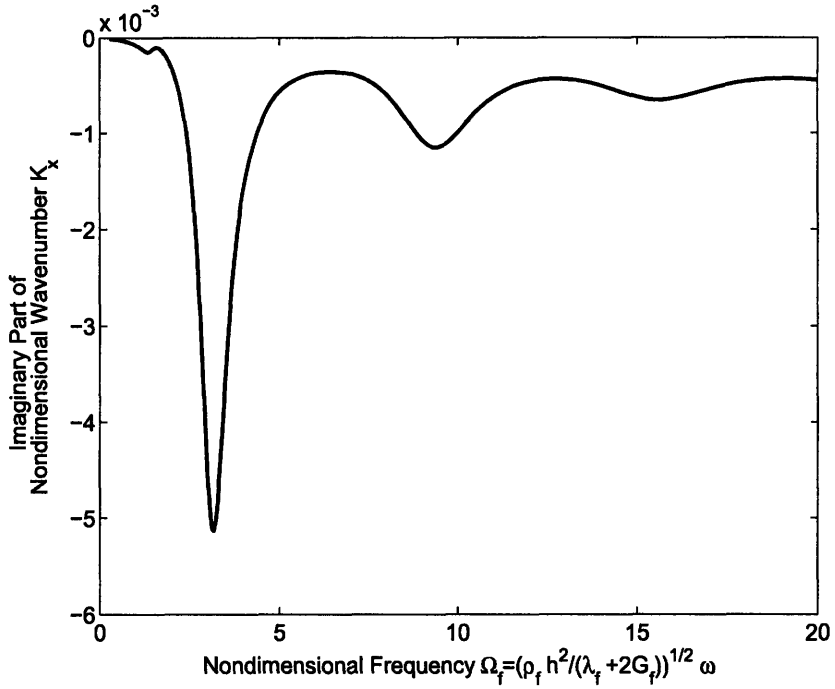

Figure 3-3: Imaginary part of the dispersion relation for an Euler-Bernoulli beam with a layer of foam with loss factor $\eta_f = 0.3$ and 5% added mass

the column in the matrix B given in (3.18) becomes

$$\begin{bmatrix} U_i e^{s_i/2} \\ V_i e^{s_i/2} \\ U_i e^{-s_i/2} \\ V_i e^{-s_i/2} \end{bmatrix} \tag{3.25}$$

and the corresponding right hand side in (3.19) becomes

$$\begin{pmatrix} -\frac{jK_x}{2} \\ 1 \\ \frac{jK_x}{2} \\ 1 \end{pmatrix} \tag{3.26}$$

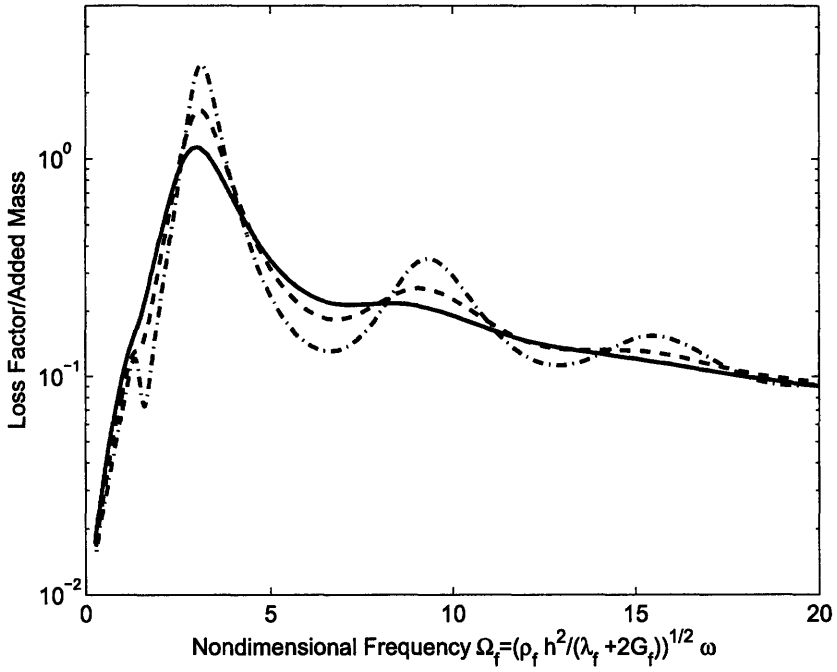

Figure 3-4: Typical dimensionless plot of loss factor as a function of frequency for an Euler-Bernoulli beam with a layer of foam with loss factors of η_f =0.3 (dash-dot), 0.5 (dashed), 0.8 (solid)

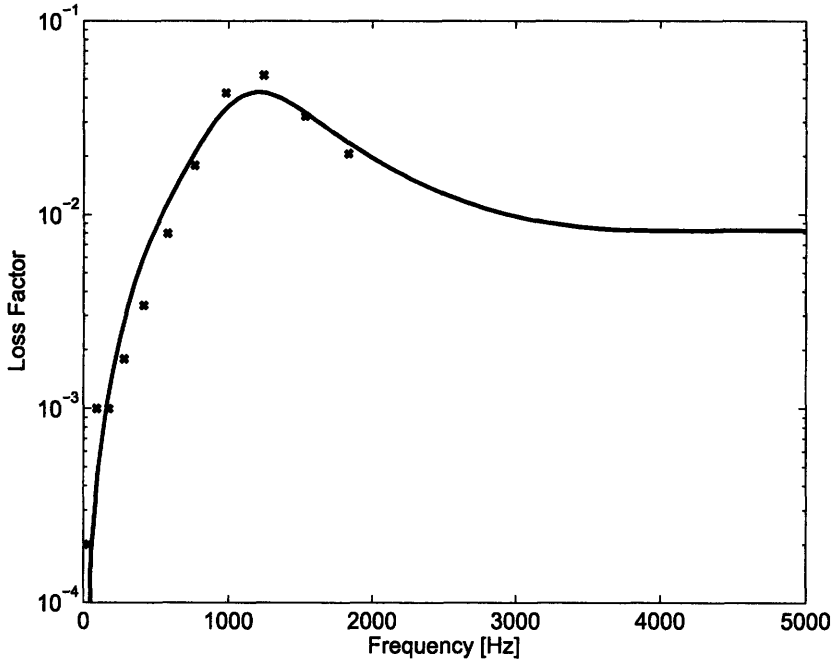

Figure 3-5: Loss factor as a function of frequency for aluminum beam (38.1 mmwide × 12.7 mm high × 1.448 m long) with a layer of EAR C-3201 foam (12.7 mm thick, 3.9% added mass): theory (solid), experiment (×). Experimental results from Varanasi and Nayfeh [66].

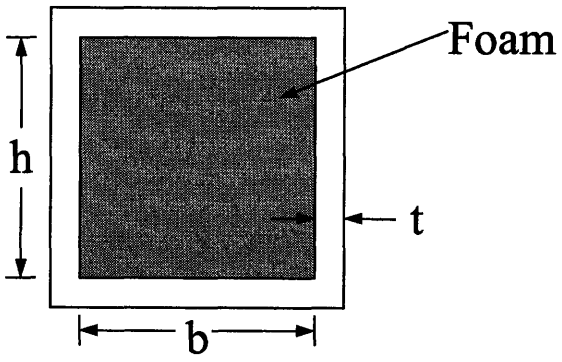

Figure 3-6: Sketch of box beam with low-wave-speed damping treatment

Finally, the dispersion relation for the coupled systerm given in (3.20) becomes

$$K_x^4 = \Omega^2 + \frac{bh^3}{EI}\left(\left(\sum_{i=1}^{4}\lambda_f j K_x c_{i,W} U_i e^{-s_i/2} + (\lambda_f + 2G_f) s_i c_{i,W} V_i e^{-s_i/2}\right)\right.$$
$$\left. - \left(\sum_{i=1}^{4}\lambda_f j K_x c_{i,W} U_i e^{s_i/2} + (\lambda_f + 2G_f) s_i c_{i,W} V_i e^{s_i/2}\right)\right)$$
$$- \frac{bh^3}{2EI} G_f \left(\left(\sum_{i=1}^{4} s_i c_{i,W} U_i e^{-s_i/2} + j K_x c_{i,W} V_i e^{-s_i/2}\right)\right.$$
$$\left. + \left(\sum_{i=1}^{4} s_i c_{i,W} U_i e^{s_i/2} + j K_x c_{i,W} V_i e^{s_i/2}\right)\right) \quad (3.27)$$

Again, this equation must be solved iteratively as described above. The loss factor is then calculated using (3.22).

3.3.1 Results

Figures 3-7 and 3-8 show the dispersion relation for a beam filled with foam. As with the beam with a layer of foam, the dispersion curve for the undamped beam is practically indistinguishable from the real part of the dispersion curve for the damped beam. Again, the minima and maxima in the imaginary part of the dispersion curve correspond to the maxima and minima in the system loss factor, which is shown in Figure 3-9.

3.4 Timoshenko beam with a layer of foam

The nondimensional governing equations for a uniform Timoshenko beam under steady, harmonic motion subjected to a force and moment per unit length are

$$-\beta^2 \frac{\partial^2 \phi}{\partial x^2} + \phi - \frac{\partial w}{\partial x} - \Omega^2 \beta^2 \gamma^2 \phi = \hat{M}(x, \Omega) \quad (3.28)$$
$$-\frac{\partial^2 w}{\partial x^2} + \frac{\partial \phi}{\partial x} - \beta^2 \Omega^2 w = \beta^2 \hat{P}(x, \Omega) \quad (3.29)$$

where ϕ is the rotation of the cross section, lengths and displacements are nondimensionalized by the height of the beam h, and

$$\beta^2 = \frac{EI}{kAGh^2} \quad (3.30)$$
$$\gamma^2 = \frac{I}{Ah^2} \quad (3.31)$$
$$\Omega^2 = \frac{\rho A h^4}{EI}\omega^2 \quad (3.32)$$

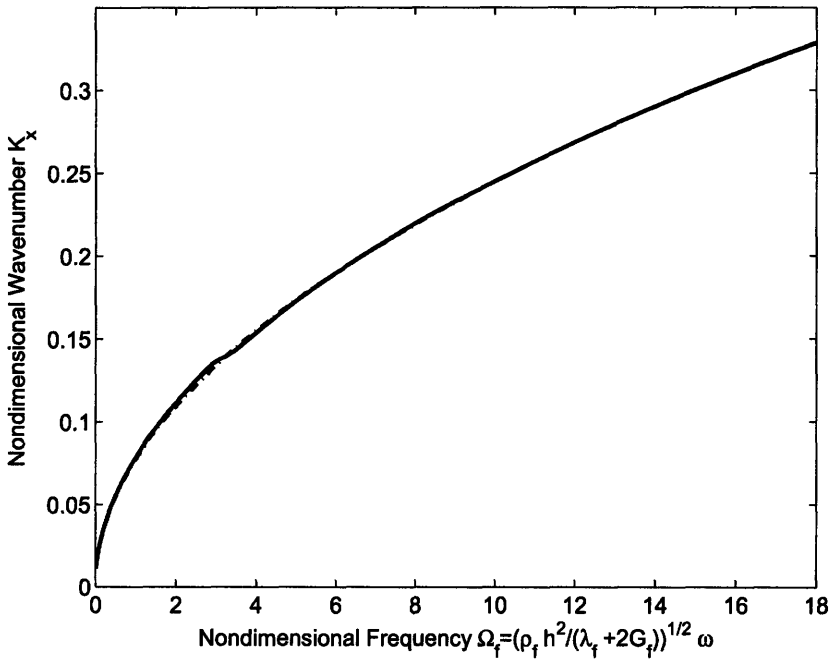

Figure 3-7: Real part of the dispersion curve for an Euler-Bernoulli beam filled with layer of foam with loss factor $\eta_f = 0.3$ and 5% added mass. The dispersion curve of the undamped beam is indistinguishable from the real part of the dispersion curve of the damped beam.

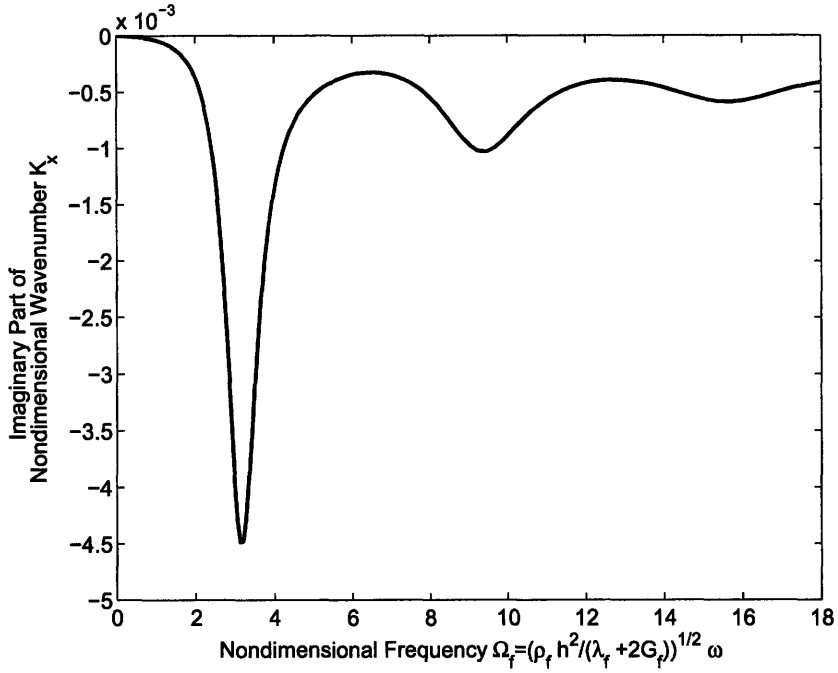

Figure 3-8: Imaginary part of dispersion relation for Euler-Bernoulli beam filled with foam whose loss factor is $\eta_f = 0.3$ and 5% added mass

where k is the shear parameter determined by the geometry of the cross section and G is the shear modulus of the beam. The forcing due to the stress at the beam-foam interface is given by

$$\frac{M(x,\Omega)}{kAG} = -\frac{bh}{2kAG}\tau_{xy}(x, y = 0, \Omega) \tag{3.33}$$

$$\frac{hP(x,\Omega)}{kAG} = \frac{bh}{kAG}\sigma_y(x, y = 0, \Omega) \tag{3.34}$$

The equations for the foam remain unchanged from above. The deformation of the foam is obtained using the eigenvalue problem in (3.12). The boundary conditions on the foam are imposed using

$$B\begin{pmatrix} c_1 \\ c_2 \\ c_3 \\ c_4 \end{pmatrix} = \begin{pmatrix} -\frac{1}{2}N \\ W \\ 0 \\ 0 \end{pmatrix} \tag{3.35}$$

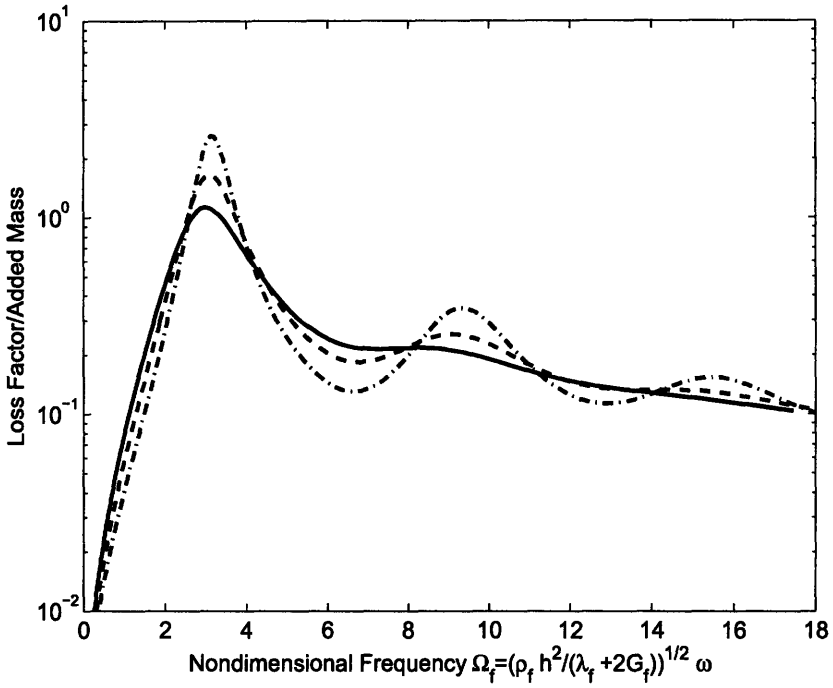

Figure 3-9: Typical dimensionless plots of loss factor as a function of frequency for an Euler-Bernoulli beam filled with foam which has loss factors of $\eta_f = 0.3, 0.5, 0.8$ and 5% added mass

where each column of B is given by (3.18). We use the principle of superposition to write $c_i = c_{i,N}N + c_{i,W}W$ to obtain to sets of equations for the $c_{i,N}$ and $c_{i,W}$

$$B\begin{pmatrix} c_{1,N} \\ c_{2,N} \\ c_{3,N} \\ c_{4,N} \end{pmatrix} = \begin{pmatrix} -\frac{1}{2} \\ 0 \\ 0 \\ 0 \end{pmatrix} \tag{3.36}$$

$$B\begin{pmatrix} c_{1,W} \\ c_{2,W} \\ c_{3,W} \\ c_{4,W} \end{pmatrix} = \begin{pmatrix} 0 \\ 1 \\ 0 \\ 0 \end{pmatrix} \tag{3.37}$$

Applying the results of the foam deformation the forcing terms (3.33) and (3.34) in the Timoshenko beam equations (3.28) and (3.29), we obtain a polynomial eigenvalue problem

$$\left(A_2K_x^2 + A_1K_x + A_0 + A_f\right)\begin{pmatrix} N \\ W \end{pmatrix} = \begin{pmatrix} 0 \\ 0 \end{pmatrix} \tag{3.38}$$

where

$$A_2 = \begin{bmatrix} \beta^2 & 0 \\ 0 & 1 \end{bmatrix} \tag{3.39}$$

$$A_1 = \begin{bmatrix} 0 & -j \\ j & 0 \end{bmatrix} \tag{3.40}$$

$$A_0 = \begin{bmatrix} 1-\Omega^2\beta^2r^2 & 0 \\ 0 & -\Omega^2\beta^2 \end{bmatrix} \tag{3.41}$$

$$A_f = \begin{bmatrix} \frac{bhG_f}{2kAG}\left(\sum_{i=1}^{4} c_{i,N}\left(s_iU_i + jK_xV_i\right)\right) & \\ \frac{-bh}{kAG}\left(\sum_{i=1}^{4} c_{i,N}\left(\lambda_f jK_xU_i + (\lambda_f + 2G_f)s_iV_i\right)\right) & \\ & \frac{bhG_f}{2kAG}\left(\sum_{i=1}^{4} c_{i,W}\left(s_iU_i + jK_xV_i\right)\right) \\ & \frac{-bh}{kAG}\left(\sum_{i=1}^{4} c_{i,W}\left(\lambda_f jK_xU_i + (\lambda_f + 2G_f)s_iV_i\right)\right) \end{bmatrix} \tag{3.42}$$

To solve this equation for the wavenumber K_x, we solve iteratively for each frequency Ω of interest. First, we solve for the dispersion relation of the undamped beam by setting $A_f = 0$. This solution results in four values of the wavenumber. Only two of them are correct, one corresponding to the right travelling wave and one corresponding to the left travelling wave [58]. Then, the correct value of the wavenumber is used to solve for the foam displacements and obtain A_f. Then, a new estimate of the wavenumber is obtained. Again, we must ensure that we are choosing the proper root consistently. We continue this iterative procedure until the error in the wavenumber estimation is sufficiently small.

After obtaining the complex wavenumber, we calculate the loss factor using an

equivalent empty beam. The resulting equation for the loss factor is

$$\eta = \frac{\text{Im}\,\frac{1}{\Omega^2}}{\text{Re}\,\frac{1}{\Omega^2}} \tag{3.43}$$

To obtain Ω^2 from the complex wavenumber, we use the dispersion relation for the empty beam given by the determinant of (3.38) with $A_f = 0$. Again, we must maintain consistency in choosing the appropriate solution that agrees with the Timoshenko beam model.

3.4.1 Results

The dispersion curve and loss factor plots for a solid beam with a layer of foam using the Timoshenko beam model are indistinguishable from those obtained using the Euler-Bernoulli beam model (see Figures 3-2, 3-7, and 3-4). We perform the comparison below for thin-walled beams, in which the differences between the two models are more pronounced.

3.5 Timoshenko beam filled with foam

The procedure to obtain the loss factor for a Timoshenko beam filled with foam is the same as the procedure above but with changes to some equations because of the different boundary conditions at the interface of the beam and foam.

The forcing of the

$$\frac{M(x,\Omega)}{kAG} = \frac{bh}{2kAG}\left(\tau_{xy}(x, y = -1/2, \Omega) + \tau_{xy}(x, y = 1/2, \Omega)\right) \tag{3.44}$$

$$\frac{hP(x,\Omega)}{kAG} = \frac{bh}{kAG}\left(\sigma_y(x, y = -1/2, \Omega) - \sigma_y(x, y = 1/2, \Omega)\right) \tag{3.45}$$

The homogeneous equations for the foam remain unchanged. The change in the boundary conditions causes (3.36) to become

$$B\begin{pmatrix} c_1 \\ c_2 \\ c_3 \\ c_4 \end{pmatrix} = \begin{pmatrix} -\frac{1}{2}N \\ W \\ \frac{1}{2}N \\ W \end{pmatrix} \tag{3.46}$$

which we separate into

$$B\begin{pmatrix} c_{1,N} \\ c_{2,N} \\ c_{3,N} \\ c_{4,N} \end{pmatrix} = \begin{pmatrix} -\frac{1}{2} \\ 0 \\ \frac{1}{2} \\ 0 \end{pmatrix} \tag{3.47}$$

and

$$B \begin{pmatrix} c_{1,W} \\ c_{2,W} \\ c_{3,W} \\ c_{4,W} \end{pmatrix} = \begin{pmatrix} 0 \\ 1 \\ 0 \\ 1 \end{pmatrix} \tag{3.48}$$

as before where the i-th column of B is given by

$$\begin{bmatrix} U_i e^{s_i/2} \\ V_i e^{s_i/2} \\ U_i e^{-s_i/2} \\ V_i e^{-s_i/2} \end{bmatrix} \tag{3.49}$$

After obtaining the foam displacements and resulting stresses, the governing equation for the beam-foam system is still a polynomial eigenvalue problem given by (3.38), but A_f becomes

$$A_f = \begin{bmatrix} -\frac{bhG_f}{2kAG}\left(\sum_{i=1}^{4} c_{i,N}\left(e^{-s_i/2}+e^{s_i/2}\right)\left(s_i U_i + jK_x V_i\right)\right) \\ -\frac{bh}{kAG}\left(\sum_{i=1}^{4} c_{i,N}\left(\lambda_f jK_x U_i + \left(\lambda_f + 2G_f\right) s_i V_i\right)\left(e^{-s_i/2}-e^{s_i/2}\right)\right) \\ -\frac{bhG_f}{2kAG}\left(\sum_{i=1}^{4} c_{i,W}\left(e^{-s_i/2}+e^{s_i/2}\right)\left(s_i U_i + jK_x V_i\right)\right) \\ -\frac{bh}{kAG}\left(\sum_{i=1}^{4} c_{i,W}\left(\lambda_f jK_x U_i + \left(\lambda_f + 2G_f\right) s_i V_i\right)\left(e^{-s_i/2}-e^{s_i/2}\right)\right) \end{bmatrix} \tag{3.50}$$

3.5.1 Results

Figures 3-10 and 3-11 compare the dispersion relation for a beam filled with foam using the Timoshenko and Euler-Bernoulli beam models. The differences are negligible except at high frequencies. The loss factor curves are compared in Figure 3-12 and reveal no noticeable difference. The same result is observed even as the shear parameter k is made smaller to accentuate the difference between the two models.

3.6 Conclusions

Based on the comparisons between the loss factor curves obtained using the Euler-Bernoulli and Timoshenko beam models, we conclude that the model of the foam is the element in obtaining an accurate estimate of the loss factor and that the Euler-Bernoulli model is sufficient to predict the loss factor of beam bending vibrations in systems with LWSM.

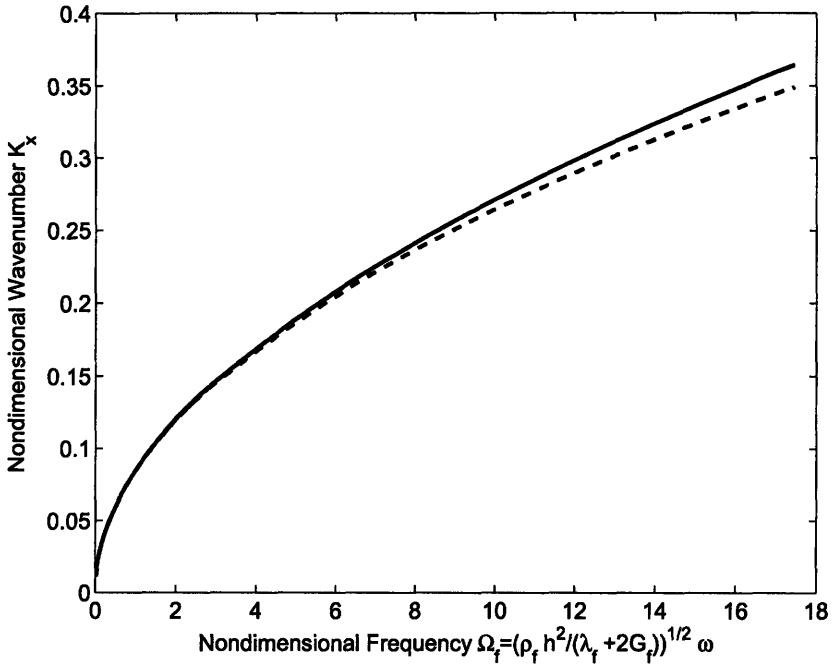

Figure 3-10: Comparison of the real part of the dispersion curve for a beam filled with foam using the Euler-Bernoulli model (dashed) and Timoshenko model (solid) with a foam loss factor $\eta_f = 0.8$

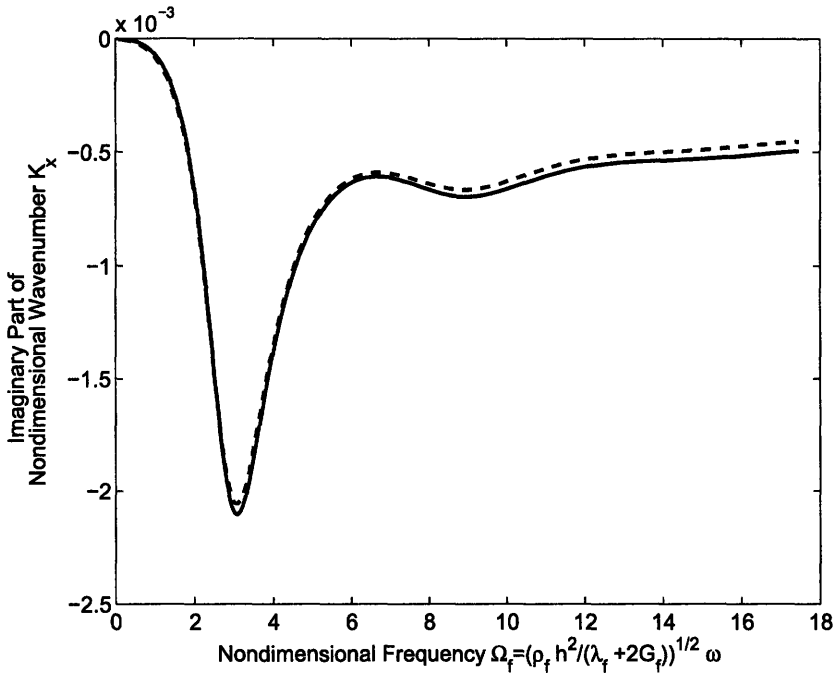

Figure 3-11: Comparison of the imaginary part of the dispersion curve for a beam filled with foam using the Euler-Bernoulli model (dashed) and Timoshenko model (solid) with a foam loss factor $\eta_f = 0.8$

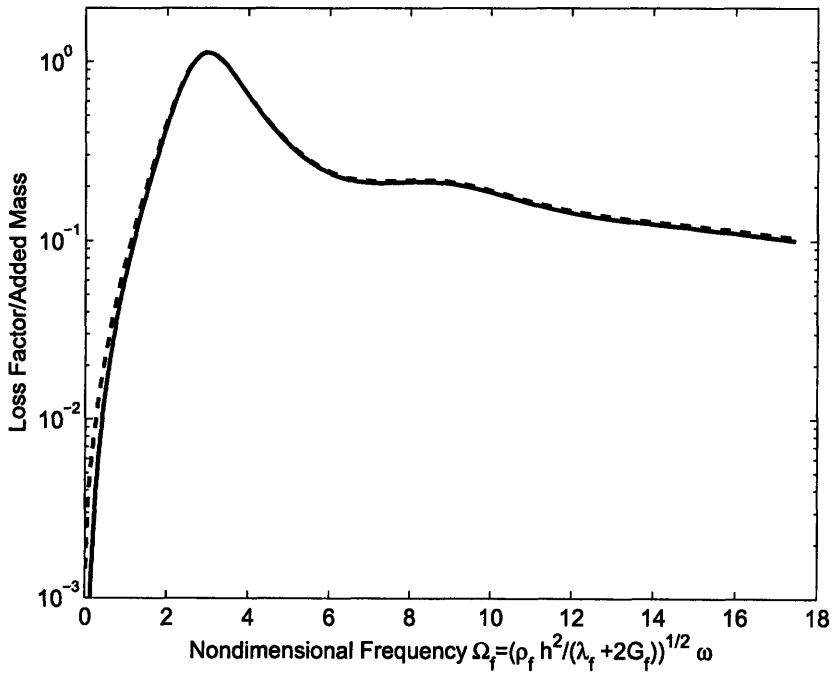

Figure 3-12: Comparison of loss factor for a beam filled with foam obtained using the Euler-Bernoulli beam model (dashed) and Timoshenko beam model (solid)

Chapter 4

Comparison of constrained-layer damping and damping via coupling to low-wave-speed media

4.1 Introduction

Contrained-layer damping (CLD) is a common method of adding damping to structures. A constrained layer damper consists of a thin layer of a viscoelastic material glued to the primary structure and then "constrained" by a layer of metal glued to the top, as sketched in Figure 4-1. Formulas exist for analysis and design of constrained layer dampers e.g., Nayfeh [42], Marsh and Hale [38]. To demonstrate the effectiveness of low-wave-speed damping, we present a comparison of CLD and LWSM damping with equal added mass for a solid beam and a box beam. We consider a simply-supported beam, which is equivalent to an infinite beam, and design CLD and LWSM damping treatments for the first two bending modes subject to a constraint of 5% added mass. For the case of the box beam, we impose the additional constraint that the damping treatment must be fully contained within the tube. Pamley *et al* [45] compare constrained-layer damping, free-layer damping, and low-wave-speed damping using viscoelastic spheres for a thin-walled steel box beam and conclude through experiments that the low-wave-speed treatment is the most mass efficient.

4.2 Comparison for solid beam

We compare the attainable damping of a five-layer symmetric constrained layer damper to a single layer of low-wave-speed foam for a simply-supported square steel beam 50 mm wide, 50 mm tall, and 1 m long (see Figures 4-1, 4-2 and 4-3). Both damping treatments are designed with 5% added mass.

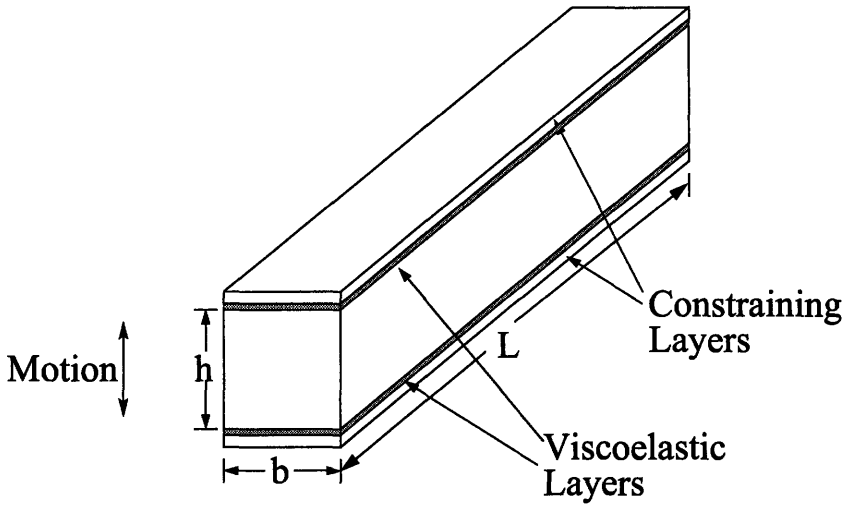

Figure 4-1: Sketch of solid beam with constrained-layer damper

4.2.1 Design of constrained-layer damper

For a given added mass and assuming a symmetric five layer configuration, the constrained-layer damper is designed in the following manner. We also assume that the viscoelastic material has a loss factor $\eta_v = 1$ and that the constraining layers are steel for its high stiffness.

Assuming that the damper spans the width of the beam and that the mass of the viscoelastic material is negligible compared to the constaining layers, we calculate the height of the constraining layers using

$$h_2 = \frac{\mu \rho_1 A_1}{2 \rho_2 b_2} \tag{4.1}$$

where μ is the allowable damper-to-beam mass ratio, ρ_1 is the density of the primary beam, ρ_2 is the density of the constraining layers, A_1 is the cross sectional area of the primary beam, and b_2 is the width of the constraining layers. The stiffness parameter is given by

$$Y = \frac{2c^2 E_2 A_2}{E_1 I_1 + 2 E_2 I_2} \tag{4.2}$$

where c is the distance between the neutral axis of the primary beam and the neutral axis of the constraining layer as shown in Figure 4-2 given by

$$c = t_v + \frac{h_1 + h_2}{2} \tag{4.3}$$

which simplifies for a thin viscoelastic layer to

$$c = \frac{h_1 + h_2}{2} \tag{4.4}$$

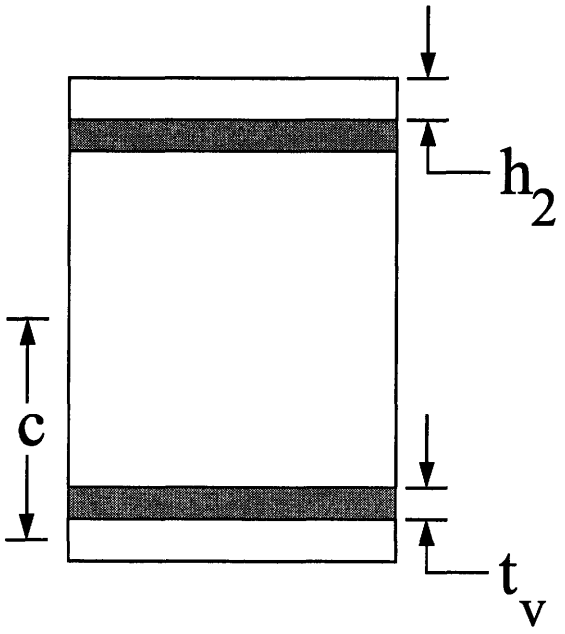

Figure 4-2: Geometry of constrained layer damper

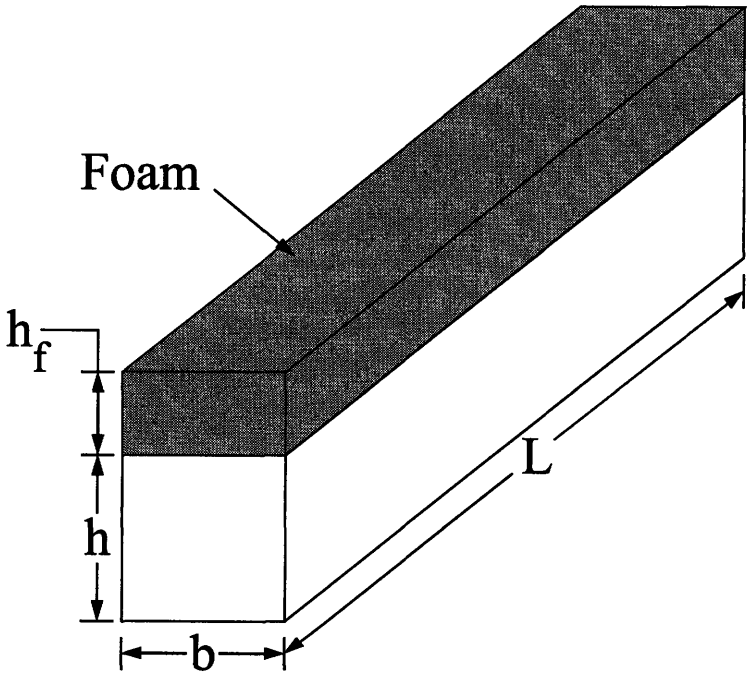

Figure 4-3: Sketch of solid beam with low-wave-speed damping treatment

The coupling or shear parameter is given by

$$g = \frac{GH}{t_v E_2 A_2 k_x^2} \tag{4.5}$$

where $2H$ is the width of the viscoelastic layer and in this case is given by $H = b_2/2$, k_x is the wavenumber, and G is the shear modulus of the viscoelastic layer. The loss factor is given by

$$\eta = \frac{g\eta_v Y}{g^2(1+Y)(1+\eta_v^2) + g(2+Y) + 1} \tag{4.6}$$

The optimal value for the shear parameter from Nayfeh [42] is given by

$$g_{opt}^2 = \frac{1}{(1+Y)(1+\eta_v^2)} \tag{4.7}$$

The corresponding maximum loss factor is

$$\eta_{max} = \frac{Y\eta_v}{Y + 2 + 2\sqrt{(1+Y)(1+\eta_v^2)}} \tag{4.8}$$

Using g_{opt}, we can solve for the optimal ratio of G/t_v for a wavenumber corresponding to the shape and frequency at which we would like to obtain maximum damping. The damping for any wavenumber can then be calculated.

4.2.2 Design of LWSM damper

A simplified method of designing the low-wave-speed damping treatment involves estimating the frequency of the first thickness resonance at which maximum damping is obtained. For a free layer of foam, this condition occurs when the thickness of the foam layer is one quarter of the wavelength. To calculate this frequency, we use the plane equations of elasticity and constrained to only allow vertical motion of the foam and obtain

$$\omega_{opt}^2 = \left(\frac{\pi}{2h_f}\right)^2 \frac{\nu_f \mathrm{Re}(E_f)}{\rho_f(1-2\nu_f)(1-\nu_f)} \tag{4.9}$$

where $\pi/2h_f$ corresponds to the quarter-wave mode shape through the thickness of the foam. To relate the frequency of maximum damping to the frequency and mode shape of the simply-supported (or infinite) beam, we use the dispersion relation of the Euler-Bernoulli beam given by

$$k_x = \left(\omega^2 \frac{\rho_1 A_1}{E_1 I_1}\right)^{\frac{1}{4}} \tag{4.10}$$

to obtain the required modulus of the foam

$$\mathrm{Re}(E_f) = k_{x,opt}^4 \left(\frac{4h_f}{2\pi}\right)^2 \frac{E_1 I_1}{rho_1 A_1} \frac{\rho_f}{\nu_f}(1-\nu_f)(1-2\nu_f) \tag{4.11}$$

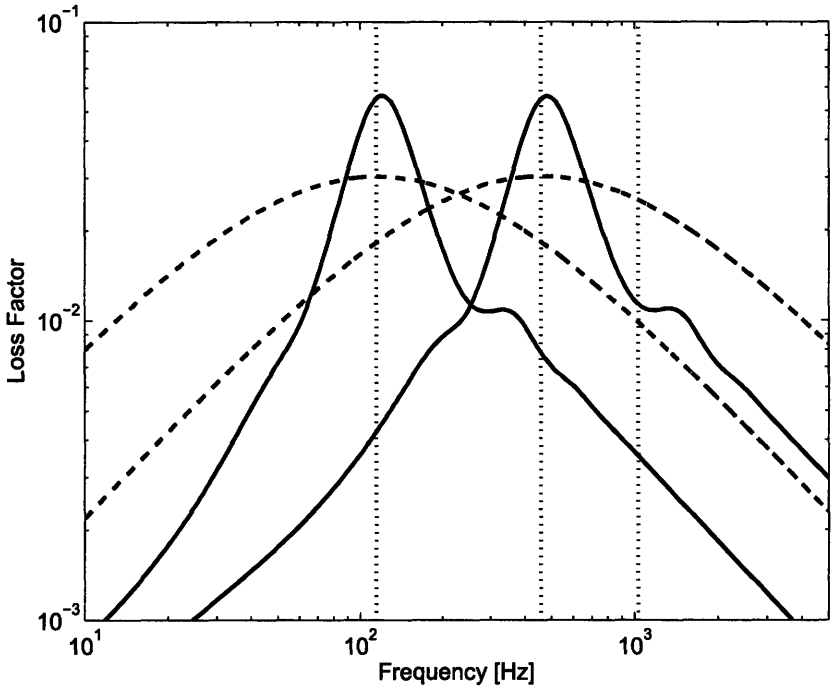

Figure 4-4: Comparison of loss factor for simply-supported steel beam with constrained-layer damper (dashed) to low-wave-speed damper (solid) for different design modes

For a simply-supported beam, the wavenumbers at resonance are

$$k_{x,ss} = \frac{n\pi}{L} \tag{4.12}$$

where L is the length of the beam and n is the mode number. For example to optimize damping for the second mode, we set $k_{x,opt} = 2\pi/L$.

To choose the foam, we constrain its geometry to have the same width as the beam and its height to be half that of the beam. Then, the modulus is calculated for the mode of interest.

4.2.3 Solid beam comparison results

Figure 4-4 compares the loss factors for the two damping treatments. The peak damping is greater for LWSM, but the CLD has a greater bandwidth.

4.3 Comparison for hollow box beam

We compare the attainable damping of a five-layer symmetric constrained layer damper to a single layer of low-wave-speed foam for a square, aluminum box beam (b =45 mm

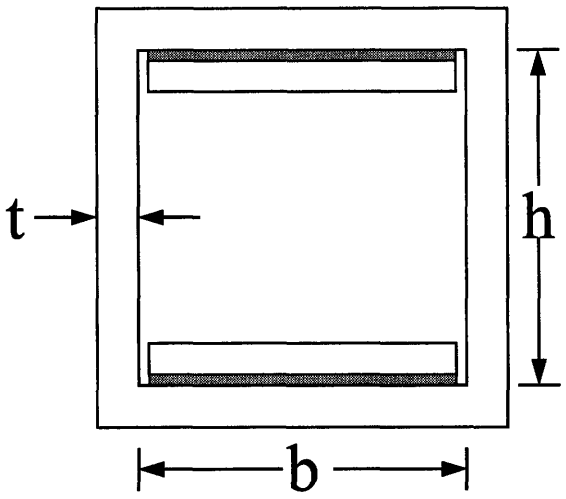

Figure 4-5: Sketch of box beam with constrained-layer damper

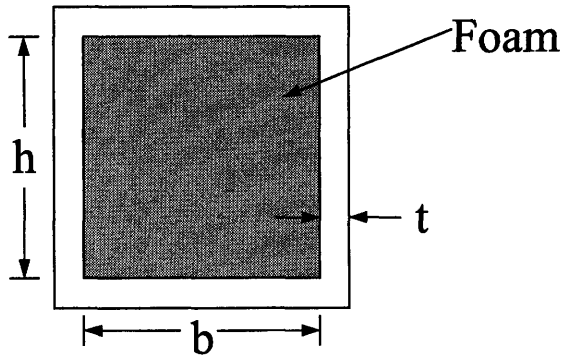

Figure 4-6: Sketch of box beam with low-wave-speed damping treatment

wide, h =45 mm tall, 5 mm wall thickness, 1 m long) as shown in Figures 4-5 and 4-6). The damping treatments have the same added mass, five percent. We require the damping treatments to be placed inside the tube so that there is no increae in height.

4.3.1 Design of constrained-layer damper

The design of the constrained-layer damper follows the same approach as given above, but the geometry constraint changes the parameter c to $c = h_1/2 - h_2/2$, if we again assume the that thickness of the viscoelastic layer is negligible.

4.3.2 Design of LWSM damper

The design of LWSM treatment follow the same approach as for the LWSM treatment on a solid beam. We assume that the foam is well described by the planar equations of elasticity and that slip can occur at the side beam-foam interfaces but that no slip

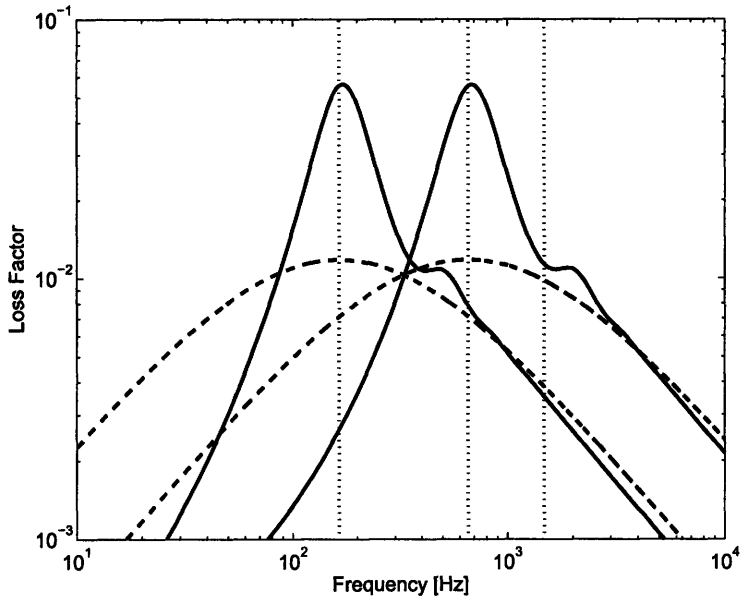

Figure 4-7: Comparison of loss factor for simply-supported aluminum box beam with constrained-layer damper (dashed) to low-wave-speed damper (solid) for different design modes

occurs at the top and bottom interfaces. The optimal frequency is given by

$$\omega_{opt}^2 = \left(\frac{\pi}{h_f}\right)^2 \frac{\nu_f \mathrm{Re}(E_f)}{\rho_f(1-2\nu_f)(1-\nu_f)} \tag{4.13}$$

because the vertical displacement of the foam is now a half wave.

We use the Euler-Bernoulli dispersion relation to determine the mode shape and to solve for the modulus of the foam.

$$\mathrm{Re}(E_f) = k_{x,opt}^4 \left(\frac{h_f}{\pi}\right)^2 \frac{E_1 I_1}{rho_1 A_1} \rho_f (1-\nu_f^2) \tag{4.14}$$

where $k_{x,opt}$ is the wavenumber of the mode shape where damping is maximum.

4.3.3 Results

Figure 4-7 shows the loss factor as a function of frequency for the CLD and LWSM damping treatments designed for the first and second modes of the beam. The LWSM clearly gives better performance. It has a larger peak damping and the same bandwidth as the CLD. As shown by Ungar and Kerwin [62], the low frequency asymptote of the LWSM damping curve has a slope of +2, and the high frequency asymptote has a slope of −1.

4.4 Conclusions

Low-wave-speed media damping outperforms constrained-layer damping in thin-walled tubes because it can attain greater peak damping and a comparable bandwidth. For solid beams, LWSM offers a higher peak damping but the bandwidth is limited. Additionally, foams examined in this thesis (EAR C-3201 and Foamex Sensus) have a stiffening frequency dependence; in other words, the modulus increases with frequency. This property increases the broadband nature of the LWSM damping. Furthermore, the LWSM treatments are easier to manufacture. CLD requires an adhesive that is very thin and very stiff. The adhesive in a LWSM damper is not subjected to large stress so almost any adhesive is sufficient. In fact for LWSM in a tube, a slightly oversized piece of foam can be held in place by a preload force without adhesive.

Chapter 5

Vibration damping of cylindrical shells using lightweight granular materials

5.1 Introduction

In this chapter, we consider the problem of damping vibration in thin-walled cylindrical tubes by filling with a granular material. We present the results of experiments on a powder-filled free-free cylindrical tube in which significant damping is attained in beam-bending and tube-wall-flexing modes. To model the damping phenomenon and obtain estimates for the damping in these modes, we consider steady harmonic wave propagation in the axial direction of an infinitely long cylindrical tube and treat the powder as a compressible fluid with a complex speed of sound. Based on the spatial decay characterized by a complex wavenumber, we obtain an estimate of the loss factor associated with motion as a function of frequency and the number of circumferential nodes.

5.2 Experiments

We conduct experiments on a welded, carbon-steel cylindrical tube of length 1.58 m, outside diameter 7.62 cm, wall thickness 1.65 mm, and mass 4.8 kg. The cylinder is filled with 3M Glass K1 Microbubbles. The average particle diameter is 65 microns [1]. The measured density of the fill is 78 kg/m^3. The total mass of the powder is 0.49 kg, or 11.8% of the mass of the cylinder. A thin latex membrane at each end encloses the particles. The cylinder is supported with strings at the quarter points to approximate free-free boundary conditions. A triaxial accelerometer (PCB 356B08) is fixed at one end of the tube, and excitation is provided by an impact hammer (PCB 086B03) in the radial direction at various points along the shell [51]. Mode shapes are fit using Star Modal analysis software [57].

A typical measured frequency response (force to acceleration) is shown in Figure 5-1. The natural frequencies, mode shapes, and damping coefficients for the empty tube

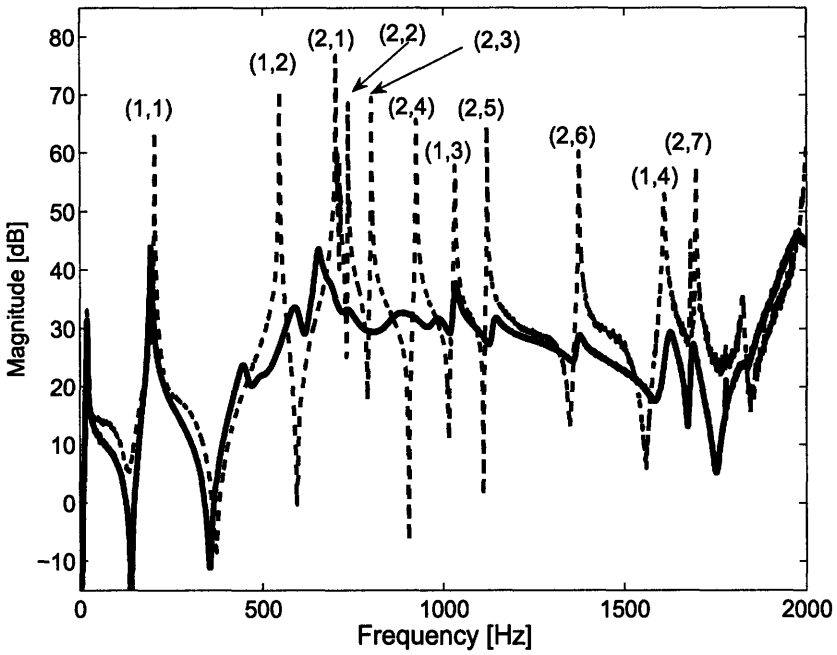

Figure 5-1: Collocated frequency response (force to acceleration) of the tube measured near the end of the tube in the radial direction (dashed line unfilled, solid line filled). Mode shape labels (n, m) refer to the number of nodal points $(2n)$ along the circumference and the number of nodal points along the length of the cylinder $(m+1)$. (See also Figure 5-2.)

are given in Table 5.1. As with many shell geometries, the modes occur in clusters. The granular material adds significant damping for modes above 400 Hz. For some modes in this range, standing waves in the powder result in an effect like that of a tuned-mass damper where the mode splits from a single lightly damped peak into two well-damped peaks. The clustering, mode splitting, and well-damped nature of the frequency response for the filled cylinder cause some difficulties in estimation of the loss factor, mode shapes, and natural frequencies from the experiments.

5.3 Modelling

The literature on the vibration of thin-walled shells contains a number of different models [32]. For the purpose of this work, we are interested in obtaining estimates of the loss factors of the lower-order modes ($n = 1$ and 2 as sketched in Figure 5-2) using the simplest model which captures the essential physics. The approach is to solve for the wavenumber as a function of frequency in a cylinder of infinite length driven at a frequency ω. The wavenumber will be complex because we model the granular medium as having a complex speed of sound. To obtain the system loss factor, we then consider a hypothetical empty tube whose wall material has a complex modulus $E_0(1 + j\eta)$. By solving for the value of $E_0(1 + j\eta)$ that renders that same complex

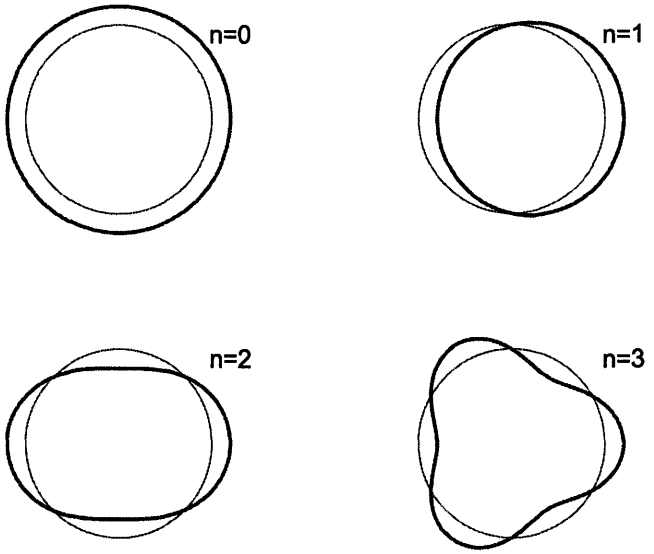

Figure 5-2: Cross sections of the mode shapes for different n

Table 5.1: Measured natural frequencies of the empty and filled tube, where n is one half the number of circumferential nodal points and $m + 1$ is the number of longitudinal nodal points.

		Empty		Filled	
Mode		Freq.	Loss Factor	Freq.	Loss Factor
n	m	[Hz]	[%]	[Hz]	[%]
1	1	204	0.16	193	1.7
1	2	546	0.08	448	6.6
1	2			593	7.8
2	1	702	0.13	664	4.0
2	2	735	0.10	682	3.5
2	3	800	0.05	738	5.0
2	4	925	0.08	898	10.
2	4			978	5.3
1	3	1030	0.16	1032	1.2
2	5	1120	0.06	1138	1.9
2	6	1380	0.12	1371	1.4
1	4	1610	0.22	1624	1.6
2	7	1680	0.06	1688	1.5

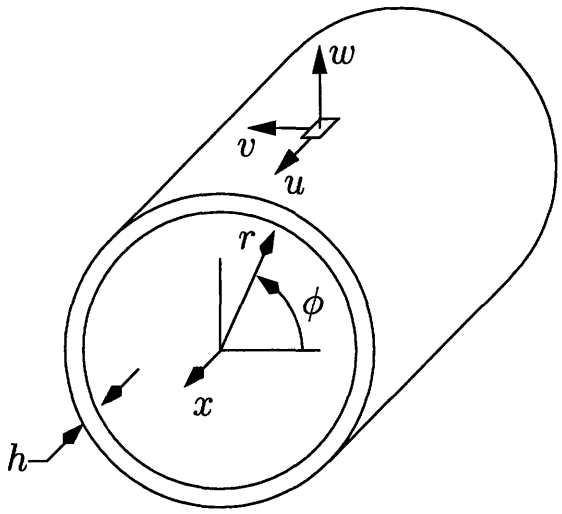

Figure 5-3: Schematic of cylinder geometry and displacements

wavenumber in the hypothetical empty tube as in the filled tube, we obtain the effective loss factor η for a given ω.

We employ Reissner's equations [30] in dimensionless form assuming steady harmonic motion:

$$\frac{\partial^2 u}{\partial x^2} + \frac{1-\nu}{2}\frac{\partial^2 u}{\partial \phi^2} + \frac{1+\nu}{2}\frac{\partial^2 v}{\partial x \partial \phi} + \nu\frac{\partial w}{\partial x} = -\Omega^2 u \tag{5.1}$$

$$\frac{1+\nu}{2}\frac{\partial^2 u}{\partial x \partial \phi} + \frac{1-\nu}{2}(1+\beta^2)\frac{\partial^2 v}{\partial x^2} + (1+\beta^2)\frac{\partial^2 v}{\partial \phi^2} + \frac{\partial w}{\partial \phi} - \beta^2\left(\frac{\partial^3 w}{\partial x^2 \partial \phi} + \frac{\partial^3 w}{\partial \phi^3}\right) = -\Omega^2 v \tag{5.2}$$

$$-\nu\frac{\partial u}{\partial x} - \frac{\partial v}{\partial \phi} + \beta^2\left(\frac{\partial^3 v}{\partial x^2 \partial \phi} + \frac{\partial^3 v}{\partial \phi^3}\right) - w - \beta^2\left(\frac{\partial^4 w}{\partial x^4} + 2\frac{\partial^4 w}{\partial x^2 \partial \phi^2} + \frac{\partial^4 w}{\partial \phi^4}\right) = -\Omega^2 w - \frac{R}{h}q_3 \tag{5.3}$$

where x is the coordinate along the axis of the cylinder normalized by its mean radius R; h is the thickness of the cylinder; u, v, and w are respectively the axial, circumferential, and radial displacements which have been nondimensionalized by R; β is a dimensionless geometric parameter given by

$$\beta^2 = \frac{h^2}{12R^2} \tag{5.4}$$

and Ω is the dimensionless frequency

$$\Omega = \frac{\omega R}{c_p} \tag{5.5}$$

where ω is the dimensional angular frequency and c_p is the speed of compressional waves in a flat plate:

$$c_p^2 = \frac{E}{\rho_s(1-\nu^2)} \tag{5.6}$$

The parameters E, ρ_s, and ν are respectively the Young's modulus, volumetric density, and Poisson's ratio of the cylinder material, and q_3 is the complex magnitude of the applied stress in the radial direction nondimensionalized by the factor $E/(1-\nu^2)$. In our problem, this applied stress is the pressure exerted by the powder on the tube wall from within.

We seek solutions of the form

$$u(x,\phi) = U\cos K_x x\,\cos n\phi \tag{5.7}$$

$$v(x,\phi) = V\sin K_x x\,\sin n\phi \tag{5.8}$$

$$w(x,\phi) = W\sin K_x x\,\cos n\phi \tag{5.9}$$

where K_x is the nondimensional wavenumber in the axial direction and n is an integer.

Following the approach of Varanasi and Nayfeh [65] and based on the experiments described earlier, we model the granular medium as a compressible fluid with a complex speed of sound c. For steady harmonic motion at a frequency ω, the pressure p in this fluid is nondimensionalized by the plane-strain modulus of the tube material $E/(1-\nu^2)$ and is governed by

$$\nabla^2 p + \frac{\Omega^2 c_p^2}{c^2} p = 0 \tag{5.10}$$

with the boundary condition that the pressure at the tube wall must be proportional to the acceleration of the wall. That is,

$$\left.\frac{\partial p}{\partial r}\right|_{r=\frac{R_i}{R}} = \frac{\rho_f \Omega^2}{\rho_s} W\sin K_x x\,\cos n\phi \tag{5.11}$$

where ρ_f is the density of the granular medium and we have made use of the expression given by (5.9).

The condition given by (5.11) suggests that we take

$$p(r,\phi,x) = \overline{p}(r)\sin K_x x\,\cos n\phi \tag{5.12}$$

Then, the governing equation (5.10) for the pressure in the cylinder becomes Bessel's equation of order n for $\overline{p}(r)$. We obtain a solution of the form

$$\overline{p}(r) = c_1 J_n(K_r r) + c_2 Y_n(K_r r) \tag{5.13}$$

where c_1 and c_2 are constants, J_n is the Bessel function of the first kind of order n, Y_n is the Bessel function of the second kind of order n, and K_r is given by

$$K_r = \sqrt{\frac{\Omega^2 c_p^2}{c^2} - K_x^2} \tag{5.14}$$

The constant c_2 must be zero to maintain finite pressure in the pipe at the origin. The boundary condition at the wall gives c_1, and the resulting solution for the pressure in the tube is

$$\overline{p}(r) = \frac{\rho_f}{\rho_s} W \Omega^2 \frac{J_n(K_r r)}{\left.\frac{dJ_n(K_r r)}{dr}\right|_{r=\frac{R_i}{R}}} \tag{5.15}$$

Returning to the equations governing motion of the shell and making use of (5.7)–(5.9), (5.12), and (5.15), we obtain algebraic equations for U, V, and W in the form

$$\left(K_x^4 A_4 + K_x^2 A_2 + K_x A_1 + A_0 - \Omega^2 M\right) \begin{pmatrix} U \\ V \\ W \end{pmatrix} = \begin{pmatrix} 0 \\ 0 \\ 0 \end{pmatrix} \tag{5.16}$$

where

$$A_4 = \begin{bmatrix} 0 & 0 & 0 \\ 0 & 0 & 0 \\ 0 & 0 & \beta^2 \end{bmatrix} \tag{5.17}$$

$$A_2 = \begin{bmatrix} 1 & 0 & 0 \\ 0 & \frac{1-\nu}{2}(1+\beta^2) & n\beta^2 \\ 0 & n\beta^2 & 2\beta^2 n^2 \end{bmatrix} \tag{5.18}$$

$$A_1 = \begin{bmatrix} 0 & -n\frac{1+\nu}{2} & -\nu \\ -n\frac{1+\nu}{2} & 0 & 0 \\ -\nu & 0 & 0 \end{bmatrix} \tag{5.19}$$

$$A_0 = \begin{bmatrix} \frac{1-\nu}{2}n^2 & 0 & 0 \\ 0 & n^2(1+\beta^2) & n+n^3\beta^2 \\ 0 & n+n^3\beta^2 & 1+\beta^2 n^4 \end{bmatrix} \tag{5.20}$$

$$M = \begin{bmatrix} 1 & 0 & 0 \\ 0 & 1 & 0 \\ 0 & 0 & 1+\frac{\rho_f R}{\rho_s h}\frac{J_n\left(K_r\frac{R_i}{R}\right)}{K_r J_n'\left(K_r\frac{R_i}{R}\right)} \end{bmatrix} \tag{5.21}$$

where J_n' is the derivative of the Bessel function of the first kind. Setting the determinant of the coefficient matrix in (5.16) equal to zero, we obtain a dispersion relation relating wavenumber K_x to frequency Ω. Because of the dependence of $J_n(K_r)$ on K_x and Ω, we use an iterative approach to the solution as outlined in the following.

First, we solve for the wavenumber K_x in an empty tube, for which the inertia matrix (5.21) is given by the identity matrix. There are multiple solutions for K_x, and the appropriate one is chosen through examination of the corresponding mode shapes

and comparison to a desired reference. The reference mode shapes can be taken using the plane strain mode shapes (see Figure 5-2). For example, beam bending modes ($n = 1$) have eigenvectors approximately given by $\begin{bmatrix} 0 & 1 & -1 \end{bmatrix}^T$, and the lowest frequency variety of $n = 2$ modes have approximate eigenvectors $\begin{bmatrix} 0 & 0.5 & -1 \end{bmatrix}^T$.

Based on this initial estimate of K_x, we evaluate the inertia matrix given by (5.21) with where the value of K_r set by the estimate of K_x, and solve again the eigenvalue problem for K_x. We continue this iterative procedure until the value of K_x converges.

Once K_x has been determined, we estimate the equivalent loss factor as a function of frequency. To do this, we again consider an empty cylinder, now characterized by an "effective" complex Young's modulus $\tilde{E} = E_0(1 + j\eta)$ and solve for the value of $\tilde{E}$ that yields the same value for the complex wavenumber K_x as computed for the filled tube.

As a result of the nondimensionalization, the modulus of the tube only appears in the nondimensional frequency parameter Ω given by (5.5). For each value of n, we substitute the value of K_x obtained above into (5.16) with the inertia matrix given by the identity matrix and solve the resulting eigenvalue problem for Ω^2. In solving the eigenvalue problem we obtain multiple solutions for Ω^2, and the appropriate value is chosen after examination of the corresponding mode shape. Finally, the loss factor is obtained using

$$\eta = \frac{\operatorname{Im} \tilde{E}}{\operatorname{Re} \tilde{E}} = \frac{\operatorname{Im} \frac{1}{\Omega^2}}{\operatorname{Re} \frac{1}{\Omega^2}} \tag{5.22}$$

5.4 Results

Figures 5-4 and 5-5 show the predicted and measured loss factors based on the measured complex speed of sound $c = 69(1 + 0.13j)$ m/s and density $\rho_f = 78$ kg/m^3. The loss factor curves for $n = 1$ and $n = 2$ agree qualitatively with the experimental results. Based on these figures, it appears that the estimates of the value of the real part of the speed of sound c_0 is too high and the loss factor η_f is too low because the peaks in the theoretical loss-factor curves are sharper and occur at higher frequency than indicated by the data.

The model and experiments both demonstrate that the powder can behave like a tuned-mass damper. Like the tuned-mass damper, the powder adds an additional degree of freedom to the system so that near a resonance in the undamped structure there may exist two resonances in the damped structure, Furthermore, the powder may act to stiffen the primary structure at some frequencies while softening it at others. Experimental results in Table 5.1 and Figure 5-1 show that modes $n = 1$, $m = 2$ and $n = 2$, $m = 4$ undergo "splitting". When splitting occurs, the powder moves in phase with the structure in the lower-frequency mode and out of phase with the structure in the higher frequency mode.

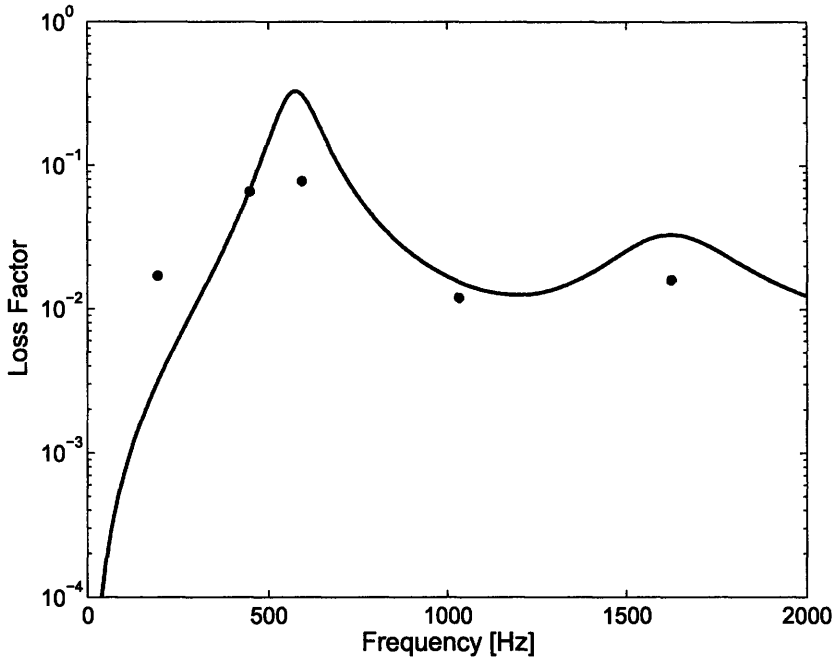

Figure 5-4: Loss factor as a function of frequency for $n = 1$. Asterisks denote data from Table 1.

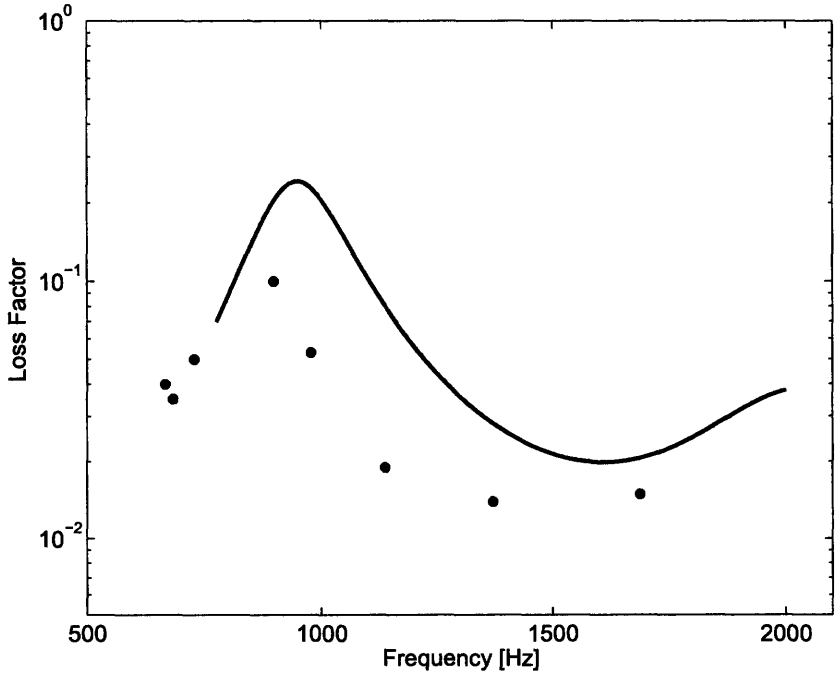

Figure 5-5: Loss factor as a function of frequency for $n = 2$. Asterisks denote data from Table 2.

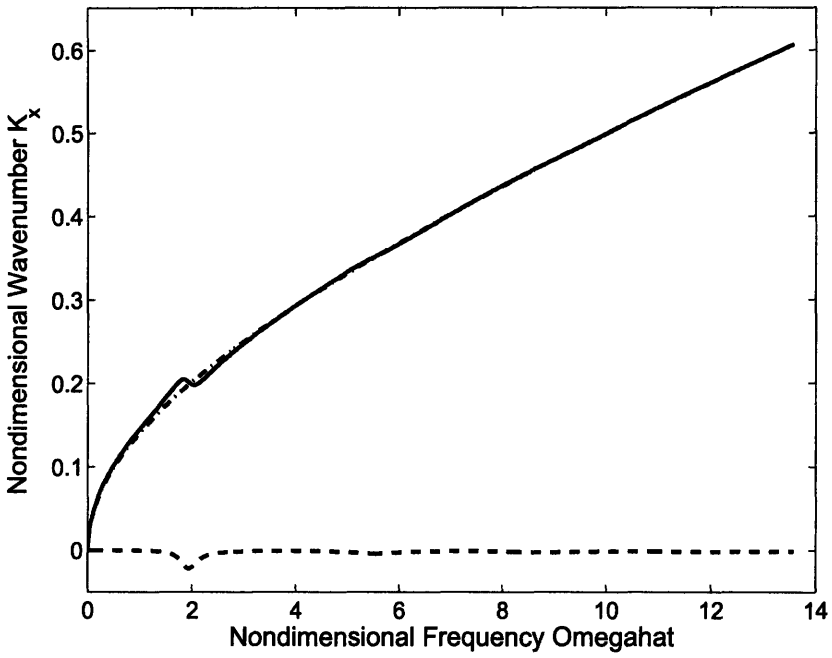

Figure 5-6: Nondimensional dispersion relation for $n = 1$ and granular material loss factor $\eta_f = 0.10$ (dash-dot, wavenumber of empty cylinder; solid, real part of complex wavenumber of filled cylinder; dashed, imaginary part of complex wavenumber of filled cylinder)

5.5 Discussion

We define a new, nondimensional frequency that is normalized by the parameters of the powder given by

$$\hat{\Omega} = \frac{c_p}{c_0}\Omega = \frac{\omega R}{c_0} \tag{5.23}$$

Damping attains local maxima and minima when $\hat{\Omega}$ is order unity.

Typical dimensionless dispersion relations for $n = 1$ and $n = 2$ are given in Figures 5-6 and 5-7, respectively. The dispersion curve gives the relation between the wavenumber and frequency for a travelling wave in an infinite cylinder. The standing wave behavior (i.e., natural frequencies) for a finite tube can be approximated using the dispersion curve. A resonance in the finite tube occurs when the wavenumber is approximately an integer multiple of the inverse of the length of the cylinder. The values of the wavenumber at which resonances occur should not vary significantly from the empty to filled cylinders; therefore, a comparison between the dispersion relation for the filled cylinder and the real part of the dispersion relation for the unfilled cylinder can be used to explain the differences in behavior of the filled and unfilled finite cylinders.

At low frequencies, the real part of the wavenumber is greater than the wavenumber of the empty shell because the powder tends to act primarily as an added mass

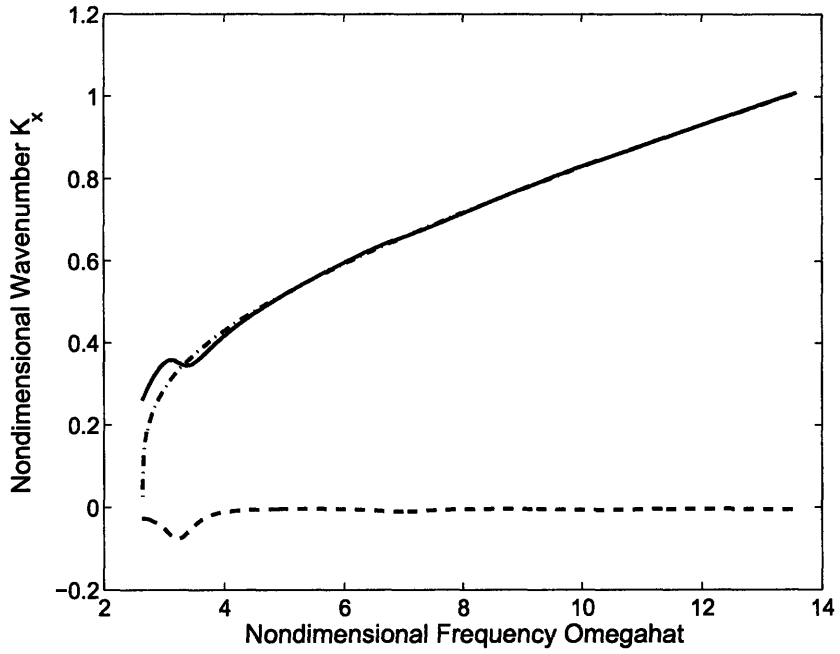

Figure 5-7: Nondimensional dispersion relation for $n = 2$ and granular material loss factor $\eta_f = 0.10$ (dash-dot, wavenumber of empty cylinder; solid, real part of complex wavenumber of filled cylinder; dashed, imaginary part of complex wavenumber of filled cylinder)

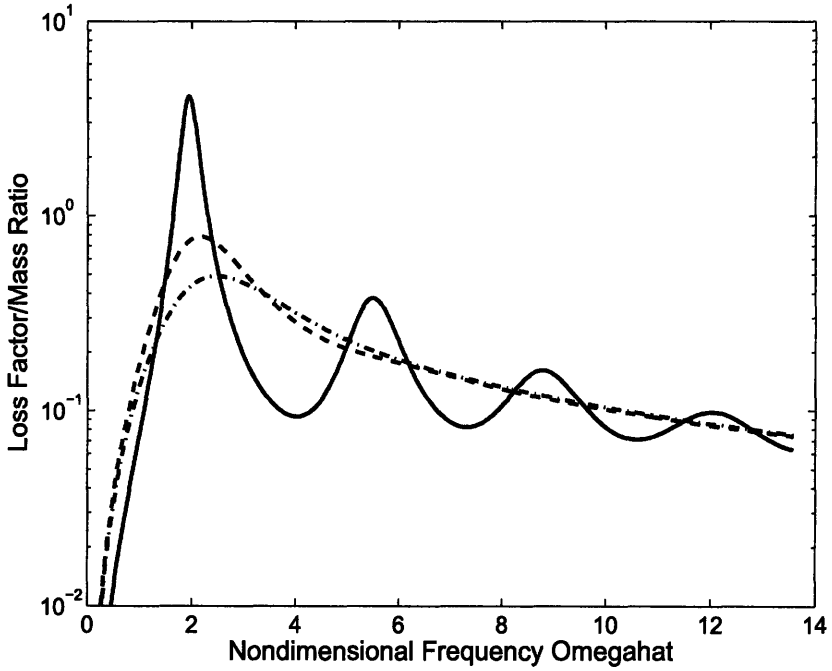

Figure 5-8: System loss factor as a function of nondimensional frequency for $n = 1$ for granular material loss factors 0.1 (solid), 0.5 (dashed), 0.8 (dash-dot)

and lower the resonant frequencies. At a value of the wavenumber K_x which corresponds to a resonance in the finite, empty tube, the value of the nondimensional frequency $\hat{\Omega}$ at the same value of K_x is smaller for the filled cylinder than for the empty cylinder.

Above a resonant frequency of the powder, the real part of the dispersion relation may lie above or below the original dispersion curve, indicating whether the powder acts primarily as an added mass or stiffness on the tube, respectively. For small perturbations (i.e., a small added mass), the powder typically acts to stiffen the cylinder just above the first resonance as shown in Figures 5-6 and 5-7.

When the real part of the dispersion relation is not monotonically increasing, one finds three frequency values for a given value of the wavenumber and mode-splitting can occur. The smallest and largest of the three frequency values correspond to the observed vibration modes of the finite tube. The intermediate frequency, which has a negative slope corresponding to a negative group velocity, is not observed in experiments.

Representative loss factor curves for $n = 1$ and $n = 2$ are given in Figures 5-8 and 5-9, respectively. The peaks in the loss factor curves are caused by resonances in the granular medium, and the valleys are caused by anti-resonances in the granular medium. The curves for $n = 2$ do not start at zero frequency because this mode has a non-zero cutoff frequency.

Using the plane wave approximation of Ungar and Kerwin [62] because the wavelength in the axial direction is much great than the radius of the cylinder, we can

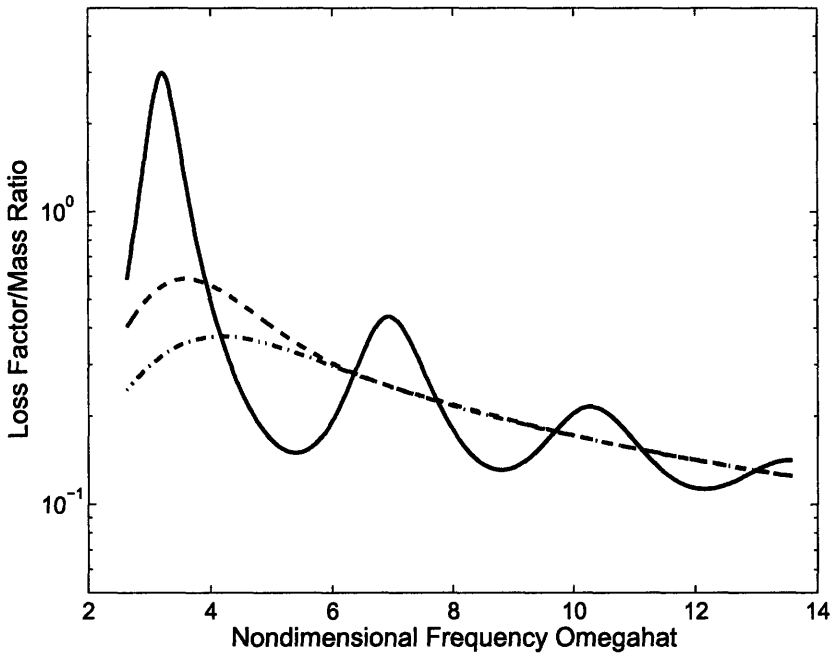

Figure 5-9: System loss factor as a function of nondimensional frequency for $n = 2$ for granular material loss factors 0.1 (solid), 0.5 (dashed), 0.8 (dash-dot)

ignore K_x in (5.14) to obtain $\hat{\Omega} \approx K_r$. The method for calculating the dispersion relation and loss factor remain the same and the resulting differences are negligible. This approach can be used to estimate the critical nondimensional frequencies. The resonance frequencies of the powder are determined by setting $J_n'(\hat{\Omega}) = 0$ to obtain $\hat{\Omega} \approx 1.8412, 5.3314, \ldots$ for $n = 1$ and $\hat{\Omega} \approx 3.0542, 6.7061, \ldots$ for $n = 2$. The anti-resonance frequencies are determined by setting $J_n(\hat{\Omega}) = 0$ to obtain for $n = 1$: $\hat{\Omega} \approx 3.8317, 7.0156, \ldots$ and for $n = 2$: $\hat{\Omega} \approx 5.1356, 8.4172, \ldots$.

5.6 Conclusions

The results of the experiments described in this chapter demonstrate that filling a thin-walled cylinder with a low-density granular material can provide considerable damping in a simple and inexpensive manner. We have developed a model that couples shell vibrations to a lossy, compressible fluid and compute dispersion relations and loss factor curves as functions of frequency for the various mode shapes. The travelling-wave behavior described by the dispersion relations is used to approximate the damping in the standing-wave behavior observed in resonant response of finite cylinders.

The theoretical loss factor curves agree reasonably well with the measured results for beam bending modes and tube-wall-flexing modes. Both theory and experiments show that there is little damping at low frequencies, but significant damping occurs above 400 Hz. The differences between the measurements and theory are attributable

in large part to difficulties in obtaining an accurate model of the powder. This is still an active research area (see e.g., [26]).

Potential applications of this damping method include autmotive driveshafts whose modes are excited by gear teeth meshing as well as other closed structures where moderate frequency vibrations are a nuisance, especially high-temperature applications because many granular materials (like the glass spheres used in our experiment) are heat resistant. Further work is needed to identify and characterize granular materials that are lightweight, lossy, and have a low speed of sound.

Chapter 6

Vibration damping of cylindrical shells using lightweight, low-wave-speed media

6.1 Introduction

The introduction of foam into a machine or structure is a simple, low-cost method of reducing noise and vibration. Oberst [43], Morris [40], and James [27] observed damping in structures consisting of metal and a soft, lossy laminate such as foam or rubber due to resonances through the thickness of the lossy material. Ungar and Kerwin [62] developed a model to estimate the loss factor of plates and beams with a viscoelastic layer due to resonances through the thickness and compared the model with experimental measurements. They modelled the viscoelastic material with a one-dimensional wave equation (through the thickness) and a complex Young's modulus. Other researchers (e.g., [10, 4, 45, 66]) have studied damping caused by resonance through the thickness of granular media. Göransson [22] discusses the energy dissipation mechanisms of foams as described by Biot's model [3] and shows acoustic and vibration experiments for plates with attached layers of foam. Vigran *et al* [67] use finite elements to obtain the forced response of a sandwich plate in which the core is modelled using Biot's equations for a porous material. Jaouen *et al* [28] use a mixed pressure-displacement finite element formulation of the Biot-Allard model to study forced vibrations of a metal plate covered with a layer of foam

In this chapter, we consider the problem of damping vibration in thin-walled cylindrical tubes. We present the results of experiments on a foam-filled free-free cylindrical tube in which significant damping is attained in beam-bending and tube-wall-flexing modes. To model the damping phenomenon and obtain estimates for the damping in these modes, we consider steady harmonic wave propagation in the axial direction of an infinitely long cylindrical tube and treat the foam as an elastic solid with a complex modulus. Based on the spatial decay characterized by a complex wavenumber, we obtain an estimate of the loss factor associated with motion as a function of frequency and the number of circumferential nodes.

6.2 Experiments

We conduct experiments on a welded, carbon-steel cylindrical tube of length 1.83 m, outside diameter 10.2 cm, wall thickness 3.0 mm. The cylinder is filled with Foamex Sensus viscoelastic memory foam [17]. The nominal diameter of the foam is 10.2 cm resulting in a 6% preload when loaded inside the tube. The unloaded density of the foam is 67.4 kg/m^3. The total mass of the foam is 1.00 kg, or 7.1% of the mass of the cylinder. The effective density of the foam loaded inside the tube is 76.7 kg/m^3. The cylinder is supported with strings at the quarter points to approximate free boundary conditions. A triaxial accelerometer (PCB 356B08) is fixed at one end of the tube, and excitation is provided by an impact hammer (PCB 086B03) in the radial direction at various points along the shell [51]. Mode shapes are fit using Star Modal analysis software [57].

A typical measured frequency response (force to acceleration) is shown in Figure 6-1. The natural frequencies, mode shapes, and damping coefficients for the empty tube are given in Tables 6.1–6.4. As with many shell geometries, the modes occur in clusters. The clustering and well-damped nature of the frequency response for the filled cylinder cause some difficulties in estimation of the loss factor, mode shapes, and natural frequencies from the experiments. Some modes, such as those with $n = 2$ and $m = 10$, appear twice because the weld line of the tube breaks the symmetry and allows the same qualitative mode shape to appear at two close but distinct frequencies.

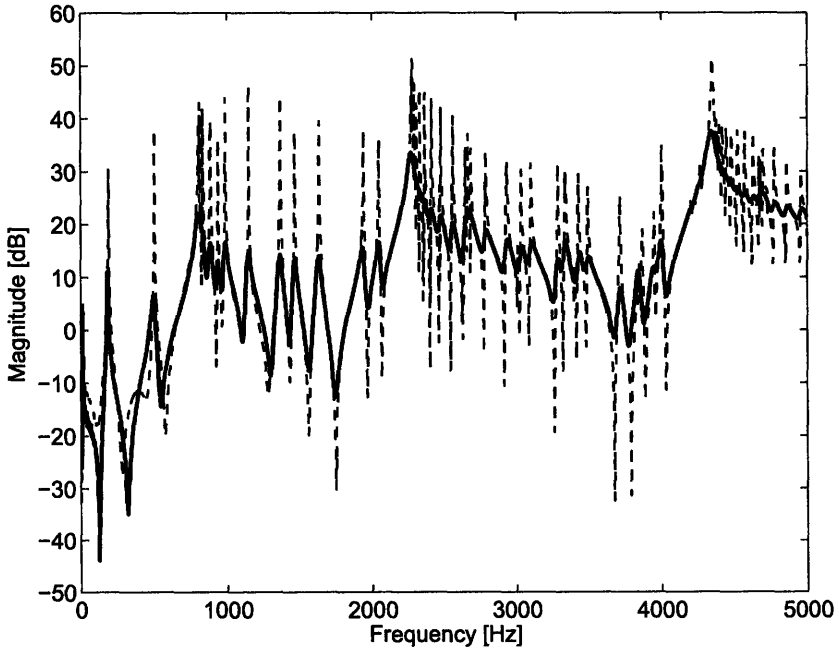

Figure 6-1: Typical measured freqency response of cylinder empty (dashed) and filled (solid)

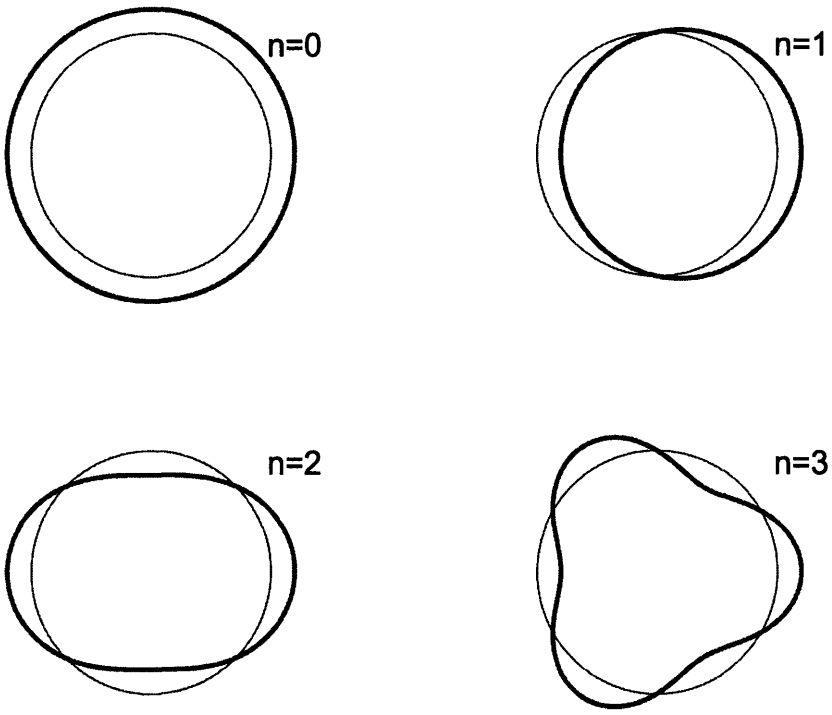

Figure 6-2: Cross-sections of deformation of vibration modes for various n

Table 6.1: Measured natural frequencies of the empty and filled tube for the beam bending modes ($n = 1$, see also Figure 6-2)

	Empty		Filled	
Mode m	Freq. [Hz]	Loss Factor [%]	Freq. [Hz]	Loss Factor [%]
1	188	0.98	182	3.0
2	501	0.61	496	4.6
3	937	0.27	934	2.7
4	1462	0.27	1461	1.7
5	2046	0.21	2050	1.3
6	2684	0.15	2675	1.4
7	3339	0.13	3335	1.1
8	4006	0.11	4004	0.70
9	4669	0.12	4676	0.69

Table 6.2: Measured natural frequencies of the empty and filled tube for the $n = 2$ modes (see also Figure 6-2)

	Empty		Filled	
Mode m	Freq. [Hz]	Loss Factor [%]	Freq. [Hz]	Loss Factor [%]
0			800.	4.2
1	814	0.32	805	2.1
2	832	0.25	827	2.7
3	885	0.23	881	3.0
4	986	0.18	982	2.2
5	1144	0.18	1142	1.3
6	1363	0.21	1359	1.1
7	1630	0.21	1627	1.9
8	1938	0.19	1935	1.7
9	2646	0.19	2643	1.3
10	3007	0.18	3035	1.1
10	3031	0.16		
12	3427	0.15	3422	1.1
13	3856	0.25	3843	0.89
14	4230	0.11		
14	4265	0.14	4258	0.71

Table 6.3: Measured natural frequencies of the empty and filled tube for the $n = 3$ modes (see also Figure 6-2)

	Empty		Filled	
Mode m	Freq. [Hz]	Loss Factor [%]	Freq. [Hz]	Loss Factor [%]
1	2279	0.27	2269	1.9
2	2295	0.15	2290.	1.7
3	2306	0.14	2312	1.7
4	2329	0.14	2318	1.3
5	2363	0.15	2351	1.3
6	2412	0.15	2400.	1.2
7	2476	0.16	2463	1.3
8	2559	0.15	2552	1.6
9	2662	0.14	2652	1.4
10	2787	0.16	2780.	1.3
11	2931	0.24	2928	1.4
12	3100.	0.2 7	3096	1.4
13	3286	0.18	3289	1.3
14	3492	0.16	3488	1.1
15	3714	0.16	3714	1.0
16	3950	0.15	3949	0.88
17	4199	0.15	4200.	0.89
18	4725	0.17		
19	4995	0.18		

Table 6.4: Measured natural frequencies of the empty and filled tube for the $n = 4$ modes (see also Figure 6-2)

	Empty		Filled	
Mode m	Freq. [Hz]	Loss Factor [%]	Freq. [Hz]	Loss Factor [%]
0			4324	1.2
1	4346	0.27		
2	4358	0.09		
3	4374	0.17	4346	1.2
4	4393	0.16	4390.	0.79
5	4415	0.14		
6	4444	0.14	4446	1.3
7	4478	0.15	4482	1.2
8	4521	0.15	4524	1.2
9	4570	0.15	4574	1.2
10	4628	0.13	4628	1.0
11	4691	0.17	4693	0.87
12	4772	0.13	4771	0.77
13	4858	0.13	4857	0.72
14	4955	0.14	4957	0.89

6.3 Foam Material Properties

6.3.1 Introduction

The goal of this section is to obtain a simple description of the dynamic properties of the foam used for vibration damping. Porous materials are very common, and models of their behavior have been studied by many researchers in a variety of fields. In materials science (see e.g., [20]) the approach is usually to predict bulk properties of a foam from factors such as cell shape and density. However, these approaches are typically concerned with quasi-static not dynamic behavior. Biot [3] developed a model, that is widely used in acoustics and geology for the deformation of the solid and surrounding fluid that does not require a detailed, geometric description of the porous microstructure. Allard [2] expanded on this work, but this model is cumbersome to use when coupled to a structure. Acoustic materials are commonly measured using an impedance tube (see e.g., [74]). Properties such as firmness, compression set, tear strength, and sometimes acoustic absorption are typically quoted for commercially available foams (e.g., [16]), but moduli are not quoted since the stress-strain curve is often nonlinear. The simplest models for the purpose of this work are an effective Young's modulus, an effective shear modulus, and loss factor.

To measure the dynamic properties of the foam, we use the methods of Varanasi and Nayfeh [66], which consist of non-resonant shear and uniaxial tests. The foam

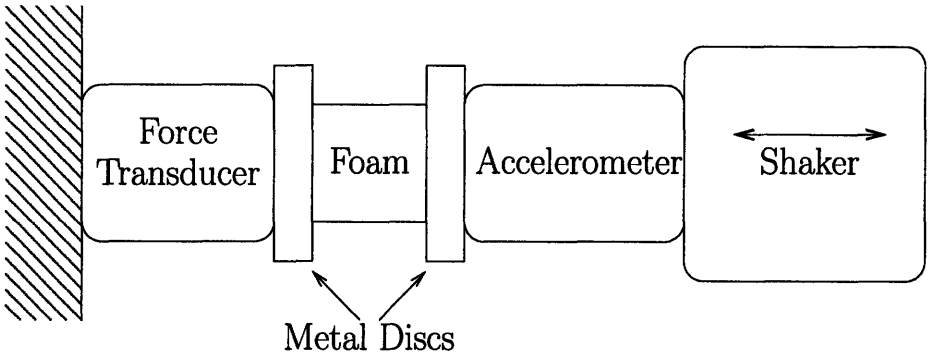

Figure 6-3: Schematic of compression test

used in these experiments is Foamex Sensus viscoelastic, or "memory," foam and has a measured density of 64.7 kg/m^3.

6.3.2 Uniaxial Test

The test setup (see schematic in Figure 6-3) consists of a layer of foam (9.3 mm thick undeformed, 29.2 mm diameter) glued between two metal discs. One disc is connected to an electromagnetic shaker (Vibration Test Systems VG100M-4), and the other disc is connected to ground. The motion of the shaker is measured with an acclerometer (PCB 356B21, 1.05 mV/(m/s^2)), and the force applied to the foam sample is measured using a forced transducer (PCB 208C01, 108.2 mV/N) placed between the fixed disc and ground. The shaker is driven using an amplifier (Techron 7541) in current mode. A signal analyzer (Spectral Dynamics Siglab 20-42) is used to drive the system, measure the sensor outputs, and create the transfer functions. The system is driven with a random excitation. To minimize nonlinear effects, we use the smallest force amplitude that yields a reasonable signal-to-noise ratio.

The uniaxial stress-strain curve of a foam under quasi-static deformation often demonstrates nonlinear behavior [20]. To obtain the material properties in the presence of material nonlinearity, we measure the dynamic stiffness of the foam at a variety of initial strains, which are implemented by applying a DC offset in addition to the driving signal.

A typical measured transfer function (force/acceleration) is shown in Figure 6-4. The modulus as a function of frequency is calculated; a typical plot is shown in Figure 6-5. Above approximately 100 radians/second, the modulus of the foam is approximately linear on logarithmic axes and hence well modelled by the relation $E(\omega) = E_0(1 + j\eta)\omega^m$. The loss factor is nearly independent of frequency so we use its average value as the material loss factor. Figures 6-6, 6-7, and 6-8 show the initial modulus E_0, loss factor η, and slope m, resectively, of the modulus model as a function of initial strain.

Figure 6-6 shows that the modulus can be significantly increased or decreased by applying an initial strain to the foam. An initial compression of the foam results in much softer behavior when the elements of the matrix that composes the foam begin

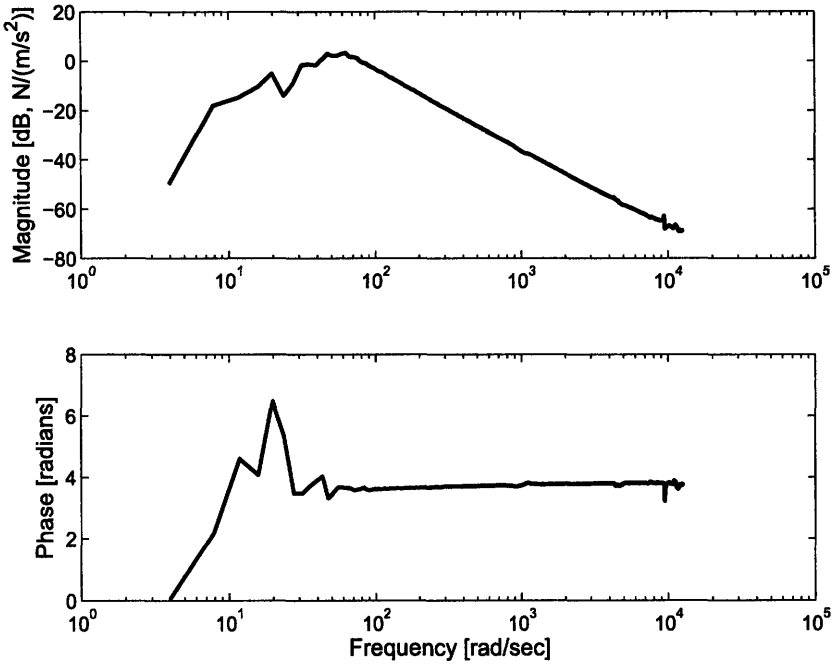

Figure 6-4: Typical measured transfer function (force/acceleration) for uniaxial tension/compression test

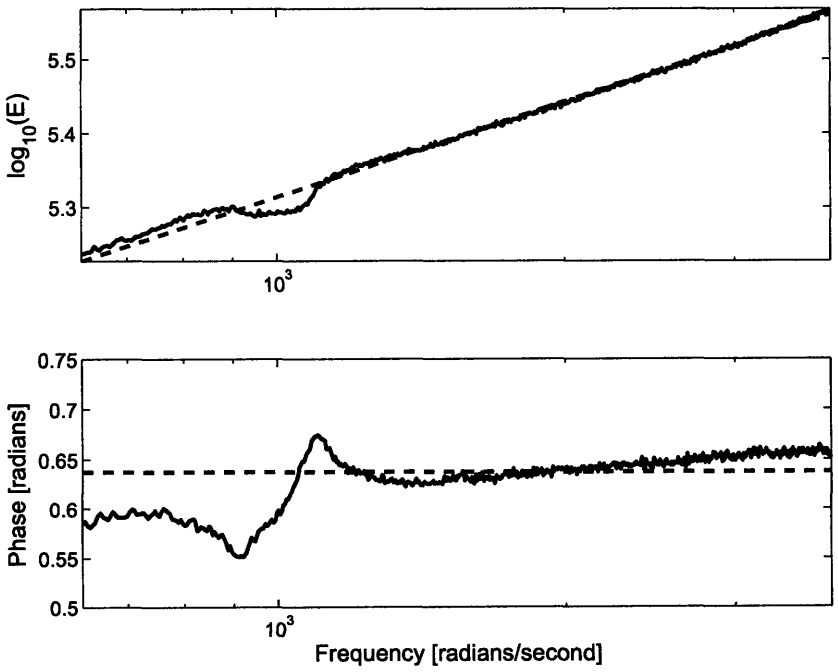

Figure 6-5: Typical measured Young's modulus as a function of frequency

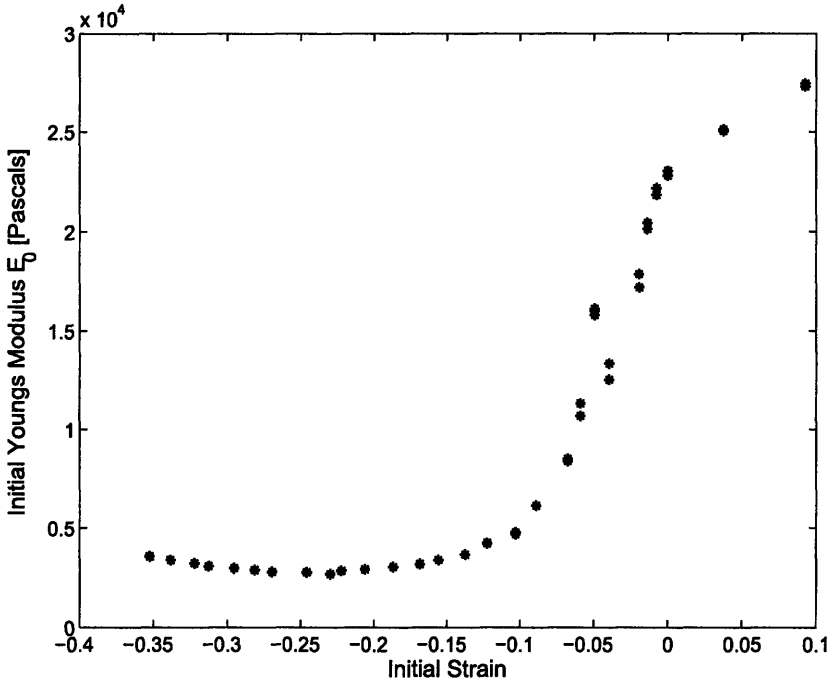

Figure 6-6: Measured values of E_0 as a function of initial strain

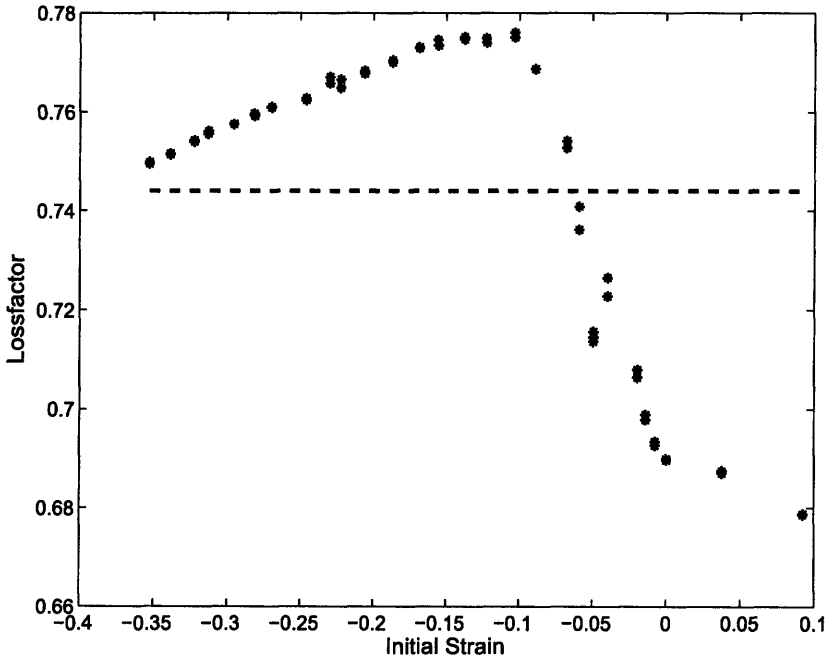

Figure 6-7: Measured loss factor as a function of initial strain (asterisk), average value (dashed)

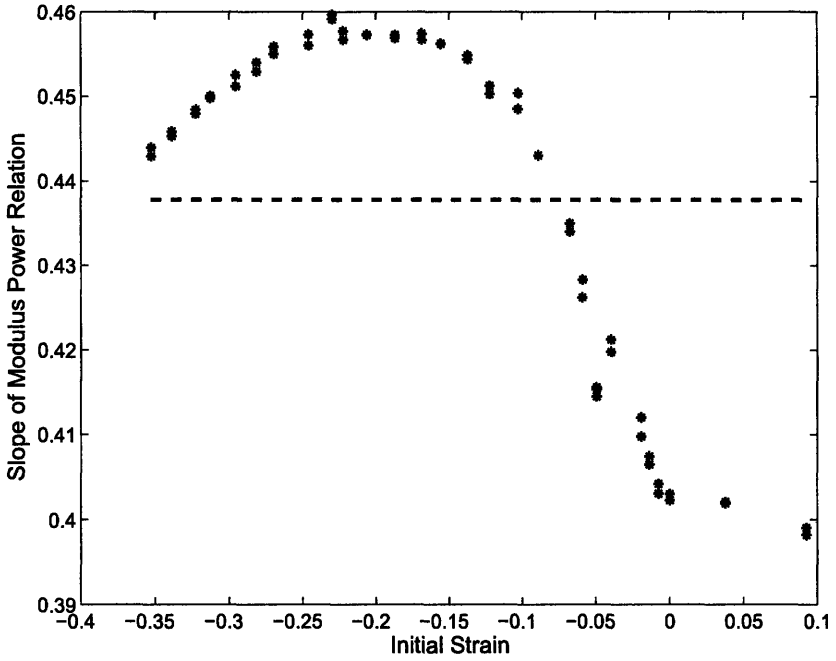

Figure 6-8: Measured slope as a function of initial strain (asterisk), average value (dashed)

to buckle [20]. An initial tension leads to a stiffening effect because deformation is tension dominated, as opposed to bending dominated in the undeformed state.

6.3.3 Shear Test

A shear test is used to calculate the shear modulus. Once the shear modulus is known, we calculate the Poisson ratio using the relation

$$\nu = \frac{E}{2G} - 1 \tag{6.1}$$

The test setup (see schematic in Figure 6-9) consists of two thin pieces of foam (2 cm × 2.5 cm × 6.1 mm thick) glued between opposites side of a metal block and the inner faces of a metal U-shaped channel. The walls of the U-channel are adjustable to vary the initial compressive/tensile strain on the foam. The metal block is actuated by an electromagnetic shaper. The U-shaped channel is connected to ground. An accelerometer measures the motion of the block, and a force transducer between the ground and the U-channel measures the force applied to the foam. Again, a dynamic signal analyzer is used to drive the shaker and measure the sensor outputs. The system is driven with a random excitation. To minimize nonlinear effects, we use the smallest force amplitude that yields a reasonable signal-to-noise ratio.

The measured transfer function and modulus curves resemble Figures 6-4 and 6-5, respectively. Using the same model for the shear modulus as for the Young's

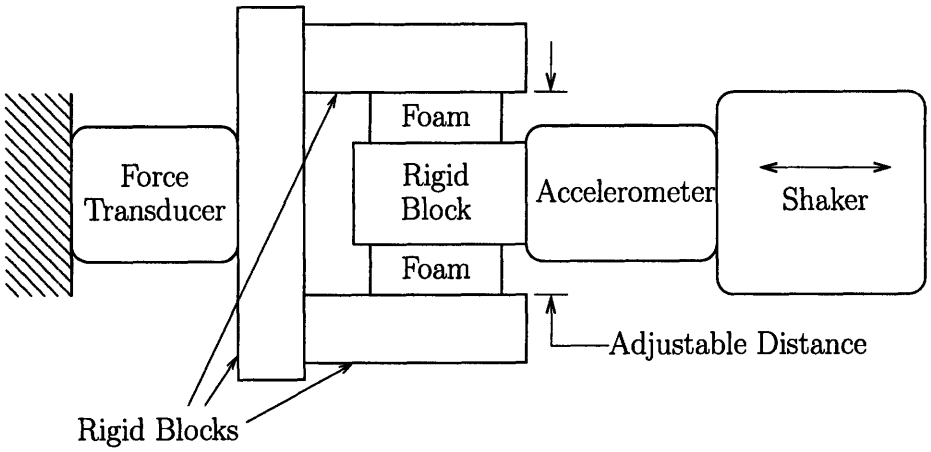

Figure 6-9: Schematic of shear test

Table 6.5: Values for logarithmic model $E = E_0(1 + j\eta)\omega^m$, $G = G_0(1 + j\eta)\omega^m$ at -6% strain

Property	Value
E_0	8000 Pa
G_0	3200 Pa
slope m	0.4
loss factor η	0.7
Poisson ratio	0.25

modulus ($G(\omega) = G_0(1+1j\eta)\omega^m$), we find that the shear modulus has approximately the same loss factor $\eta = 0.7$ (see Figure 6-12) and slope $m = 0.4$ (see Figure 6-11). The variation of the shear modulus parameter G_0 with initial strain does not follow a clear trend like the Young's modulus (see Figure 6-10). A search of the literature does not suggest that there should be a significant and well-defined correlation. Once the initial strain is known, the values of E_0 and G_0 can be determined, and the Poisson ratio is calculated using (6.1).

For the experiment of the cylinder filled with foam, the undeformed diameter of the foam is 10.2 cm, and the internal diameter of the cylinder is 9.5 cm resulting in an intial strain of -6%. Using this initial strain and the data from the shear and compression tests, the resulting parameters for the logarithmic model are calculated and given in Table 6.5.

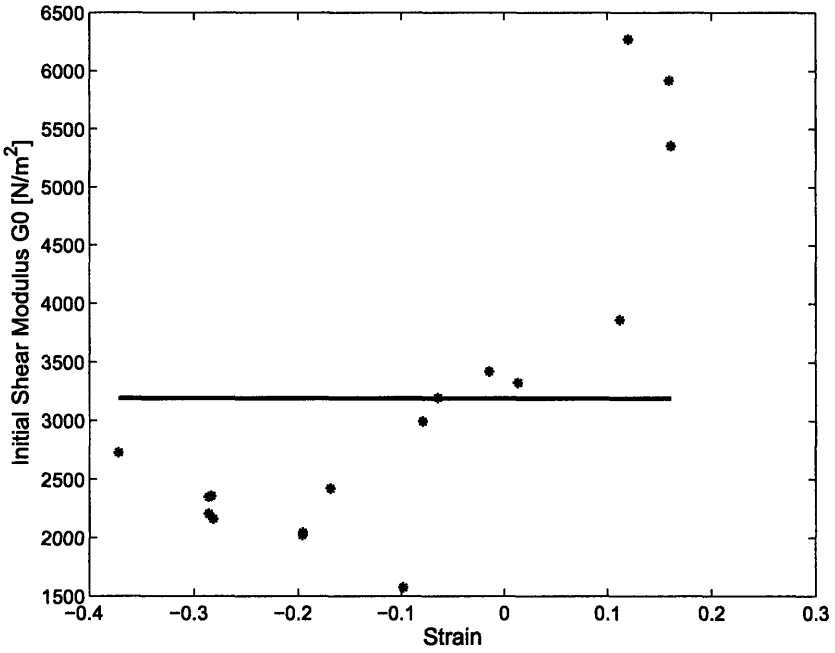

Figure 6-10: Measured values of initial shear modulus G_0 as a function of initial strain

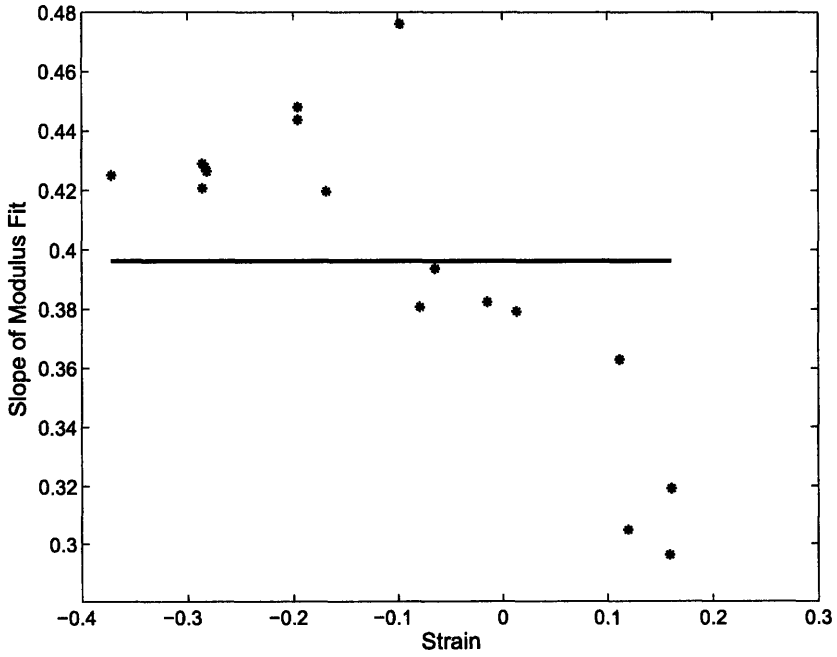

Figure 6-11: Measured values of the slope for the shear modulus as a function of initial strain

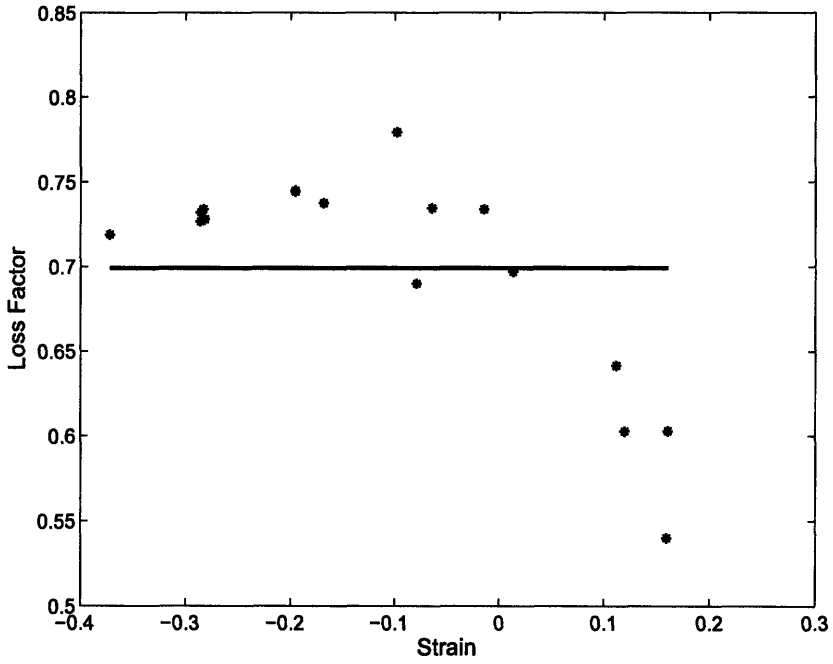

Figure 6-12: Measured loss factor for shear modulus tests as a function of initial strain

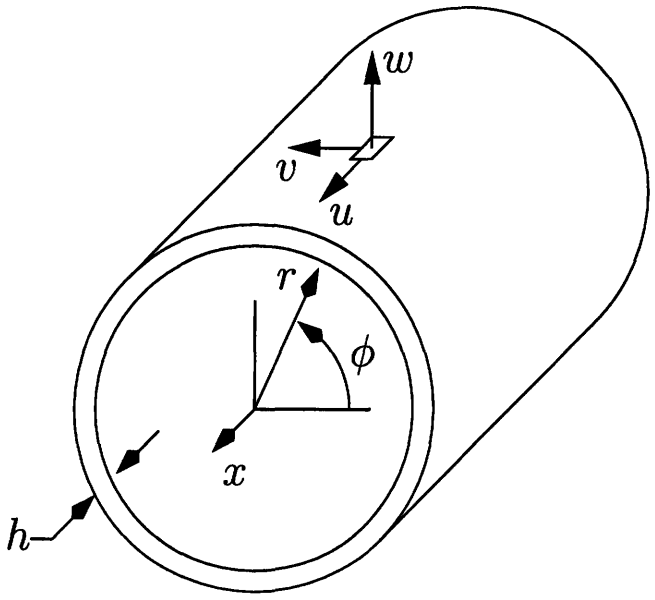

Figure 6-13: Schematic of cylinder geometry and displacements

6.4 Modelling

6.4.1 Cylindrical Shell

We employ Reissner's equations [30] in dimensionless form assuming steady harmonic motion:

$$\frac{\partial^2 u}{\partial x^2} + \frac{1-\nu}{2}\frac{\partial^2 u}{\partial \phi^2} + \frac{1+\nu}{2}\frac{\partial^2 v}{\partial x \partial \phi} + \nu\frac{\partial w}{\partial x} = -\Omega^2 u - \frac{R}{h}\frac{1-\nu^2}{E}q_r \tag{6.2}$$

$$\begin{aligned}\frac{1+\nu}{2}\frac{\partial^2 u}{\partial x \partial \phi} + \frac{1-\nu}{2}(1+\beta^2)\frac{\partial^2 v}{\partial x^2} + (1+\beta^2)\frac{\partial^2 v}{\partial \phi^2} \\ + \frac{\partial w}{\partial \phi} - \beta^2\left(\frac{\partial^3 w}{\partial x^2 \partial \phi} + \frac{\partial^3 w}{\partial \phi^3}\right) = -\Omega^2 v - \frac{R}{h}\frac{1-\nu^2}{E}q_\phi\end{aligned} \tag{6.3}$$

$$\begin{aligned}-\nu\frac{\partial u}{\partial x} - \frac{\partial v}{\partial \phi} + \beta^2\left(\frac{\partial^3 v}{\partial x^2 \partial \phi} + \frac{\partial^3 v}{\partial \phi^3}\right) \\ - w - \beta^2\left(\frac{\partial^4 w}{\partial x^4} + 2\frac{\partial^4 w}{\partial x^2 \partial \phi^2} + \frac{\partial^4 w}{\partial \phi^4}\right) = -\Omega^2 w - \frac{R}{h}\frac{1-\nu^2}{E}q_r\end{aligned} \tag{6.4}$$

where x is the coordinate along the axis of the cylinder normalized by its radius R; h is the mean thickness of the cylinder; u, v, and w are respectively the axial, circumferential, and radial displacements; β is a dimensionless geometric parameter given by

$$\beta^2 = \frac{h^2}{12R^2} \tag{6.5}$$

Ω is the dimensionless frequency

$$\Omega = \frac{\omega R}{c_p} \tag{6.6}$$

where ω is the dimensional angular frequency and c_p is the speed of compressional waves in a flat plate:

$$c_p^2 = \frac{E}{\rho_s(1-\nu^2)} \tag{6.7}$$

E, ρ_s, and ν are respectively the Young's modulus, volumetric density, and Poisson's ratio of the cylinder material; and q_3 is the complex magnitude of the applied stress in the radial direction which has been nondimensionalized by the factor $E/(1-\nu^2)$. In our problem this applied stress is the pressure exerted by the powder on the tube wall from within.

We seek solutions of the form

$$u(x,\phi) = U\cos k_x x\,\cos n\phi \tag{6.8}$$
$$v(x,\phi) = V\sin k_x x\,\sin n\phi \tag{6.9}$$
$$w(x,\phi) = W\sin k_x x\,\cos n\phi \tag{6.10}$$

where k_x is the nondimensional wavenumber in the axial direction and n is an integer.

We assume stress loadings of the form

$$q_x = -\tau_{xr}\cos k_x x\,\cos n\phi \tag{6.11}$$
$$q_\phi = -\tau_{r\phi}\sin k_x x\,\sin n\phi \tag{6.12}$$
$$q_r = -\tau_{rr}\sin k_x x\,\cos n\phi \tag{6.13}$$

where the negative sign is necessary because the foam is on the inside of the shell.

Returning to the equations governing motion of the shell (6.2–6.4) and making use of (6.8)–(6.10) (6.11)–(6.13), we obtain algebraic equations for U, V, and W in the form

$$\left(k_x^4 A_4 + k_x^3 A_3 + k_x^2 A_2 + k_x A_1 + A_0 - \Omega^2 M\right)\begin{pmatrix} U \\ V \\ W\end{pmatrix} = -\frac{R}{h}\frac{1-\nu^2}{E}\begin{pmatrix}\tau_{xr}\\ \tau_{r\phi}\\ \tau_{rr}\end{pmatrix} \tag{6.14}$$

where

$$A_4 = \begin{bmatrix} 0 & 0 & 0 \\ 0 & 0 & 0 \\ 0 & 0 & \beta^2 \end{bmatrix} \tag{6.15}$$

$$A_3 = \begin{bmatrix} 0 & 0 & 0 \\ 0 & 0 & 0 \\ 0 & 0 & 0 \end{bmatrix} \tag{6.16}$$

$$A_2 = \begin{bmatrix} 1 & 0 & 0 \\ 0 & \frac{1-\nu}{2}(1+\beta^2) & n\beta^2 \\ 0 & n\beta^2 & 2\beta^2 n^2 \end{bmatrix} \tag{6.17}$$

$$A_1 = \begin{bmatrix} 0 & -n\frac{1+\nu}{2} & -\nu \\ -n\frac{1+\nu}{2} & 0 & 0 \\ -\nu & 0 & 0 \end{bmatrix} \tag{6.18}$$

$$A_0 = \begin{bmatrix} \frac{1-\nu}{2}n^2 & 0 & 0 \\ 0 & n^2(1+\beta^2) & n+n^3\beta^2 \\ 0 & n+n^3\beta^2 & 1+\beta^2 n^4 \end{bmatrix} \tag{6.19}$$

$$M = \begin{bmatrix} 1 & 0 & 0 \\ 0 & 1 & 0 \\ 0 & 0 & 1 \end{bmatrix} \tag{6.20}$$

6.4.2 Foam in Cylindrical Coordinates

The nondimensional equations of elasticity for a cylindrical solid (see Figure 6-14) under steady harmonic motion are given by

$$\begin{bmatrix} L_{11} & L_{12} & L_{13} \\ L_{21} & L_{22} & L_{23} \\ L_{31} & L_{23} & L_{33} \end{bmatrix} \begin{pmatrix} u_f \\ v_f \\ w_f \end{pmatrix} + \hat{\Omega}^2 \begin{bmatrix} 1 & 0 & 0 \\ 0 & 1 & 0 \\ 0 & 0 & 1 \end{bmatrix} \begin{pmatrix} u_f \\ v_f \\ w_f \end{pmatrix} = \begin{pmatrix} 0 \\ 0 \\ 0 \end{pmatrix} \tag{6.21}$$

where lengths and displacements have been nondimensionalized by the mean radius of the shell R,

$$L_{11} = (1-2\nu_f)\left(\frac{\partial^2}{\partial r^2} + \frac{1}{r}\frac{\partial}{\partial r} + \frac{1}{r^2}\frac{\partial^2}{\partial \phi^2}\right) + 2(1-\nu_f)\frac{\partial^2}{\partial x^2} \tag{6.22}$$

$$L_{12} = L_{21} = \frac{1}{r}\frac{\partial^2}{\partial \phi \partial x} \tag{6.23}$$

$$L_{13} = \frac{\partial^2}{\partial r \partial x} + \frac{1}{r}\frac{\partial}{\partial x} \tag{6.24}$$

$$L_{22} = (1-2\nu_f)\left(\frac{\partial^2}{\partial r^2} + \frac{1}{r}\frac{\partial}{\partial r} - \frac{1}{r^2} + \frac{\partial^2}{\partial x^2}\right) + 2(1-\nu_f)\frac{1}{r^2}\frac{\partial^2}{\partial \phi^2} \tag{6.25}$$

$$L_{23} = \frac{\partial^2}{\partial r \partial \phi} + (3-4\nu_f)\frac{1}{r^2}\frac{\partial}{\partial \phi} \tag{6.26}$$

$$L_{31} = \frac{\partial^2}{\partial r \partial x} \tag{6.27}$$

$$L_{32} = \frac{1}{r}\frac{\partial^2}{\partial r \partial \phi} - (3-4\nu_f)\frac{1}{r^2}\frac{\partial}{\partial \phi} \tag{6.28}$$

$$L_{33} = 2(1-\nu_f)\left(\frac{\partial^2}{\partial r^2} + \frac{1}{r}\frac{\partial}{\partial r} - \frac{1}{r^2}\right) + (1-2\nu_f)\left(\frac{1}{r^2}\frac{\partial^2}{\partial \phi^2} + \frac{\partial^2}{\partial x^2}\right) \tag{6.29}$$

and the nondimensional frequency is given by

$$\hat{\Omega}^2 = 2R_i^2(1+\nu_f)(1-2\nu_f)\frac{\rho_f}{E_f}\omega^2 = \frac{c_p^2}{\left(\frac{E_f}{2\rho_f(1+\nu_f)(1-2\nu_f)}\right)}\Omega^2 \tag{6.30}$$

Using the methods of Mirsky (1965) (also see Leissa [32]), we find the solutions to be

$$u(x,r,\phi) = U_f(r)\cos k_x x \cos n\phi \tag{6.31}$$

$$v(x,r,\phi) = V_f(r)\sin k_x x \sin n\phi \tag{6.32}$$

$$w(x,r,\phi) = W_f(r)\sin k_x x \cos n\phi \tag{6.33}$$

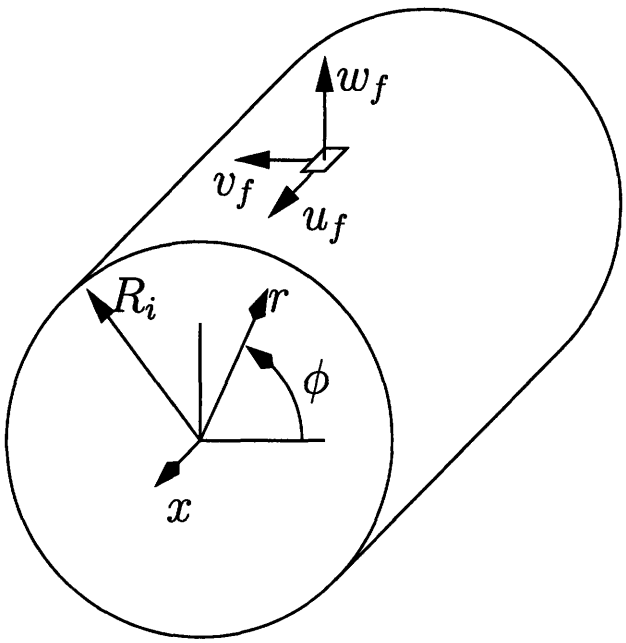

Figure 6-14: Schematic of cylinder geometry and displacements

where

$$U_f(r) = k_x A_{mn} J_n(p_1 r) + k_x B_{mn} Y_n(p_1 r) - \frac{p_2^2}{k_x} C_{mn} J_n(p_2 r) - \frac{p_2^2}{k_x} D_{mn} Y_n(p_2 r) \quad (6.34)$$

$$V_f(r) = -\left(\frac{n}{r} A_{mn} J_n(p_1 r) + \frac{n}{r} B_{mn} Y_n(p_1 r) + \frac{n}{r} C_{mn} J_n(p_2 r) + \frac{n}{r} D_{mn} Y_n(p_2 r) + E_{mn} \frac{dJ_n(p_2 r)}{dr} + F_{mn} \frac{dY_n(p_2 r)}{dr}\right) \quad (6.35)$$

$$W_f(r) = A_{mn} \frac{dJ_n(p_1 r)}{dr} + B_{mn} \frac{dY_n(p_1 r)}{dr} + C_{mn} \frac{dJ_n(p_2 r)}{dr} + D_{mn} \frac{dY_n(p_2 r)}{dr} + \frac{n}{r} E_{mn} J_n(p_2 r) + \frac{n}{r} F_{mn} Y_n(p_2 r) \quad (6.36)$$

where A_{mn}, B_{mn}, C_{mn}, D_{mn}, E_{mn}, and F_{mn} are constants, J_n is the Bessel function

of the first kind, Y_n is the Bessel function of the second kind and

$$p_1^2 = \frac{\hat{\Omega}^2}{2(1-\nu_f)} - k_x^2 \tag{6.37}$$

$$p_2^2 = \frac{\hat{\Omega}^2}{1-2\nu_f} - k_x^2 \tag{6.38}$$

The boundary conditions are

$$U_f(r=0) < \infty \tag{6.39}$$

$$V_f(r=0) < \infty \tag{6.40}$$

$$W_f(r=0) < \infty \tag{6.41}$$

$$U_f\left(r = \frac{R_i}{R}\right) = \overline{U} \tag{6.42}$$

$$V_f\left(r = \frac{R_i}{R}\right) = \overline{V} \tag{6.43}$$

$$W_f\left(r = \frac{R_i}{R}\right) = \overline{W} \tag{6.44}$$

The boundary conditions at $r = 0$ require $B_{mn} = 0 = D_{mn} = F_{mn}$. The remaining constants are found using

$$\begin{bmatrix} k_x J_n\left(p_1 \frac{R_i}{R}\right) & -\frac{p_2^2}{k_x} J_n\left(p_2 \frac{R_i}{R}\right) & 0 \\ -\frac{n}{\frac{R_i}{R}} J_n\left(p_1 \frac{R_i}{R}\right) & -\frac{n}{\frac{R_i}{R}} J_n\left(p_2 \frac{R_i}{R}\right) & -\frac{dJ_n\left(p_2 \frac{R_i}{R}\right)}{dr} \\ \frac{dJ_n\left(p_1 \frac{R_i}{R}\right)}{dr} & \frac{dJ_n\left(p_2 \frac{R_i}{R}\right)}{dr} & \frac{n}{\frac{R_i}{R}} J_n\left(p_2 \frac{R_i}{R}\right) \end{bmatrix} \begin{pmatrix} A_{mn} \\ C_{mn} \\ E_{mn} \end{pmatrix} = \begin{pmatrix} \overline{U} \\ \overline{V} \\ \overline{W} \end{pmatrix} \tag{6.45}$$

To facilitate a later step, we divide the solutions for A_{mn}, C_{mn}, and E_{mn} into parts corresponding to the cases where the right hand side is given by $\begin{pmatrix} 1 & 0 & 0 \end{pmatrix}^T$, $\begin{pmatrix} 0 & 1 & 0 \end{pmatrix}^T$, and $\begin{pmatrix} 0 & 0 & 1 \end{pmatrix}^T$ such that

$$\overline{U} \begin{pmatrix} A_{mnU} \\ C_{mnU} \\ E_{mnU} \end{pmatrix} + \overline{V} \begin{pmatrix} A_{mnV} \\ C_{mnV} \\ E_{mnV} \end{pmatrix} + \overline{W} \begin{pmatrix} A_{mnW} \\ C_{mnW} \\ E_{mnW} \end{pmatrix} = \begin{pmatrix} A_{mn} \\ C_{mn} \\ E_{mn} \end{pmatrix} \tag{6.46}$$

Using the displacements, the stresses at the interface of the foam and the cylin-

drical shell are given by

$$\tau_{rx} = \frac{E_f}{(1+\nu_f)\left(\frac{R_i}{R}\right)^2}\left\{k_x\frac{R_i}{R}\left[nJ_n\left(p_1\frac{R_i}{R}\right) - p_1\frac{R_i}{R}J_{n+1}\left(p_1\frac{R_i}{R}\right)\right]A_{mn}\right.$$
$$+\frac{\frac{R_i}{R}}{2k_x}(k_x^2-p_2^2)\left[nJ_n\left(p_2\frac{R_i}{R}\right) - p_2\frac{R_i}{R}J_{n+1}\left(p_2\frac{R_i}{R}\right)\right]C_{mn}$$
$$\left.+\frac{k_x\frac{R_i}{R}}{2}nJ_n\left(p_2\frac{R_i}{R}\right)E_{mn}\right\} \quad (6.47)$$

$$\tau_{r\phi} = \frac{E_f}{(1+\nu_f)\left(\frac{R_i}{R}\right)^2}\left\{\left[-n(n-1)J_n\left(p_1\frac{R_i}{R}\right) + np_1\frac{R_i}{R}J_{n+1}\left(p_1\frac{R_i}{R}\right)\right]A_{mn}\right.$$
$$+\left[-n(n-1)J_n\left(p_2\frac{R_i}{R}\right) + np_2\frac{R_i}{R}J_{n+1}\left(p_2\frac{R_i}{R}\right)\right]C_{mn}$$
$$\left.+\left[-\left(n^2-n-\frac{p_2^2r^2}{2}\right)J_n\left(p_2\frac{R_i}{R}\right) - p_2\frac{R_i}{R}J_{n+1}\left(p_2\frac{R_i}{R}\right)\right]E_{mn}\right\} \quad (6.48)$$

$$\tau_{rr} = \frac{E_f}{(1+\nu_f)\left(\frac{R_i}{R}\right)^2}\left\{\left[\frac{1}{2}\left(2n(n-1)+(k_x^2-p_2^2)\frac{R_i^2}{R^2}\right)J_n\left(p_1\frac{R_i}{R}\right)\right.\right.$$
$$\left.+p_1\frac{R_i}{R}J_{n+1}\left(p_1\frac{R_i}{R}\right)\right]A_{mn}$$
$$+\left[\left(n(n-1)-p_2^2\frac{R_i^2}{R^2}\right)J_n\left(p_2\frac{R_i}{R}\right) + p_2\frac{R_i}{R}J_{n+1}\left(p_2\frac{R_i}{R}\right)\right]C_{mn}$$
$$\left.+\left[n(n-1)J_n\left(p_2\frac{R_i}{R}\right) - np_2\frac{R_i}{R}J_{n+1}\left(p_2\frac{R_i}{R}\right)\right]E_{mn}\right\} \quad (6.49)$$

These stresses can be written in terms of the shell displacements

$$\begin{pmatrix}\tau_{rx}\\ \tau_{r\phi}\\ \tau_{rr}\end{pmatrix} = \frac{E_f}{(1+\nu_f)\frac{R_i^2}{R^2}}\begin{bmatrix}\alpha_1 & \alpha_2 & \alpha_3\\ \alpha_4 & \alpha_5 & \alpha_6\\ \alpha_7 & \alpha_8 & \alpha_9\end{bmatrix}\begin{bmatrix}A_{mnU} & A_{mnV} & A_{mnW}\\ C_{mnU} & C_{mnV} & C_{mnW}\\ E_{mnU} & E_{mnV} & E_{mnW}\end{bmatrix}\begin{pmatrix}\overline{U}\\ \overline{V}\\ \overline{W}\end{pmatrix} \quad (6.50)$$

where

$$\alpha_9 = n(n-1)J_n\left(p_2\frac{R_i}{R}\right) - np_2\frac{R_i}{R}J_{n+1}\left(p_2\frac{R_i}{R}\right) \tag{6.51}$$

$$\alpha_6 = -\left(n^2 - n - \frac{p_2^2 r^2}{2}\right)J_n\left(p_2\frac{R_i}{R}\right) - p_2\frac{R_i}{R}J_{n+1}\left(p_2\frac{R_i}{R}\right) \tag{6.52}$$

$$\alpha_3 = \frac{k_x\frac{R_i}{R}}{2}nJ_n\left(p_2\frac{R_i}{R}\right) \tag{6.53}$$

$$\alpha_8 = \left(n(n-1) - p_2^2\frac{R_i^2}{R^2}\right)J_n\left(p_2\frac{R_i}{R}\right) + p_2\frac{R_i}{R}J_{n+1}\left(p_2\frac{R_i}{R}\right) \tag{6.54}$$

$$\alpha_5 = -n(n-1)J_n\left(p_2\frac{R_i}{R}\right) + np_2\frac{R_i}{R}J_{n+1}\left(p_2\frac{R_i}{R}\right) \tag{6.55}$$

$$\alpha_2 = \frac{\frac{R_i}{R}}{2k_x}(k_x^2 - p_2^2)\left(nJ_n\left(p_2\frac{R_i}{R}\right) - p_2\frac{R_i}{R}J_{n+1}\left(p_2\frac{R_i}{R}\right)\right) \tag{6.56}$$

$$\alpha_7 = \frac{1}{2}\left(2n(n-1) + (k_x^2 - p_2^2)\frac{R_i^2}{R^2}\right)J_n\left(p_1\frac{R_i}{R}\right) + p_1\frac{R_i}{R}J_{n+1}\left(p_1\frac{R_i}{R}\right) \tag{6.57}$$

$$\alpha_4 = -n(n-1)J_n\left(p_1\frac{R_i}{R}\right) + np_1\frac{R_i}{R}J_{n+1}\left(p_1\frac{R_i}{R}\right) \tag{6.58}$$

$$\alpha_1 = k_x\frac{R_i}{R}\left(nJ_n\left(p_1\frac{R_i}{R}\right) - p_1\frac{R_i}{R}J_{n+1}\left(p_1\frac{R_i}{R}\right)\right) \tag{6.59}$$

6.4.3 Iterative Solution for the Wavenumber

Using the relations for the stresses developed at the exterior of the foam, we can write the governing equation for the foam as

$$\begin{aligned}&\left(k_x^4A_4 + k_x^3A_3 + k_x^2A_2 + k_xA_1 + A_0 - \Omega^2M\right)\begin{pmatrix}U\\V\\W\end{pmatrix}\\ &= -\frac{R}{h}\frac{1-\nu^2}{E}\frac{E_f}{(1+\nu_f)\frac{R_i^2}{R^2}}\begin{bmatrix}\alpha_1 & \alpha_2 & \alpha_3\\ \alpha_4 & \alpha_5 & \alpha_6\\ \alpha_7 & \alpha_8 & \alpha_9\end{bmatrix}\begin{bmatrix}A_{mnU} & A_{mnV} & A_{mnW}\\ C_{mnU} & C_{mnV} & C_{mnW}\\ E_{mnU} & E_{mnV} & E_{mnW}\end{bmatrix}\begin{pmatrix}U\\V\\W\end{pmatrix}\end{aligned} \tag{6.60}$$

This equation may be written in a simplified form as

$$\left(k_x^4A_4 + k_x^3A_3 + k_x^2A_2 + k_xA_1 + A_0 + A_f - \Omega^2M\right)\begin{pmatrix}U\\V\\W\end{pmatrix} = \begin{pmatrix}0\\0\\0\end{pmatrix} \tag{6.61}$$

where A_f is a matrix that represents the complex impedance of the foam given by

$$A_f = \frac{R}{h}\frac{1-\nu^2}{E}\frac{E_f}{(1+\nu_f)\frac{R_i^2}{R^2}}\begin{bmatrix}\alpha_1 & \alpha_2 & \alpha_3\\ \alpha_4 & \alpha_5 & \alpha_6\\ \alpha_7 & \alpha_8 & \alpha_9\end{bmatrix}\begin{bmatrix}A_{mnU} & A_{mnV} & A_{mnW}\\ C_{mnU} & C_{mnV} & C_{mnW}\\ E_{mnU} & E_{mnV} & E_{mnW}\end{bmatrix} \tag{6.62}$$

Now that we have an equation for the combined foam-shell system, we must solve for the wavenumber k_x. Because the matrix A_f is a nonlinear function of the wavenumber k_x and A_f is relatively small, we use an iterative approach to solve for the wavenumber. First, for each desired value of n over the desired frequency range we compute the corresponding wavenumbers for the empty shell (i.e. by setting $A_f = 0$ in (6.61)). Then, using this initial estimate for the wavenumber we calculate the stresses developed in the foam at the interface with the shell and the corresponding matrix A_f. Next, we recalculate the wavenumber using (6.61). We continue to recalculate A_f and the wavenumber until the value of the wavenumber converges to within a desired error. For an error of 1×10^{-9} in the wavenumber, usually only three iterations are necessary.

To solve (6.61) for the wavenumber k_x as a function of frequency, we treat the problem as a polynomial eigenvalue problem, which can easily be transformed into a traditional eigenvalue problem. There are multiple solutions for the wavenumber corresponding to different modes shapes and to right or left travelling waves. To select the appropriate solution, we examine the corresponding mode shape and choose a single direction of propagation for consistency.

6.4.4 Loss Factor

Once k_x has been determined, we estimate the equivalent loss factor as a function of frequency. To do this, we again consider an empty cylinder, now characterized by an "effective" complex Young's modulus $E = E_0(1 + j\eta)$. Then the loss factor is given by

$$\eta = \frac{\operatorname{Im} E}{\operatorname{Re} E} \tag{6.63}$$

As a result of the nondimensionalization, the modulus of the tube only appears in the nondimensional frequency parameter Ω given by (6.6). For each value of n, we use the set of k_x obtained above and (6.14) with the inertia matrix given by the identity matrix becomes an eigenvalue problem for Ω^2 for the empty tube. In solving the eigenvalue problem we obtain multiple solutions for Ω^2, and the appropriate value is chosen after examination of the corresponding mode shape. Finally, the loss factor is obtained using

$$\eta = \frac{\operatorname{Im} \frac{1}{\Omega^2}}{\operatorname{Re} \frac{1}{\Omega^2}} \tag{6.64}$$

6.5 Results

Figures 6-15-6-20 show the loss factor curves and experimental loss factor measurments for the cylinder filled with Foamex Sensus foam. Based on the loss factor curves, we conclude this model and solution method are a good predictor of the loss factor. In Figure 6-20 the experimental data occur at a lower frequency than theoretical curve shows. There are a few contributing factors to this result. The dispersion relation of the undamped curve is calculated beginning a small percentage above the

cutoff frequency. Even though the added mass of the foam effectively lowers the cutoff frequency, it is not easy to calculate the loss factor and dispersion relation at frequencies below the original cutoff of the empty cylinder. Furthermore, the prediction of the cutoff frequency by the shell model is not exact.

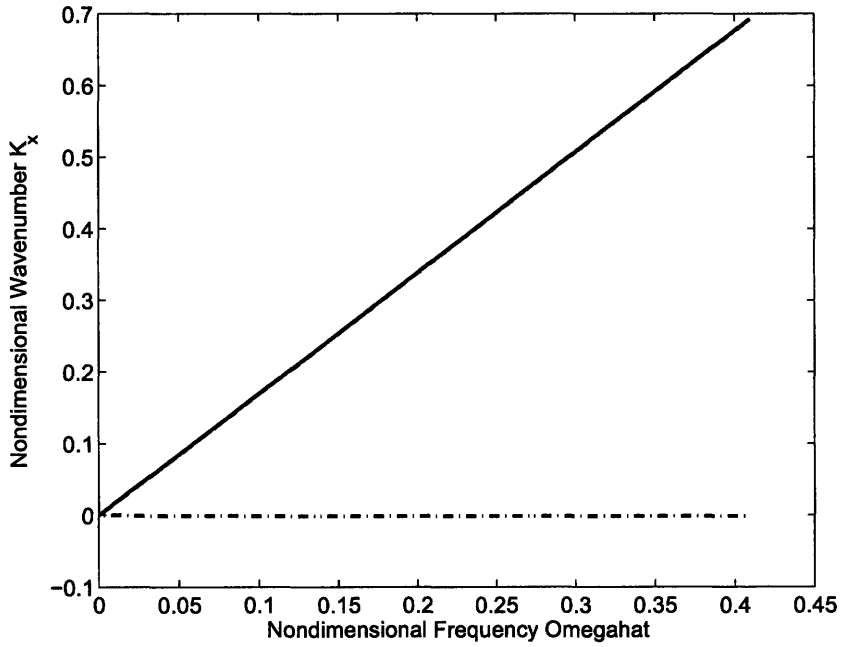

Figure 6-15: Loss factor as a function of frequency for torsional ($n = 0$) modes

6.6 Discussion

We define a new, nondimensional frequency that is normalized by the parameters of the low-wave-speed material given by

$$\hat{\Omega} = \Omega \frac{c_p}{\sqrt{\frac{\Re(E_f)}{2\rho_f(1+\nu_f)(1-2*\nu_f)}}} \tag{6.65}$$

Damping attains local maxima and minima when $\hat{\Omega}$ is order unity.

Typical dimensionless dispersion relations for $n = 0$ (torsion), $n = 1$ and $n = 2$ are given in Figures 6-21-6-26, respectively. The dispersion curve gives the relation between the wavenumber and frequency for a travelling wave in an infinite cylinder. The standing wave behavior (i.e., natural frequencies) for a finite tube can be approximated using the dispersion curve. A resonance in the finite tube occurs when the wavenumber is approximately an integer multiple of the inverse of the length of the cylinder. The values of the wavenumber at which resonances occur should not vary significantly from the empty to filled cylinders; therefore, a comparison between the

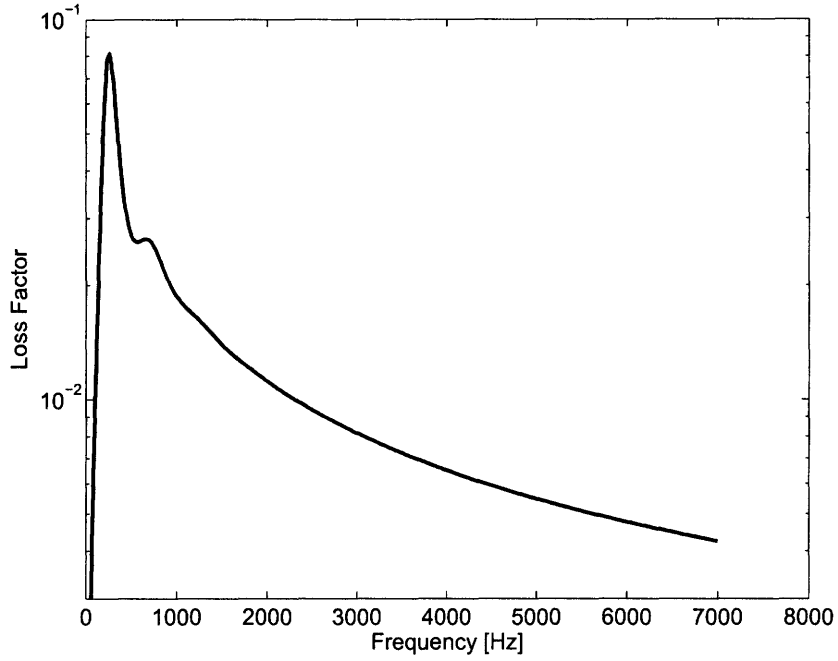

Figure 6-16: Loss factor as a function of frequency for axial ($n = 0$) modes

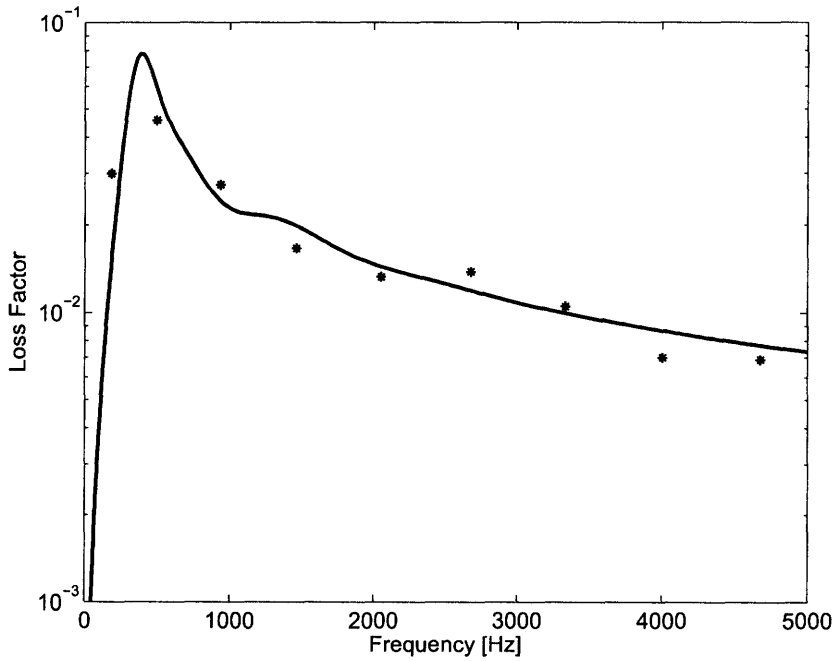

Figure 6-17: Loss factor as a function of frequency for $n = 1$. Asterisks denote data from Table 6.1.

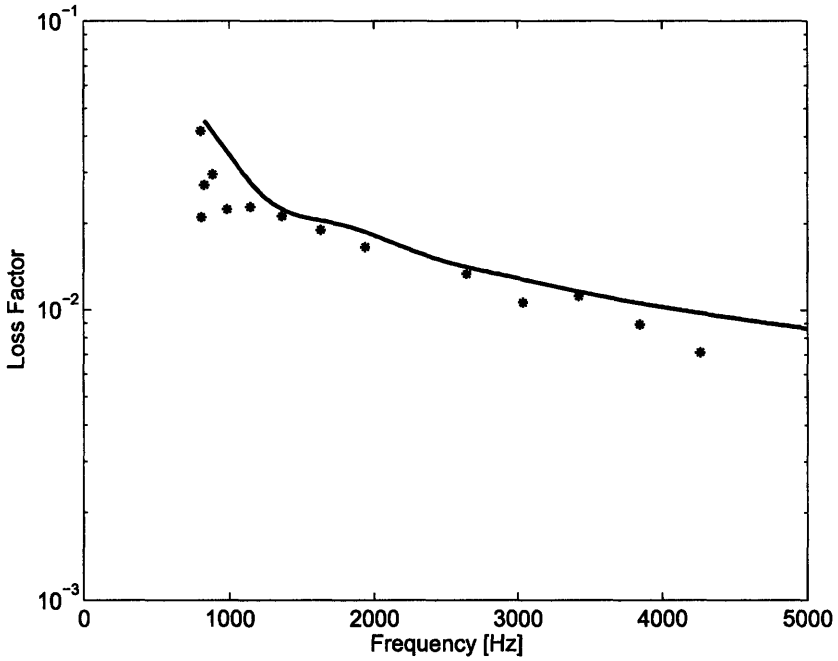

Figure 6-18: Loss factor as a function of frequency for $n = 2$. Asterisks denote data from Table 6.2.

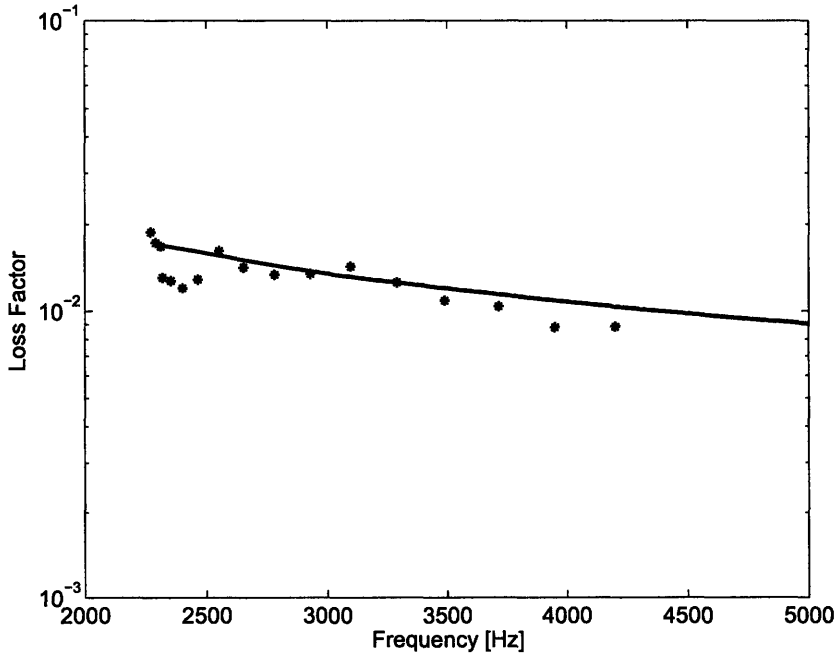

Figure 6-19: Loss factor as a function of frequency for $n = 3$. Asterisks denote data from Table 6.3.

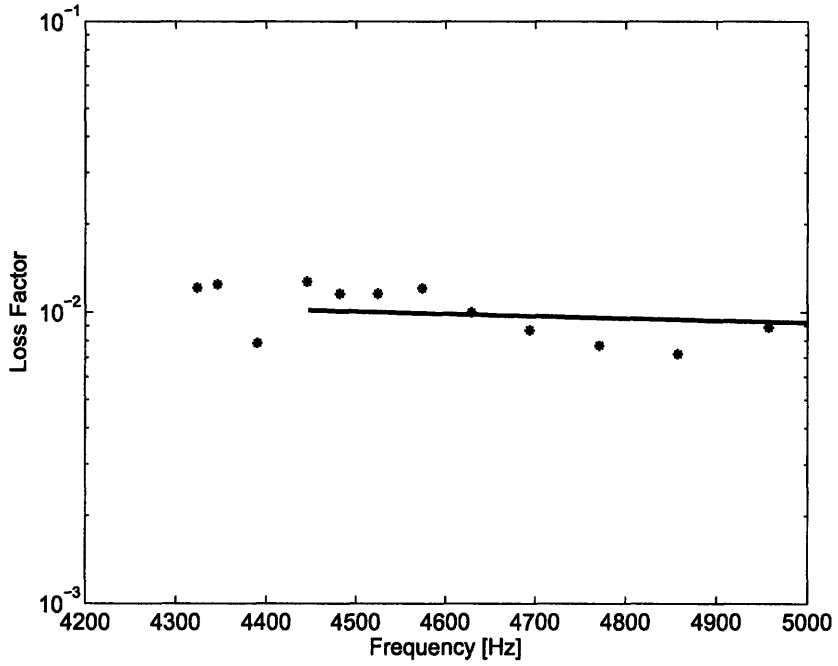

Figure 6-20: Loss factor as a function of frequency for $n = 4$. Asterisks denote data from Table 6.4.

dispersion relation for the filled cylinder and the real part of the dispersion relation for the unfilled cylinder can be used to explain the differences in behavior of the filled and unfilled finite cylinders.

The axial and torsional ($n = 0$) modes have linear dispersion relations because those waves are nondispersive. The bending and wall flexing modes are dispersive and have nonlinear dispersion relations. For $n > 1$ and the $n = 0$ breathing modes, there is a non-zero cutoff frequency so the dispersion relation does not start at zero frequency.

The real part of the dispersion relation does not vary significantly from the dispersion relation for the empty cylinder. At frequencies where the real part of the dispersion relation for the filled cylinder lies above the dispersion relation for the empty cylinder, the low-wave-speed material is acting as an added mass, lowering the resonant frequencies for a given mode shape. At frequencies where the real part of the dispersion relation of the filled cylinder lies below that of the empty cylinder, the low-wave-speed material is acting to stiffen the cylinder. For lossy low-wave-speed media, the real part of the dispersion relation of the filled cylinder will be monotonically increasing. For low-wave-speed materials with small loss factors, the real part of the dispersion curve may have inflection points near the resonant frequencies of the low-wave-speed material. Near these frequencies, the system may experience mode splitting, two resonant frequencies exist in the neighborhood where only one resonance existed in the undamped system. This behavior is analogous to a tuned-mass damper.

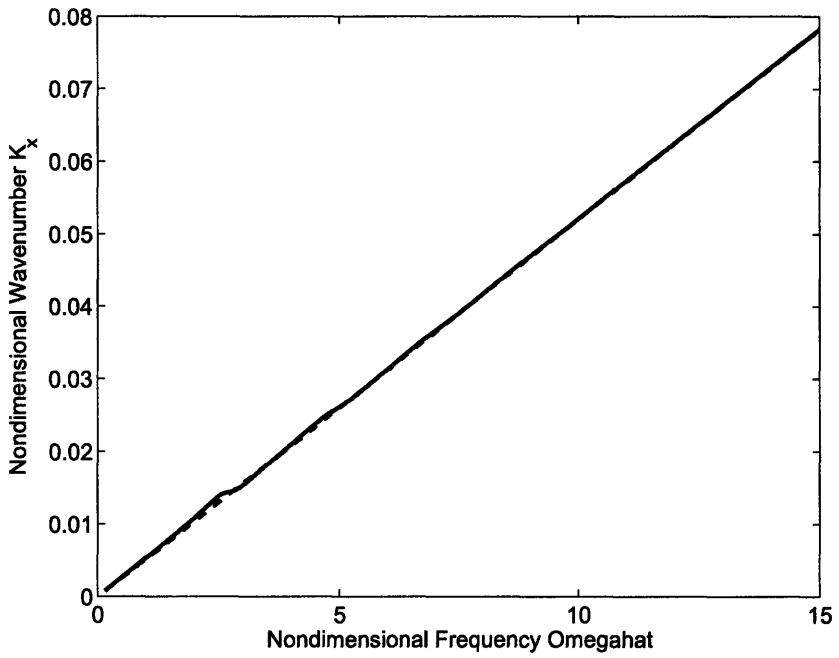

Figure 6-21: Dispersion relation of empty cylinder (dashed) and real part of dispersion relation of foam-filled cylinder (solid) for torsional ($n = 0$) modes

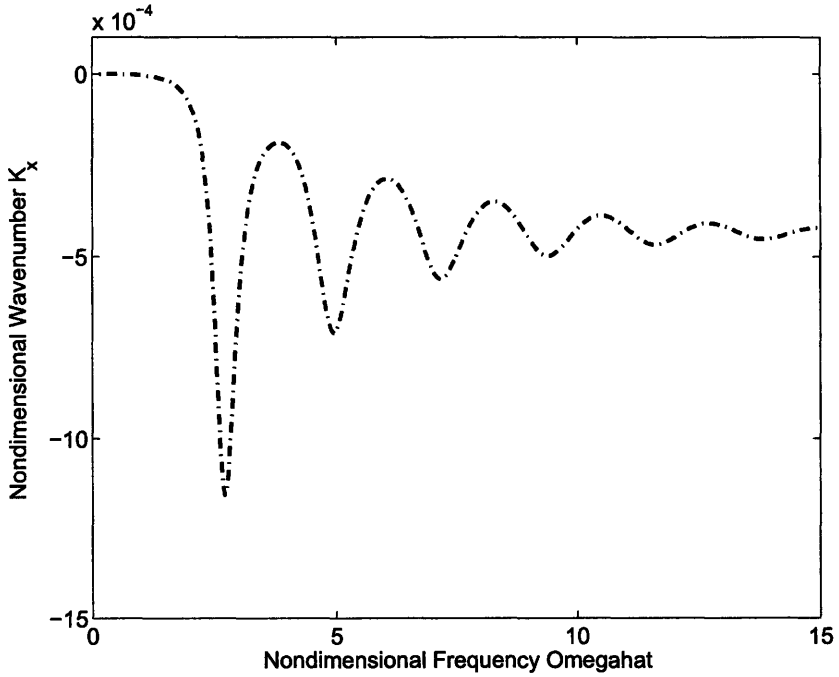

Figure 6-22: Imaginary part of the dispersion relation for foam-filled cylinder for the torsional ($n = 0$) modes and $\eta = 0.2$

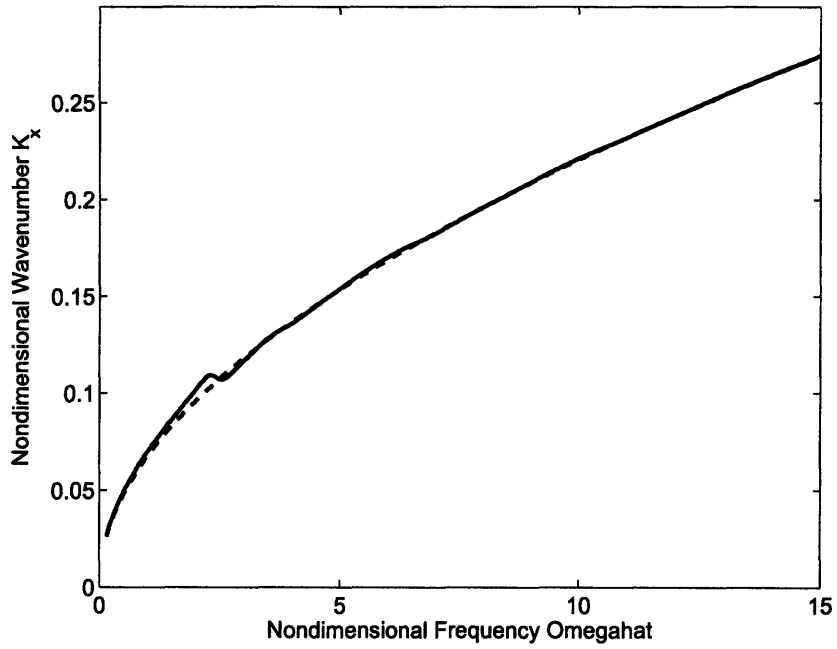

Figure 6-23: Dispersion relation of empty cylinder (dashed) and real part of dispersion relation of foam-filled cylinder (solid) for bending ($n = 1$) modes

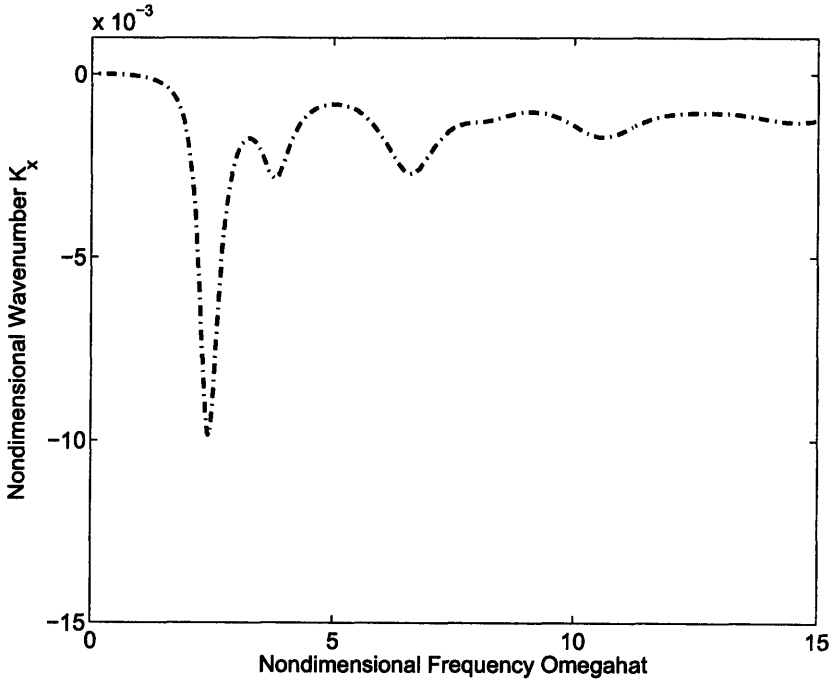

Figure 6-24: Imaginary part of the dispersion relation for cylinder filled with foam for the bending ($n = 1$) modes and $\eta = 0.2$

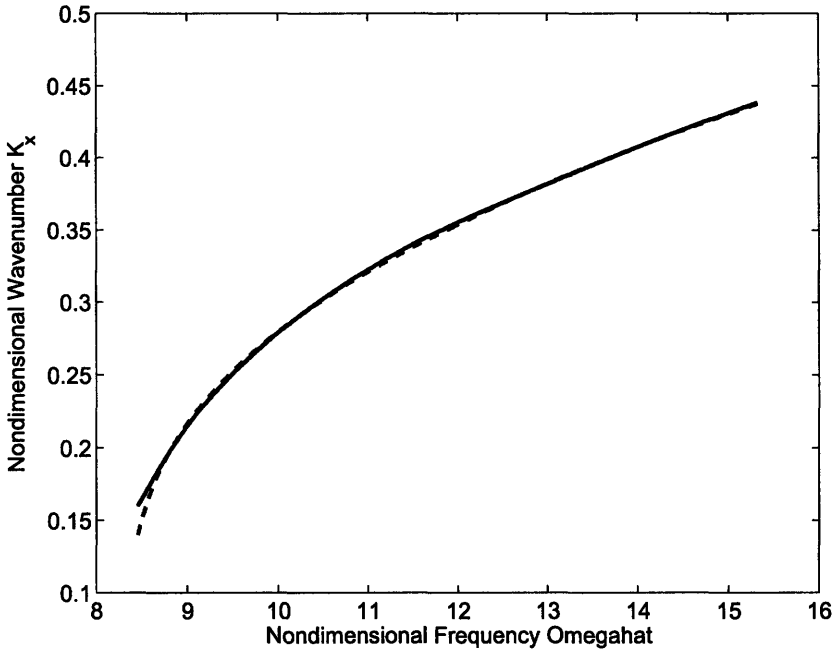

Figure 6-25: Dispersion relation of empty cylinder (dashed) and real part of dispersion relation of foam-filled cylinder (solid) for $n = 2$ modes

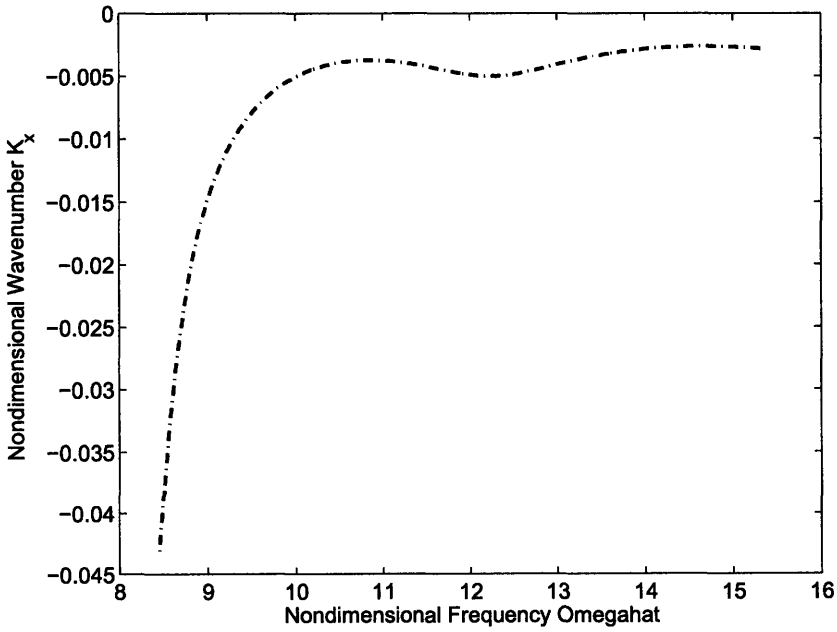

Figure 6-26: Imaginary part of the dispersion relation for cylinder filled with foam for the $n = 2$ vibratory modes and $\eta = 0.2$

The imaginary part of the dispersion relation determines the decay of the wave, or the damping. It has local maxima and minima corresponding to local minima and maxima in loss factor.

Figures 6-27 and 6-28 show typical loss factor curves for $n = 0$ (torsion) and $n = 1$.

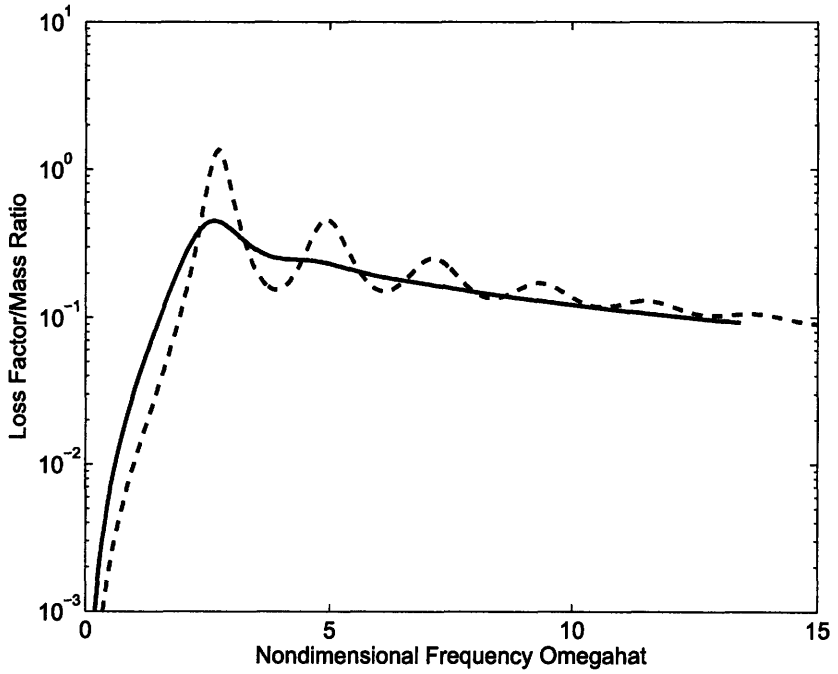

Figure 6-27: Nondimensional loss factor curves for torsional ($n = 0$) mode with $\eta = 0.2$ (dashed) and $\eta = 0.7$ (solid)

6.7 Conclusions

The results of the experiments described in this paper demonstrate that filling a thin-walled cylinder with a soft, low-density foam material can provide considerable damping in a simple and inexpensive manner. We have developed a model that couples shell vibrations to a lossy, elastic material and computes dispersion relations and loss factor curves as functions of frequency for the various mode shapes. The travelling-wave behavior described by the dispersion relations is used to approximate the damping in the standing-wave behavior observed in resonant response of finite cylinders. The theoretical loss factor curves agree well with the measured results for beam bending modes and tube-wall-flexing modes.

Potential applications of this damping method include reduction of structure-borne sound. Such an example is autmotive driveshafts whose modes are excited by gear teeth meshing as well as other closed structures where moderate frequency vibrations are a nuisance. Further work is needed to identify and characterize low-wave-speed materials that are lightweight and lossy.

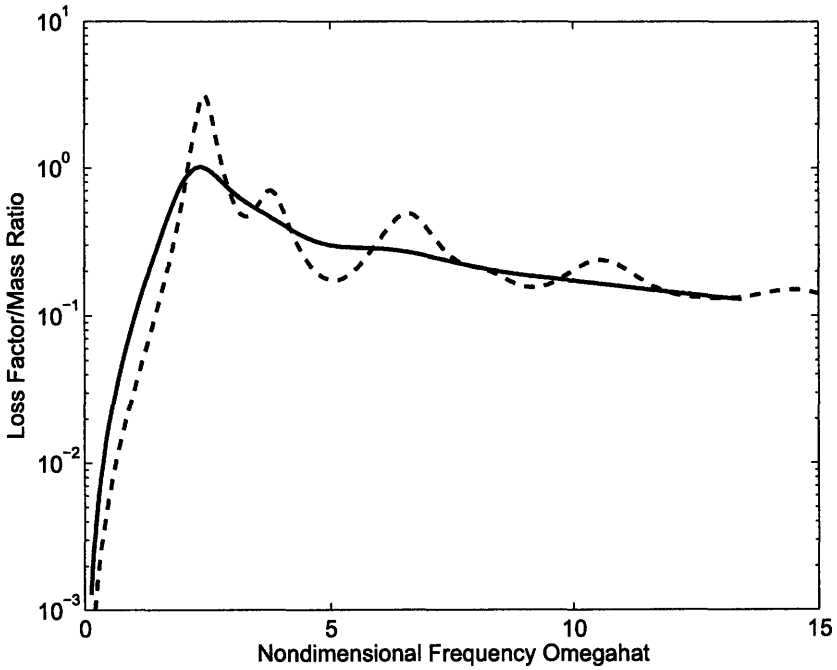

Figure 6-28: Nondimensional loss factor curves for $n = 1$ mode with $\eta = 0.2$ (dashed) and $\eta = 0.7$ (solid)

Chapter 7

Finite element analysis of structures coupled to lightweight, low-wave-speed materials

7.1 Introduction

The finite element method is a valuable tool for analysis and design of structures. Eigenvalue problems are frequently encountered when solving for mode shapes and natural frequencies. Numerical methods for the solution of eigenvalue problems are well studied (see e.g., [21]). To facilitate the solution of eigenvalue problems of structures containing low-wave-speed media, a numerical method is tailored for such problems.

The resulting eigenvalue problems of structures containing low-wave-speed media have certain characteristics, some of which make the numerical methods more difficult to implement. The addition of low-wave-speed media to a structure significantly increases the size of the discritized system matrices. The increase size of the matrices greatly increases the computation time for standard algorithms. As an example, the number of elements for a thin-walled cylinder is approximately proportional to the surface area of the cylinder, but the number of elements for a cylinder filled with LWSM is approximately proportional to the volume. In general, the low-wave-speed media has frequency dependent properties. The frequency dependence means that the eigenvalue problem becomes nonlinear, and the standard algorithms are no longer useful. Furthermore, these systems have eigenmodes which consist primarliy of motion of the LWSM and, therefore, have a very high loss factor. Hence, the modes are irrelevant to the practical engineer, and it is inefficient and unnecessary to solve for them.

Similar problems of complex eigenvalues and frequency dependent material properties arise when using finite elements to analyze structures with constrained layer damping. Johnson and Kienholz [29] obtain estimates of the loss factor using the modal strain energy method. In the modal strain energy method, the mode shapes are assumed to be real and the loss factor is calculated from a summation of the

ratio of the loss factor of each element times the strain energy in that element to the total strain energy of the structure. Leung [33] extended the common subspace iteration method to symmetric, complex matrices, which makes it useful for calculating a few eigenvalues of frequency independent systems. Ma and He [36] use an asymptotic method in which the natural frequency, loss factor, and eigenvector are expanded in a series to solve the complex eigenvalue problem of damped sandwich plates. Potier-Ferry and co-workers [11, 14, 37] extend the asymptotic method using Padé approximants and homotopy. Cortès and Elejabarrieta [8] use the undamped eigenvalues and eigenvectors as the starting point. Then, they begin an iterative loop which computes eigenvector derivatives and uses the Rayleigh quotient to find the eigenvalue. Because the method calculates each eigensolution individually, frequency dependent properties can be used by updating the frequency dependent portions of the matrices during each iteration. Wagner *et al* [68] model foam using a discrete Kelvin model in finite element simulations of automotive structures damped with foam. Chen *et al* [5] analyze finite element models of sandwich structures using a two step approach. In the first step, they calculate the eigensolution of the real part of the system using an asymptotic method. In the second step, they use order reduction on the full complex system. Dewulf and De Roeck [12] compare four approximate eigensolution methods for frequency-dependent constrained layer systems and use modal strain energy to calculate the loss factor. Wang and Wereley [69] use a spectral finite element analysis in which the elements are formulated using the travelling wave displacement solutions to analyze sandwich beams with frequency dependent constrained layer damping. Lin and Xia [34] solve the eigenproblem for undamped, frequency-dependent structures using dynamic condensation.

In this chapter, we develop an eigenvalue solution method for the finite-element discritization of a multi-degree-of freedom structure coupled to a lightweight, frequency-dependent damping material. The underlying principle of operation is that the mode shapes of the primary structure do not change significantly with the addition of the damping material, and therefore, the motion of the low-wave-speed media can be treated as a forced problem. First, the desired eigenvalues and eigenvectors of the undamped structure are calculated using a traditional method, such as subspace iteration or Lanczos method. Then, for each desired eigenvalue and eigenvector of the primary structure, the displacement of the damping material is calculated using the structure as the excitation and the eigenvalue estimate as the driving frequency. The eigenvalue of the full system is then calculated using the Rayleigh quotient. Iterations continue on the deformation of the damping material using the newest estimate of the eigenvalue until convergence. Finally, the loss factor can be calculated as the ratio of the imaginary part to the real part of the eigenvalue.

This method has the advantage that it only calculates the desired modes, not the well damped modes which are dominated by motion of the low-wave-speed medium. Furthermore, it allows for frequency dependent materials to be used. The method relies on its separation into a smaller eigenvalue problem and a smaller forced problem to attain computational efficiency.

7.2 Approximate Eigensolution Method

The finite element model of the primary structure is characterized by a mass matrix M_s and stiffness matrix K_s. The finite-element model of the damping material is characterized by a mass matrix M_f and frequency-dependent, complex stiffness matrix $K_f(\omega)$. The damping material and primary structure are coupled together without slip such that there are common degrees of freedom between the two models (see Figure 7-1). The displacement vector of the primary structure may be partitioned into the "free" and interfacial degrees of freedom

$$u_s = \begin{pmatrix} u_{sf} \\ u_i \end{pmatrix} \tag{7.1}$$

and the displacement vector of the damping material can similarly be partitioned

$$u_f = \begin{pmatrix} u_i \\ u_{ff} \end{pmatrix} \tag{7.2}$$

Based on these displacement vectors, the mass and stiffness matrices for the primary structure and damping material can be partitioned

$$M_s = \begin{bmatrix} M_{sf} & M_{si} \\ M_{si}^T & M_{sii} \end{bmatrix} \tag{7.3}$$

$$K_s = \begin{bmatrix} K_{sf} & K_{si} \\ K_{si}^T & K_{sii} \end{bmatrix} \tag{7.4}$$

$$M_f = \begin{bmatrix} M_{fii} & M_{fi} \\ M_{fi}^T & M_{ff} \end{bmatrix} \tag{7.5}$$

$$K_f(\omega) = \begin{bmatrix} K_{fii} & K_{fi} \\ K_{fi}^T & K_{ff} \end{bmatrix} \tag{7.6}$$

where $K_f(\omega)$ is complex and possibly frequency depenedent due to its nature as a lossy material.

The governing equations for the combined system are given by

$$\left(\begin{bmatrix} K_{sf} & K_{si} & 0 \\ K_{si}^T & K_{sii} + K_{fii} & K_{fi} \\ 0 & K_{fi}^T & K_{ff} \end{bmatrix} - \omega^2 \begin{bmatrix} M_{sf} & M_{si} & 0 \\ M_{si}^T & M_{sii} + M_{fii} & M_{fi} \\ 0 & M_{fi}^T & M_{ff} \end{bmatrix} \right) \begin{pmatrix} x_{sf} \\ x_i \\ x_{ff} \end{pmatrix} = \begin{pmatrix} 0 \\ 0 \\ 0 \end{pmatrix} \tag{7.7}$$

where we have not written the frequency dependence and loss factor of the damping material for compactness.

The first step is to calculate the eigensolution of the primary structure given by

$$(K_s - \omega_0^2 M_s) \begin{pmatrix} x_{sf} \\ x_i \end{pmatrix} = 0 \tag{7.8}$$

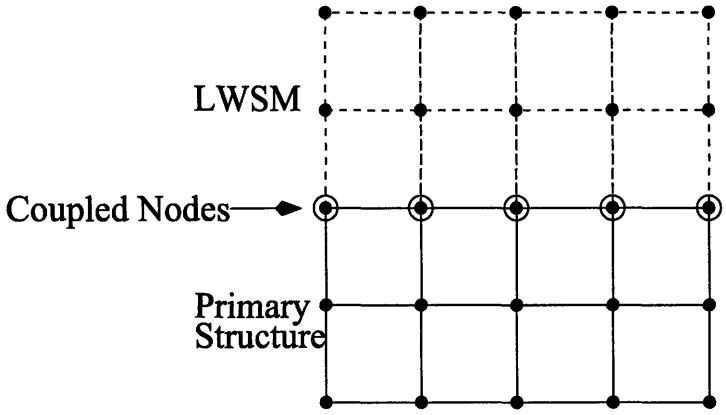

Figure 7-1: Schematic of coupled finite element mesh for primary structure and low-wave-speed material

to serve as the starting point for the damped structure. Any standard algorithm such as subspace iteration or Lanczos method can be used. For computation efficiency, only the desired number of modes should be calculated.

Then, the iterative loop begins. The displacement of the foam is calculated using dynamic condensation and is given by

$$x_{ff} = -(\hat{K}_{ff} - \hat{\omega}^2 M_{ff})^{-1}(\hat{K}_{fi}^T - \hat{\omega}^2 M_{fi}^T)x_i \tag{7.9}$$

where $\hat{\omega}$ is the current estimate of the natural freuqency. This current estimate $\hat{\omega}$ is used to evaluate the stiffness matrices if the system is frequency dependent. Matrix inversion is not used because it is computationally expensive. Rather, the system is solved using a more efficient algorithm.

Then, the eigenvalue is estimated using the complex Rayleigh quotient of the full system

$$\hat{\omega}_{k+1}^2 = \frac{v^T \begin{bmatrix} K_{sf} & K_{si} & 0 \\ K_{si}^T & K_{sii} + K_{fii} & K_{fi} \\ 0 & K_{fi}^T & K_{ff} \end{bmatrix} v}{v^T \begin{bmatrix} M_{sf} & M_{si} & 0 \\ M_{si}^T & M_{sii} + M_{fii} & M_{fi} \\ 0 & M_{fi}^T & M_{ff} \end{bmatrix} v} \tag{7.10}$$

where the eigenvector v is given by

$$v = \begin{pmatrix} x_{sf} \\ x_i \\ x_{ff} \end{pmatrix} \tag{7.11}$$

Iterations continue by recalculating x_{ff} using the newest estimate of ω until ω has converged.

An inherent assumption in this procedure is that the that changes in the interfacial

component of the eigenvector V_{si} will be small at each iteration. Because we are concerned with systems involving a small added mass and stiffness, this assumption has merit.

One possible problem is that dynamic condensation eliminates the ability to obtain certain modes. This is clearly seen in a single degree of freedom system with an attached absorber. Dynamic condensation of the absorber results in an equation with a single root even though there are two modes for this system.

7.3 Implementation and Results

The approximate eigenvalue solver and following examples are implemented using Matlab.

7.3.1 Sample Analytical Problem

In this section, we consider an example which can be solved analytically for comparison. We consider a single-degree-of-freedom spring-mass system to which is attached a uniform bar with modulus $E(1+j\eta)$, cross-section A, density ρ and length ℓ. The left end of the bar ($x = 0$) has a lumped mass M and is connected to ground with a spring K as shown in Figure 7-2. The governing equation of the bar under steady harmonic motion is

$$\frac{\partial^2 u}{\partial x^2} + \frac{\omega^2}{c^2} u = 0 \tag{7.12}$$

where c is given by

$$c^2 = \frac{E}{\rho} \tag{7.13}$$

and

$$E = E_o(1 + j\eta) \tag{7.14}$$

The boundary conditions on the ends of the bar are

$$EA\frac{\partial u(x=0)}{\partial x} = (K - \omega^2 M)u(x=0) \tag{7.15}$$

and

$$\frac{\partial u(x=\ell)}{\partial x} = 0 \tag{7.16}$$

The solution to (7.12) is

$$u(x) = c_1 \sin\frac{\omega}{c}x + c_2 \cos\frac{\omega}{c}x \tag{7.17}$$

The boundary condition at $x = 0$ gives

$$\frac{c_1}{c_2} = \frac{K - \omega^2 M}{EA\frac{\omega}{c}} \tag{7.18}$$

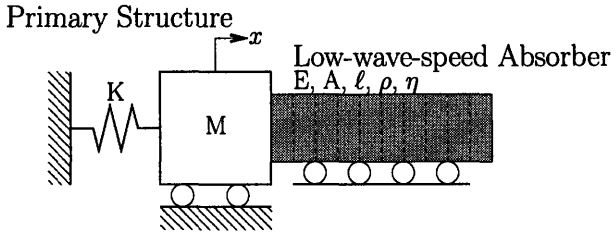

Figure 7-2: Sketch of single-degree-of-freedom system with LWSM absorber

The boundary condition at $x = \ell$ gives

$$\frac{c_1}{c_2} = \tan\frac{\omega}{c}\ell \tag{7.19}$$

Equating (7.18) and (7.19, we obtain the frequency relation

$$\frac{K - \omega^2 M}{EA} = \frac{\omega}{c}\tan\frac{\omega}{c}\ell \tag{7.20}$$

This relation must be solved numerically to obtain the natural frequencies. The mode shapes are obtained by setting $c_2 = 1$ to give

$$u(x) = \tan\frac{\omega}{c}\ell \sin\frac{\omega}{c}x + \cos\frac{\omega}{c}x \tag{7.21}$$

Figure 7-3 shows very good agreement between the analytical solution and both the full eigensolution and the approximate eigensolution of the finite element model. This figure also demonstrates the ability of the approximate eigensolution to only capture the mode of interest. A significant reason for the success of this example is that the eigenvector of the primary structure does not change with the addition of the foam. From the frequency response (see Figure 7-4), one sees that the second mode of the structure is very well damped but still has some effect on the frequency response. This mode is not captured by the approximate finite element approach.

7.3.2 Bar with layer of foam

In this section, we consider an example problem to demonstrate the ability of this method to only solve for the modes of interest. We demonstrate the utility of the proposed method and compare its results to the full eigensolution. We consider a uniform, aluminum bar of length 63.5 cm, width 12.7 mm, and height 12.7 mm constrained to move only in the axial direction. A uniform layer of low-wave-speed material is attached to the top of the bar (see Figure 7-5). The foam is modelled using plane strain such that only displacements in the plane occur. The foam has a Young's modulus of 207500 Pa, Poisson ratio of 0.36, loss factor of 0.7, and density of 67.4 kg/m^3. The bar is discritized using 10 two-node elements, and the foam is discritized using 100 four-node elements (ten along the length and ten through the

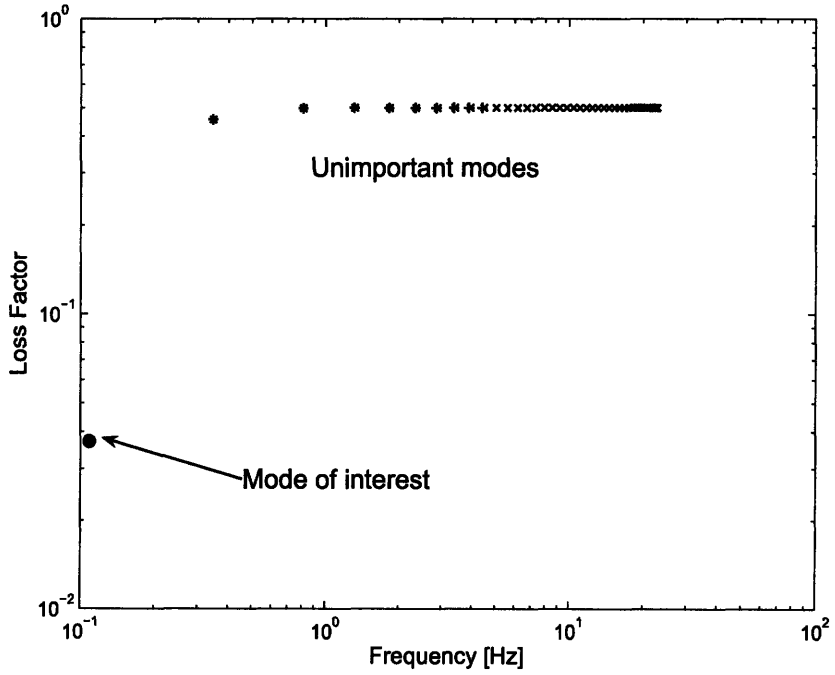

Figure 7-3: Predicted loss factor for spring-mass system with attached bar of LWSM: analytical for first few modes (×), approximate eigensolution of finite element model (○), full eigensolution of finite element model (+)

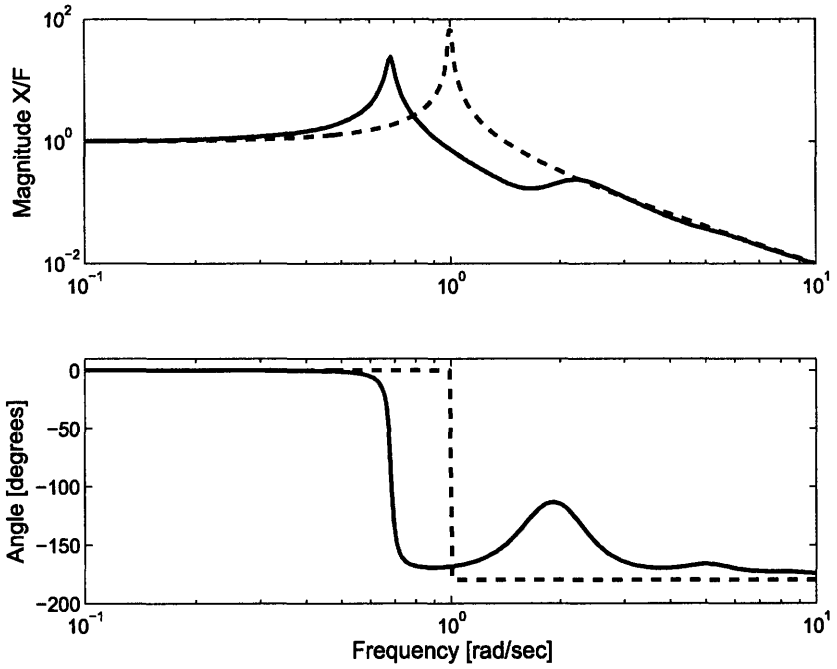

Figure 7-4: Frequency response for finite element model of spring-mass with (dashed) and without (solid) bar of LWSM

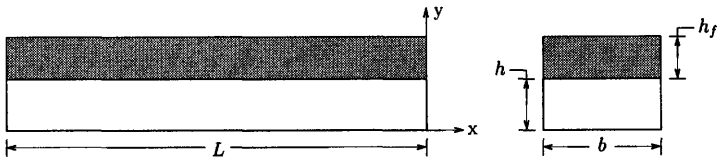

Figure 7-5: Sketch of bar with layer of foam

thickness). To calculate the first eight eigenvalues to within 10^{-9} using the approximate method, the algorithm requires on average four iterations. Figures 7-6 7-9 show the first two axial mode shapes of the bar and foam. Figures 7-10 and 7-11 show the eigenvalues and loss factors calculated

7.3.3 Timoshenko beam with layer of foam

In this example, we compare the approximate eigenvalue solver for a uniform Timoshenko beam with a layer of foam to the analytical approach developed earlier and to experimental measurements. The analytical model produces a curve displaying loss factor as a function of frequency for a uniform beam, independent of boundary conditions and length. A comparison of the analytical model using both the Timoshenko and Euler-Bernoulli beam theories shows that there is negligible difference between the loss factor curves because the deformation of the foam, which is the dominant

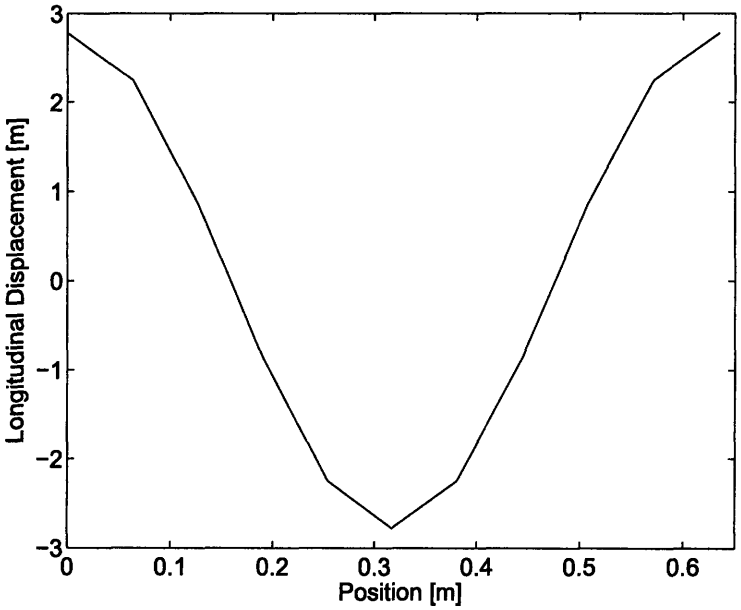

Figure 7-6: First axial mode shape of bar

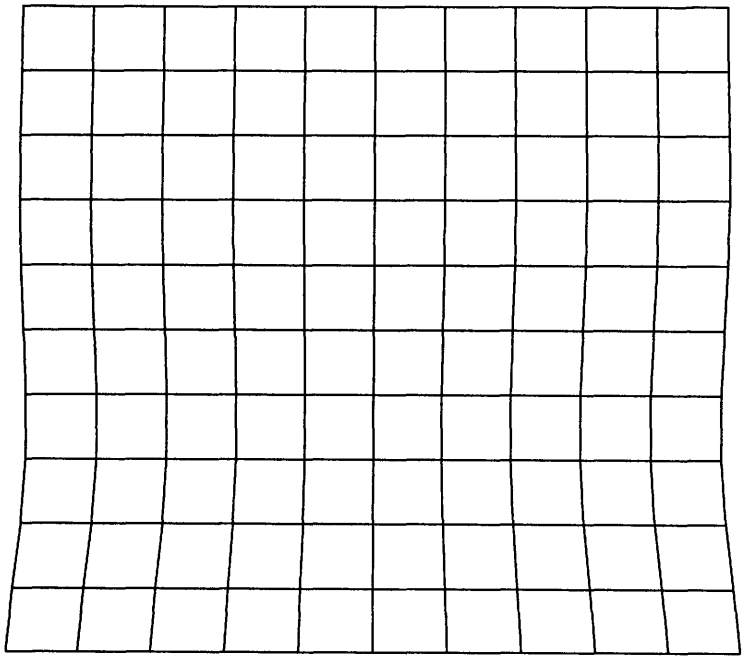

Figure 7-7: LWSM deformation for first axial mode of bar

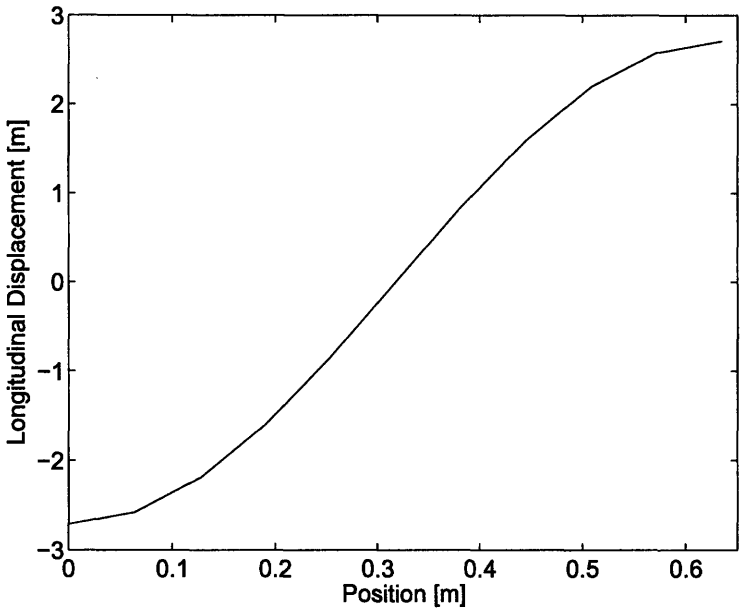

Figure 7-8: Second axial mode shape of bar

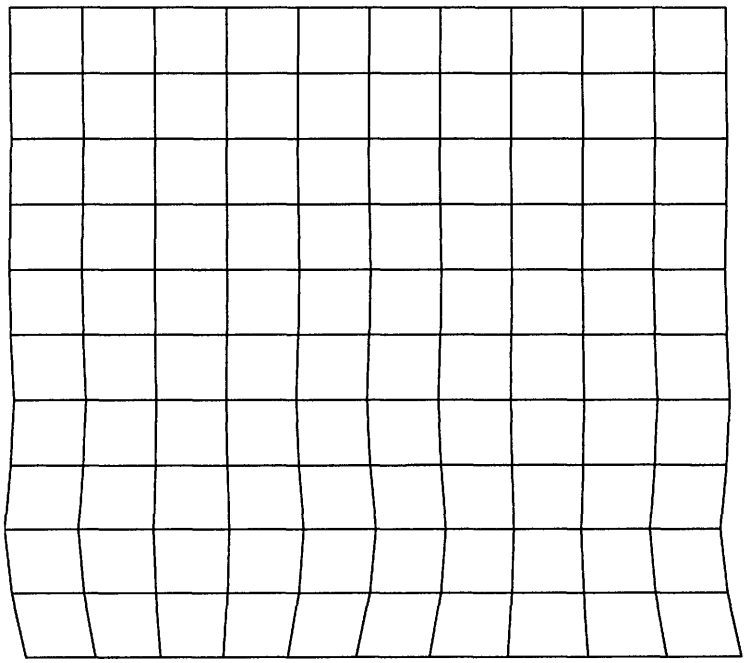

Figure 7-9: LWSM deformation for second axial mode of bar

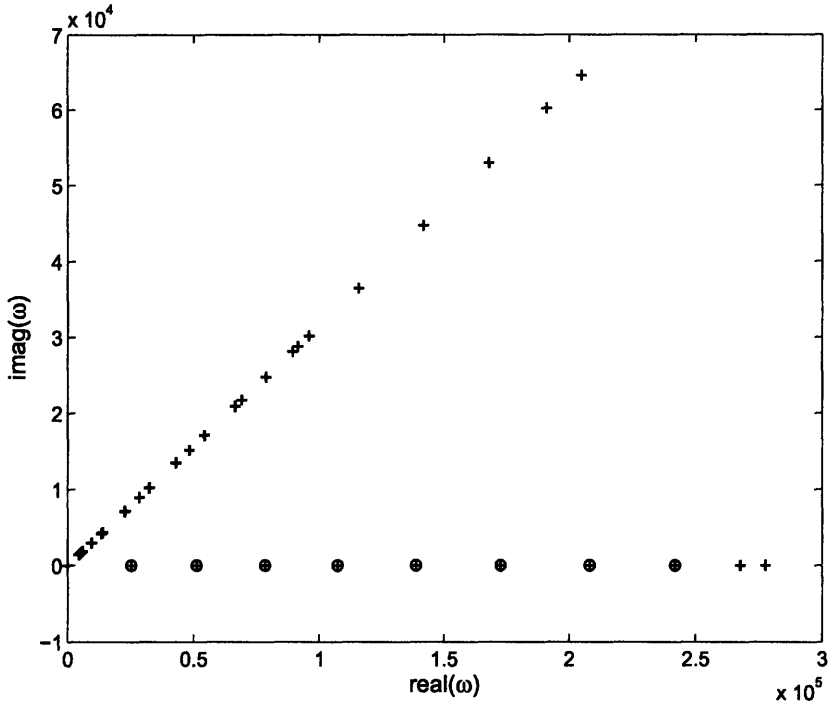

Figure 7-10: Eigenvalues of finite element model of a bar with a layer of foam: approximate eigensolutions (o), full eigensolution (+)

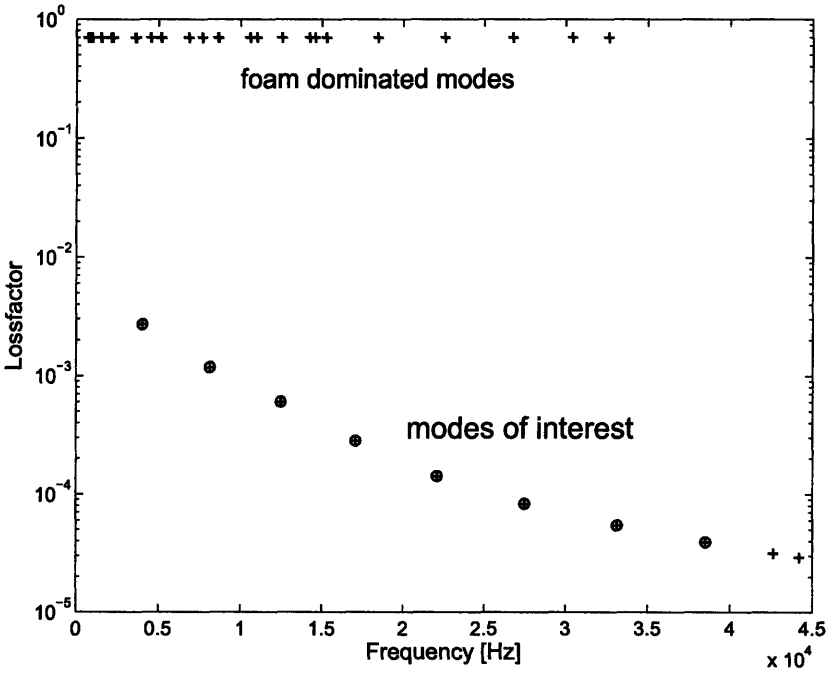

Figure 7-11: Calculated loss factor of finite element model of a bar with layer of foam: approximate eigensolutions (o), full eigensolution (+)

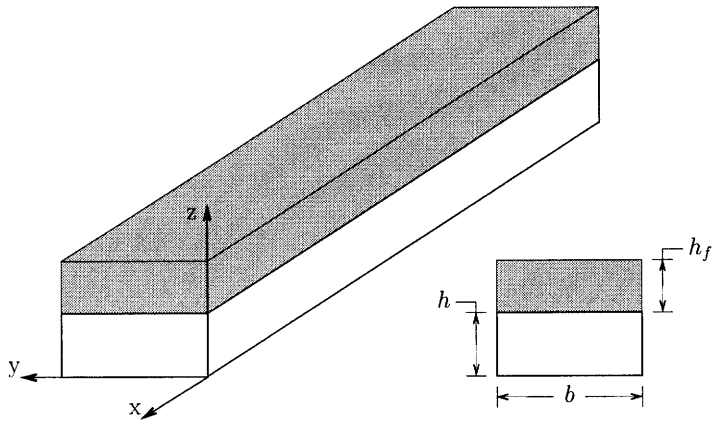

Figure 7-12: Sketch of beam covered with layer of foam

factor in determining the loss factor, does not change significantly between the two models.

We consider an aluminum, rectangular Timoshenko beam of width 38.1 mm, height 12.7 mm, and length 1.448 m vibrating in the $x-z$ plane as shown in Figure 7-12. A layer of EAR C-3201 foam of height 12.7 mm and width 38.1 mm is placed on top of the beam along its full length.

The foam has a Young's modulus of $2075\omega^{0.5}$ Pa, Poisson ratio of 0.36, loss factor of 0.8, and density of 67.4 kg/m^3 as measured by Varanasi and Nayfeh [66]. The beam is discritized using 20 three-node Timoshenko beam elements. The foam is discritized nine-node plane strain elements, 20 along the length and 10 through the thickness. A coordinate transformation assuming small displacements is used to convert rotational and transverse displacements at the centerline of the beam to axial and transverse displacements at the top of the beam, where it interfaces with the foam.

To calculate the first 20 eigenvalues to within 10^{-9} using the approximate method, the algorithm requires on average five iterations for each eigenvalue.

Figure 7-13 shows good agreement between the experimental results, the analytical estimates developed earlier based on spatial decay of the bending waves, and the approximate finite element method.

7.3.4 Cylinder filled with foam

We consider a uniform, steel cylinder of length 1.83 m, outside diameter 10.2 mm, and thickness 3.0 mm. The cylinder is filled with Foamex Sensus viscoelastic "memory" foam. The foam's properties are based on measurements described earlier. The cylinder is discritized using twenty seven node elements, one through the thickness, twenty-four around the circumference, and ten along the length (see Figure 7-14). Two simulations are run using different meshes (both utilizing 27-node brick elements) are used for the foam core. The more refined mesh is shown in Figure 7-15. Figures 7-16–7-19 compare the loss factors calculated using the finite element method with experimental and analytical results for various circumferential modes (values of n)

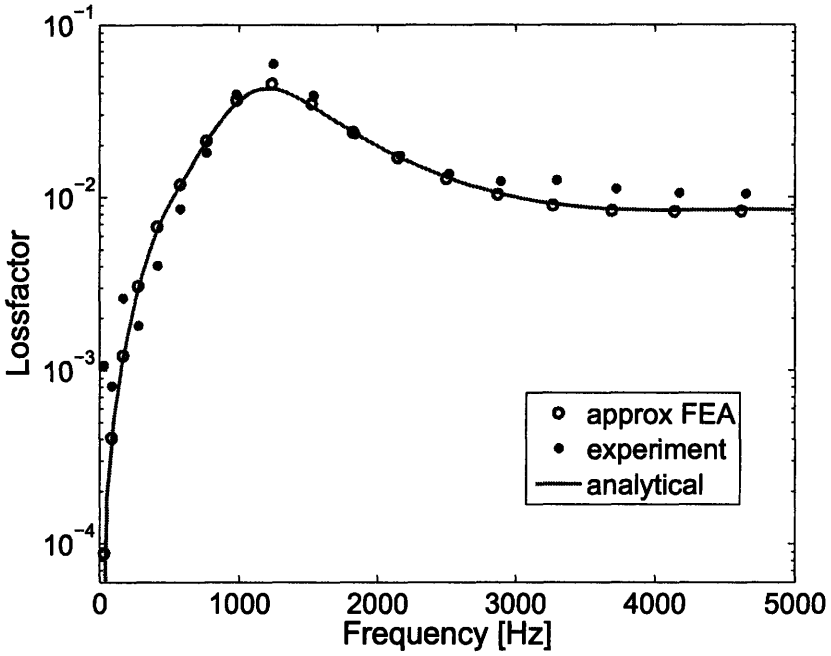

Figure 7-13: Loss factor of aluminum beam covered with a layer of EAR C-3201 foam using: solid line analytical theory, o finite element result, × experiment. Foam properties by Varanasi and Nayfeh [66]

utilizing the coarse mesh. It should be noted that Wang *et al* [70] used a finite element study to classify the mode shapes of the thick-walled cylinders into six categories instead of simply by the longitudinal and circumferential node numbers.

7.4 Discussion

Figures 7-16–7-19 show that the agreement between the loss factors calculated using the approximate eigensolution of the finite element model agree well with experimental and theoretical results below 2000 Hz. Above 2000 Hz, the approximate eigensolution overestimates the real part of the natural frequency but underestimates the loss factor. While the proofs of the properties of the Rayleigh quotient may not strictly hold for a complex stiffness, we expect that the finite element model should overestimate the real part of the natural frequencies and that the error should grow with frequency as shown.

The coarseness of the mesh is the root of these errors. Because the approximate eigenvalue solver is implemented in Matlab, we are significantly limited by the sizes of the matrices as well as the lack of an efficient solver. Improving the mesh of the cylinderical shell will improve the prediction of the real part of the eigenvalues. Refinements in the radial direction do not have a significant effect becuase a single element accurately captures the radial deformation of a cylinder. For the foam core,

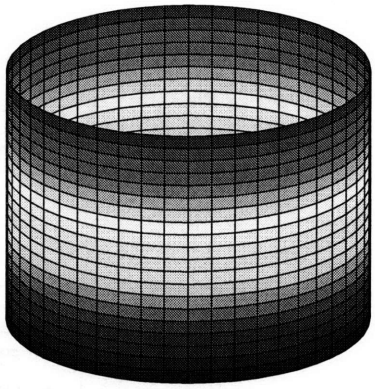

Figure 7-14: Mesh used for cylindrical shell: 24 elements (27-node bricks) in circumferential direction, 10 elements in axial direction, 1 element through the thickness

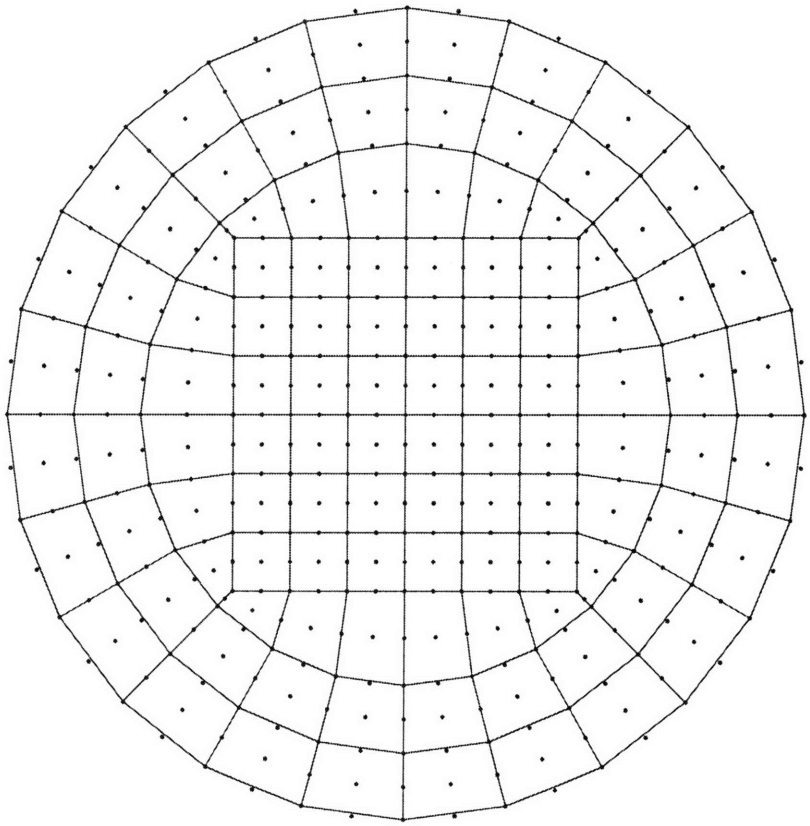

Figure 7-15: Cross section of refined mesh of foam core

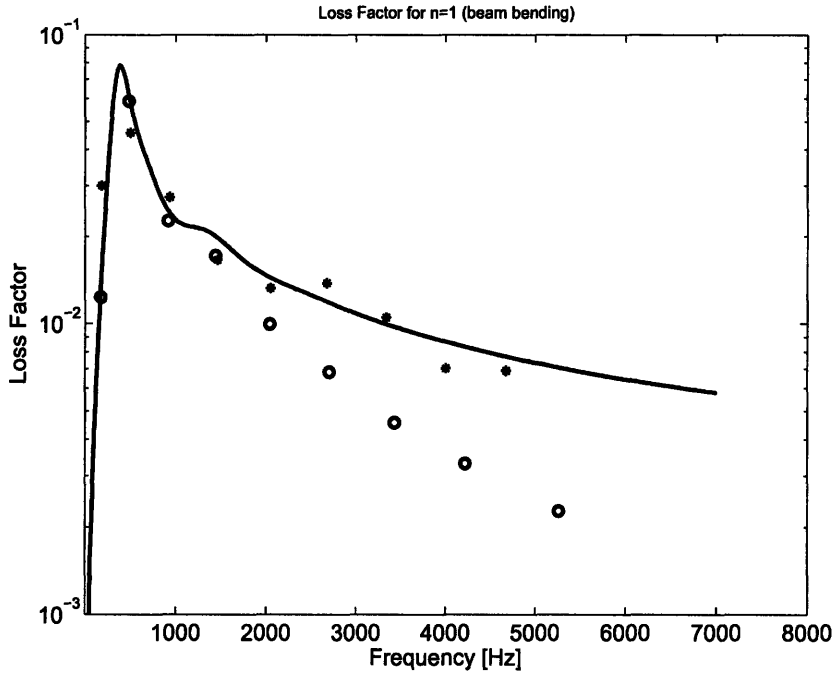

Figure 7-16: Loss factor of foam filled cylinder for bending modes ($n = 1$): approimate eigensolution of finite element (o), experiment ($*$), analytical method (solid)

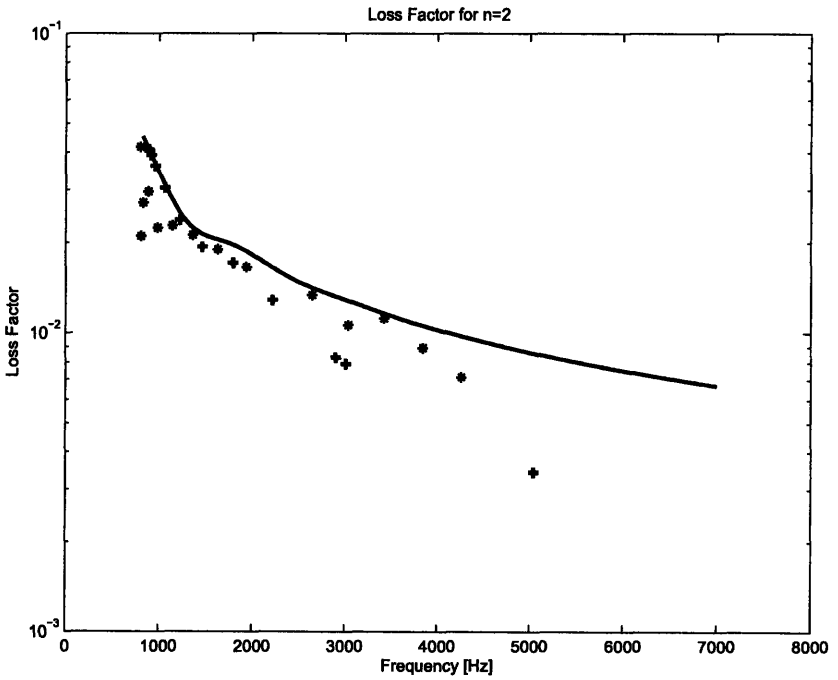

Figure 7-17: Loss factor of foam filled cylinder for $n = 2$ modes: approimate eigensolution of finite element (+), experiment ($*$), analytical method (solid)

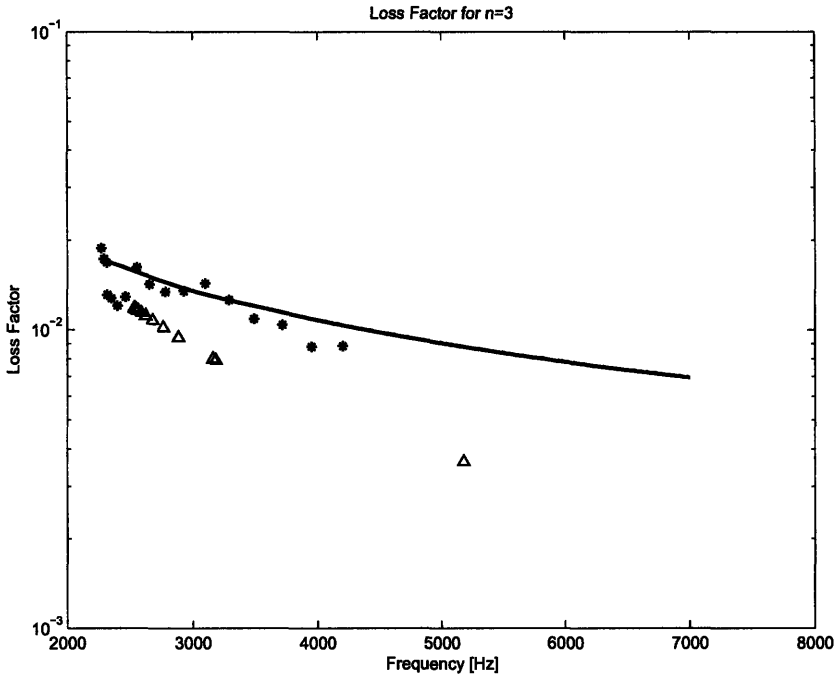

Figure 7-18: Loss factor of foam filled cylinder for $n = 3$ modes: approimate eigensolution of finite element ($\triangle$), experiment ($*$), analytical method (solid)

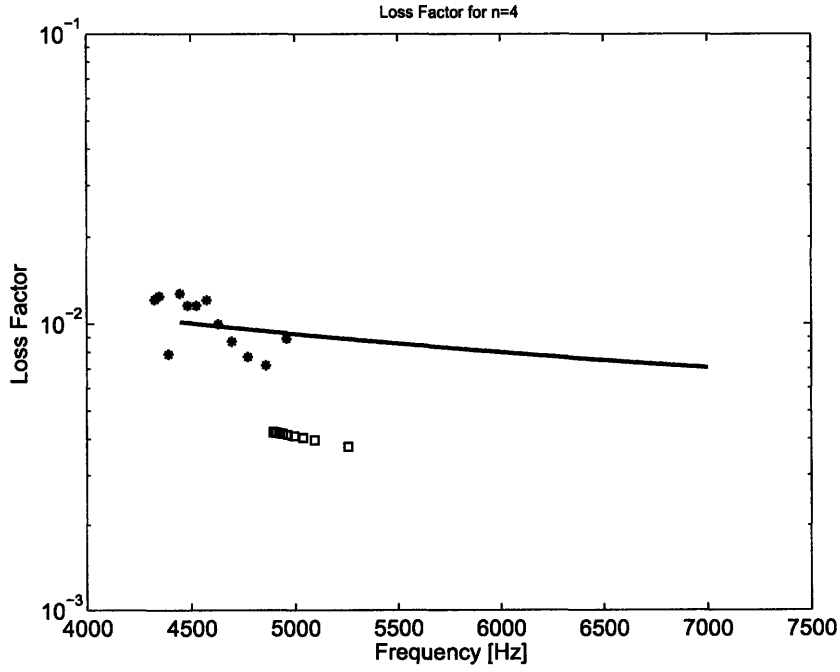

Figure 7-19: Loss factor of foam filled cylinder for $n = 4$ modes: approimate eigensolution of finite element ($\square$), experiment ($*$), analytical method (solid)

the mesh must be increased primarily in the radial direction because that is the primary direction of deformation and hence has significant effect on the accuracy of the loss factor. Figures 7-20 and 7-21 show that a refinement of the mesh of the foam core significantly improves the estimates of the loss factor. However, the error in the estimates of the real part of the natural frequency remain becuase that is a function of the mesh of the primary structure.

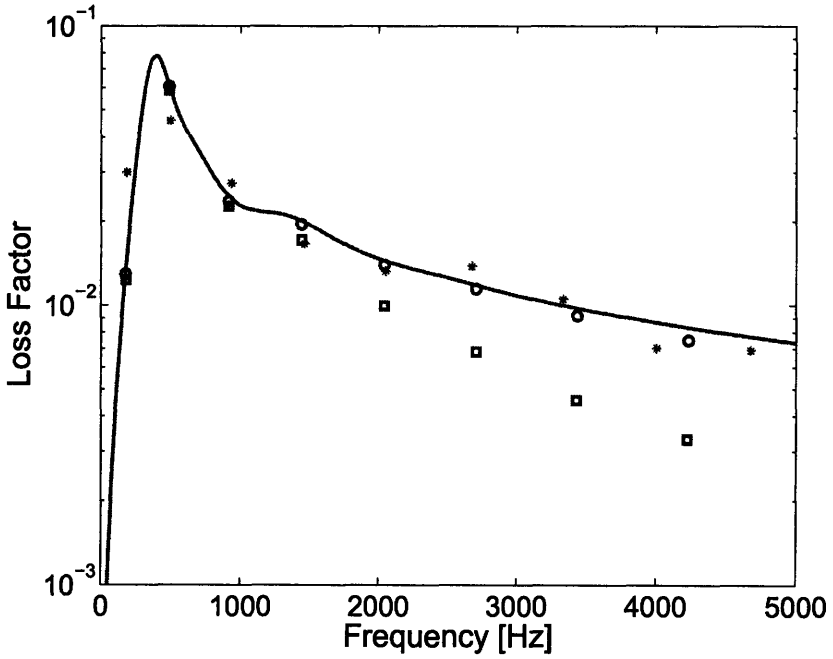

Figure 7-20: Loss factor of foam filled cylinder for bending ($n = 1$) modes: approximate eigensolution of finite element (o) with refined mesh of foam core, approximate eigensolution of finite element (□) with coarse mesh of foam core, experiment (*), analytical method (solid)

An additional complication that can occur is the appearance of mode splitting. Because of the additional degrees of freedom provided by the LWSM, pairs of vibratory modes can occur near resonant frequencies of the primary structure where only one mode previously existed. The "new" modes have approximately the same shape for the primary structure, but the LWSM vibrates in phase with the primary structure at the smaller resonant frequency and out of phase at the larger resonant frequency. This phenomenon is analogous to the behavior seen in a discrete tuned-mass damper. We leave this implementation for future work.

7.5 Conclusions

This chapter developed an approximate eigenvalue solver for finite element models of structures coupled to low-wave-speed media. The solver was developed to han-

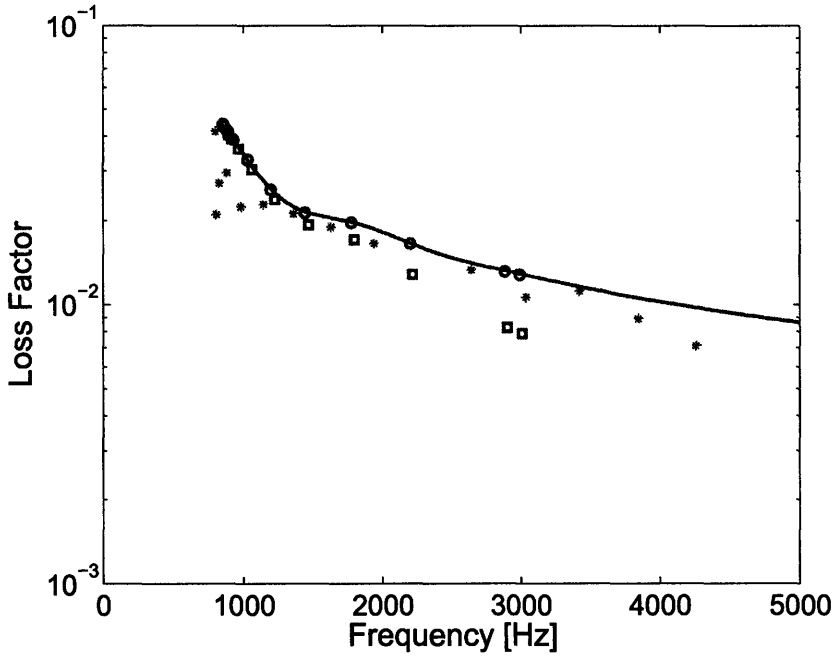

Figure 7-21: Loss factor of foam filled cylinder for bending ($n = 1$) modes: approximate eigensolution of finite element ($\circ$) with refined mesh of foam core, approximate eigensolution of finite element ($\square$) with coarse mesh of foam core, experiment ($*$), analytical method (solid)

dle certain problems encountered when a low-wave-speed material is added to finite element model of a structure, such as frequency dependent material properties, "uninteresting" modes dominated by motion of LWSM, and a significant increase in the number of degrees of freedom in the finite element model. The solver works under the assumption that the LWSM is a small perturbation to the system such that the mode shapes of the primary structure do not change significantly. Under this assumption, the eigenvalue problem is transformed into a forced harmonic problem, and the Rayleigh quotient is used to iteratively find calculate the complex eigenvalue. The solver is implemented using Matlab and results on simple structures show that it works well. Results for a more complicated structure, a cylinder filled with foam, show that the solver works well at low frequencies but that coarse mesh required by the limitations of Matlab in terms of memory size and solver efficiency prevent the eigenvalues of higher modes from being accurately calculated.

In the near future, we would like to implement this approximate solver on a commmercial finite element program. The current implementation of the solver does not make use of the banded nature of the stiffness and mass matrices for the forced problem. In a future implementation, we could either maintain that banded nature or use a solver that contains an algorithm based on graph theory that optimizes the Gaussian elmination order and hence effectively re-establishes the banding.

Chapter 8

Conclusions

8.1 Findings

The objective of this thesis has been to develop and demonstrate tools to facilitate the application of low-wave-speed media (LWSM) as a structural damping treatment. Significant levels of damping are achieved at frequencies above the first thickness resonance of the low-wave-speed material. We have shown that LWSM is an effective and mass-efficient damping treatment that compares favorably to constrained-layer damping, particularly for thin-walled tubes. We have demonstrated one such application, reduction of noise radiated from vehicle driveshafts. The analytical methods developed for beams and cylinders are shown to be accurate by comparison to experimental measurements. The approximate eigenvalue solver makes the the finite element method a practical tool for analyzing structures with LWSM.

The use of low-wave-speed materials as a damping treatment has many advantages over other damping treatments that allow it to offer superior performance in a number of different applications. The low-wave-speed materials that we have examined, such as glass microbubbles, fiberglass insulation, steel wool, and viscoelastic foam, are relatively inexpensive. Manufacturing a structure with LWSM is typically simpler than for constrained-layer damping because the materials can easily conform to a complicated geometries and a high strength glue bond is not required. Many of the materials mentioned above also have a wide temperature range. The broadband damping nature is a useful advantage. Changes to the primary system or errors in modelling the primary system do not cause significant degradation in performance. Furthermore, even though the damping is designed for a specific type of mode, such as damping the beam bending vibrations of a thin-walled tube, signicant damping is still attained in torsional, axial, and wall-flexing modes. Varanasi [64] demonstrated that LWSM can improve the performance of belt drives, which takes advantage of the ability of LWSM to accomodate large strains, and flexure stages, which take advantage of the fact that the addition of LWSM will not introduce significant creep because the stresses in the LWSM are small. Impact and shock mitigation is an attractive application of LWSM that requires further exploration because of the broadband nature of the damping, the ability to accomodate large strains, and the durability of

LWSM.

8.2 Future Work

8.2.1 Materials Modelling and Selection

There are two extensive bodies of literature on porous materials, the materials science viewpoint focusing on quasi-static behavior and design of materials and the acoustics viewpoint focusing on acoustic properties, which need to be bridged for successful development of low-wave-speed media as a damping treatment. Materials scientists have the tools to analyze foams and fibrous materials at a cellular level to predict properties and to develop low-wave-speed materials with desired properties. Acoustics researchers have done extensive testing and modelling of porous, fibrous, and granular materials. The combination of these two would allow for the development of low-wave-speed materials suited for a variety of specialized applications. The lack of material properties data is currently a hindrance to application. Additionally, exploration of existing materials like steel wool and fiberglass that can be used in cryogenic and high temperature applications is needed.

8.2.2 Mode splitting in finite element

Recalling from the experiments of structures coupled to granular materials the existence of mode-splitting, the tuned-mass-damper-like behavior in which two vibratory modes exist in the neighborhood of one mode of the undamped structure, we recognize a need to account for the possibility of this occurence in the finite element method. This scenario of mode splitting could arise in applications where selection of a lossy material is not possible, perhaps due to environmental compatibility concerns. To solve for this behavior, one must recognize that while the mode shape of the primary structure is relatively unchanged, the low-wave-speed media moves in phase with the structure for the lower frequency mode and out of phase from the structure for the higher frequency mode.

8.2.3 Implementation into commercial finite element code

The eigenvalue solver will be most useful to the engineering community if it is implemented in a commercial finite element code so that it may take advantage of all the tools currently found in a commercial package. We hope to implement this algorithm in a commercial code in the near future.

Appendix A

Damping torsional vibrations in cylinders using lightweight, low-wave-speed media

A.1 Introduction

In this section, we develop an analytical model for torsion of a circular tube filled with a low-wave-speed material. This formulation differs from the study of the cylinder filled with foam because in that case the full equations to model a cylinder were required because we were concerned with all possible mode shapes. In this case where we are only concerned with torsion, the equations for the cylinder simplify significantly.

A.2 Modelling

We model the cylinderical tube as a simple bar subject to torsion. The foam is modelled as a elastic solid with a complex modulus. The foam and cylinder are coupled together through a "no-slip" condition. To obtain estimates of the system loss factor, we study an infinite length cylinder and foam subject to steady harmonic motion. We first calculate the wavenumber as a function of frequency for the the empty cylinder. For a simple torsional model, the waves are nondispersive, and the wavenumber is proportional to frequency. Then, we calculate the motion of the foam at the corresponding frequency and wavenumber. Based on the motion of the foam, the stress at the foam-cylinder interface is calculated. This stress results in an applied torque per unit length to the cylinder. Using this applied stress, we can calculate a correction to the dispersion relation of the cylinder. Next, we use an iterative procedure to solve for the wavenumber of the combined cylinder-foam system. Finally, we use the complex wavenumber to calculate the loss factor as a function of frequency.

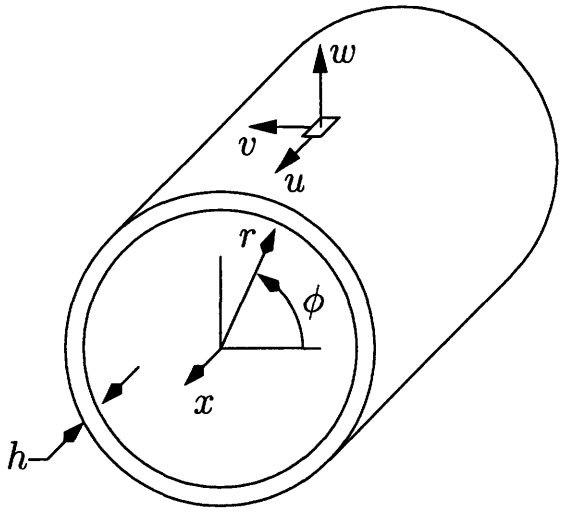

Figure A-1: Schematic of cylinder geometry and displacements

A.2.1 Hollow Cylinder

$$\frac{\partial^2 \phi}{\partial x^2} + \Omega^2 \phi = -\frac{R_i^2}{GJ} T(x, \Omega) \tag{A.1}$$

where lengths have been nondimensionalized by the inner radius R_i, G is the shear modulus, J is the moment of inertia, $T(x, \Omega)$ is the harmonic, applied torque per unit length, and

$$\Omega = \frac{\omega R_i}{c_s} \tag{A.2}$$

where

$$c_s^2 = \frac{G}{\rho} \tag{A.3}$$

We assume a solution of the form

$$\phi(x, \Omega) = N e^{j k_x x} \tag{A.4}$$

and obtain

$$\left(k_x^2 - \Omega^2\right) N = \frac{R_i^2}{GJ} T(x, \Omega) \tag{A.5}$$

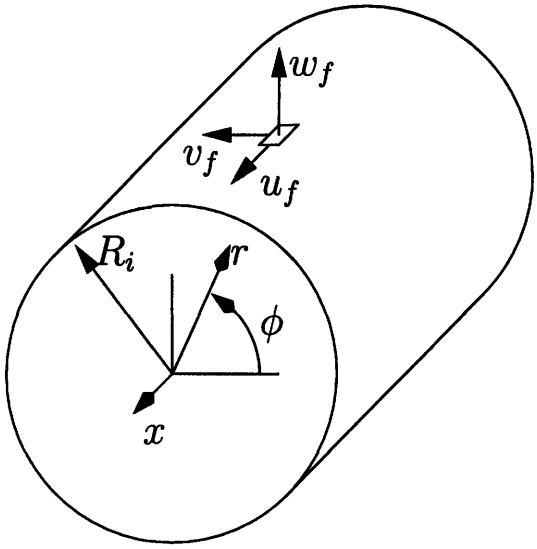

Figure A-2: Schematic of foam geometry and displacements

A.2.2 Foam

The governing differential equation in dimensionless form for the foam under plane strain and harmonic motion is

$$\left[(1-2\nu_f)\left(r^2\frac{\partial^2}{\partial r^2}+r\frac{\partial}{\partial r}+r^2\frac{\partial^2}{\partial x^2}-1\right)+2(1-\nu_f)\frac{\partial^2}{\partial\theta^2}\right.$$
$$\left.+2r^2R_i^2(1+\nu_f)(1-2\nu_f)\frac{\rho_f}{E_f}\omega^2\right]v(r,\theta,\omega)=0 \quad \text{(A.6)}$$

We assume a solution for the foam that has no dependence on the angular coordinate θ

$$v(r,\theta)=V(r)e^{jk_xx} \quad \text{(A.7)}$$

Then, (A.6) reduces to a Bessel equation

$$\left(r^2\frac{d^2}{dr^2}+r\frac{d}{dr}+r^2\left(\hat{\Omega}^2-k_x^2\right)-1\right)V(r)=0 \quad \text{(A.8)}$$

where

$$\hat{\Omega}=\frac{\omega R_i}{c_f}=\frac{c_s}{c_f}\Omega \quad \text{(A.9)}$$

where

$$c_f^2=\frac{G_f}{\rho_f} \quad \text{(A.10)}$$

where G_f is the complex shear modulus of the foam and ρ_f is the density of the foam. The solution to (A.8) is given by

$$V(r) = a_1 J_1(k_r r) + b_1 Y_1(k_r r) \tag{A.11}$$

where a_1 and b_1 are constants to be determined by the boundary conditions, $J_1(k_r r)$ is the Bessel function of the first kind of order one, $Y_1(k_r r)$ is the Bessel function of the second kind of order one, and

$$k_r^2 = \hat{\Omega}^2 - k_x^2 \tag{A.12}$$

The boundary condition at $r = 0$ requires that $V(r)$ is finite; therefore, we obtain $b_1 = 0$. We impose the no-slip boundary condition at the interface of the foam and the cylinder to obtain

$$a_1 = \frac{N}{J_1(k_r)} \tag{A.13}$$

Next, we calculate the shear stress at the cylinder-foam interface using

$$\tau_{r\phi} = G_f \, \gamma_{r\phi} \tag{A.14}$$

where shear strain $\gamma_{r\phi}$ is given by

$$\gamma_{r\phi} = \frac{dV(r)}{dr} - \frac{V(r)}{r} \tag{A.15}$$

The resulting shear stress is

$$\tau_{r\phi}(r = 1) = N \frac{G_f}{J_1(k_r)} \left(J_1'(k_r) - J_1(k_r) \right) \tag{A.16}$$

where J_1' is the derivative of the Bessel function of the first kind of order one.

The torque per unit length applied to the cylinder by the foam is

$$T(x, \Omega) = -\int_0^{2\pi} \tau_{r\phi}(r = 1) R_i^2 d\theta = 2\pi R_i^2 G_f N \left(\frac{J_1'(k_r)}{J_1(k_r)} - 1 \right) \tag{A.17}$$

where the negative sign is required because the foam is inside the tube.

A.2.3 Solution for Complex Wavenumber

Substituting for (A.17) into (A.5), we obtain

$$\left(k_x^2 - \Omega^2 \right) N = -2\pi \frac{G_f R_i^4}{GJ} \left(\frac{J_1'(k_r)}{J_1(k_r)} - 1 \right) N \tag{A.18}$$

Solving this equation for the wavenumber, we obtain

$$k_x = \sqrt{\Omega^2 + 2\pi \frac{G_f R_i^4}{GJ} \left(1 - \frac{J_1'(k_r)}{J_1(k_r)}\right)} \tag{A.19}$$

We use an iterative procedure to solve this equation because the wavenumber shows up inside the Bessel function. First, we take $k_x = \Omega$ as the initial estimate that is given by an empty tube. Next, we calculate the correction term due to the stress at the foam-tube interface using this initial guess. Then, we calculate the wavenumber using (A.19). We recalculate the foam correction term using this updated value for the wavenumber and then obtain a new estimate of the wavenumber using (A.19). We continue this iterative procedure until the wavenumber converges to within a desired error bound. Typically only one or two iterations is required for one percent error.

A.2.4 Loss Factor

To calculate the loss factor, we assume that we have an empty cylinder with a complex modulus given by $G = G_0(1 + j\eta)$ where η is the material loss factor. Using the fact that torsional waves are nondispersive and the definition of Ω (A.2), we obtain the loss factor to be

$$\eta = \frac{\text{Im}\left(\frac{1}{k_x^2}\right)}{\text{Re}\left(\frac{1}{k_x^2}\right)} \tag{A.20}$$

A.3 Results

The real part dispersion curve for the filled tube crosses the that of the empty tube. From (A.19) the these two curves cross when

$$\text{Re}(J_1(k_r)) = \text{Re}(J_1'(k_r)) \tag{A.21}$$

These intersections occur in pairs, one in which the imaginary part of is a minimum and one in which the imaginary part is approximately zero. The case in which the imaginary part is a minimum occurs when $J_1(k_r)$ is close to zero and corresponds to local maximum in the system loss factor. The value of k_r corresponds to the roots of J_1 3.8317, 7.0156, 10.1735,... Because we assume the wavenumber to be small, $k_r \approx \hat{\Omega}$ and the roots of J_1 are approximately the nondimensional frequencies of maximum damping. The other case occurs when $J_1(k_r) \approx J_1'(k_r)$ and corresponds to a local minimum of damping. This corresponds to the case when the stress at interface is a minimum. In fact, one obtains this equality when solving for free vibration of a cylindrical solid by imposing the zero stress condition at the surface. The corresponding values of k_r are 4.5700, 7.7715, 10.9374,...

These results could easily be modified for a layer of foam on the inside or outside of the tube. A similar analysis could be performed to calculate the loss factor of axial

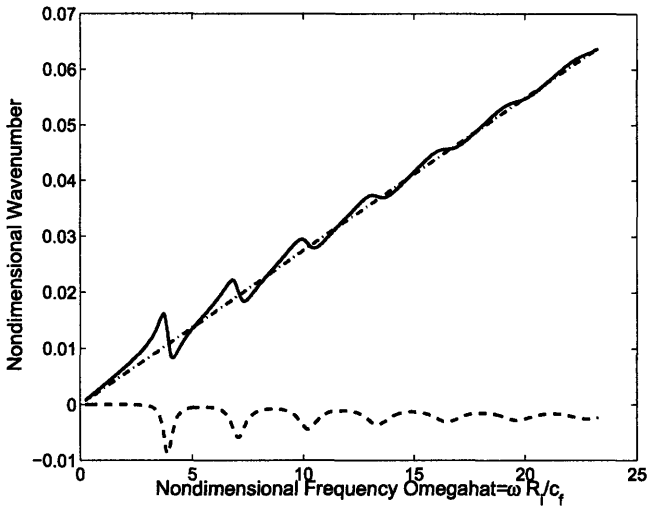

Figure A-3: Dispersion curve for torsional vibrations: empty (dash-dot), real part of wavenumber for foam-filled tube (solid), imaginary part of wavenumber for foam-filled tube (dashed). Fourteen percent mass ratio, foam material loss factor of 0.1

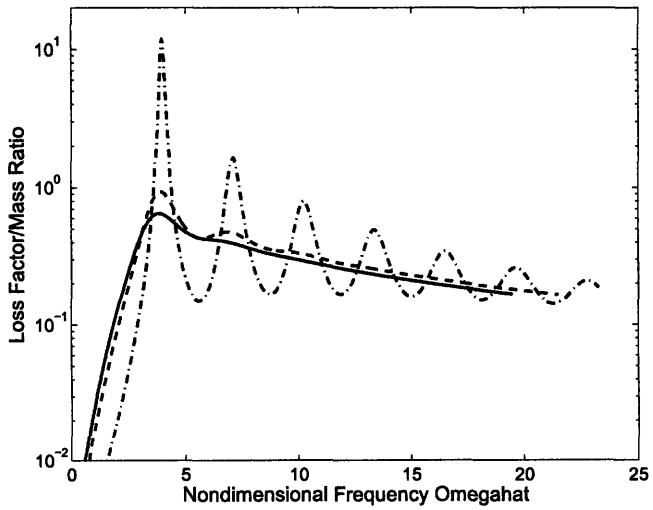

Figure A-4: Loss factor curves as a function of nondimensional frequency $\hat{\Omega}$ for various material loss factors: $\eta = 0.1$ (dash-dot), 0.5 (solid), 0.8 (dashed)

vibration of uniform tubes filled with low-wave-speed media. In that case a circular or rectangular cross section is tractable.

Bibliography

[1] 3M Speciality Materials, St. Paul, MN. *3M Microspheres Selection Guide.*

[2] J.F. Allard. *Propagation of sound in porous media: modelling sound absorbing materials.* Elsevier Applied Science, 1993.

[3] M.A. Biot. Theory of propagation of elastic waves in a fluid-saturated porous solid. I. low-frequency range. II. higher frequency range. *Journal of the Acoustical Society of America*, 28:168–191, 1956.

[4] J.M. Bourinet and D. Le Houedec. A dynamic stiffness analysis of damped tubes filled with granular material. *Computers and Structures*, 73:395–406, 1999.

[5] X. Chen, H.L. Chen, and X.L. Hu. Damping predication of sandwich structures by order-reduction-iteration approach. *Journal of Sound and Vibration*, 222(5):803–812, 1999.

[6] Chih-Hung Chung, Glen Steyer, Takeshi Abe, Mark Clapper, and Chandra Shah. Gear noise reduction through transmission error control and gear blank dynamic tuning. In *Proceedings of the 1999 Noise and Vibration Conference*, May 1999. P-342.

[7] Mark L. Clapper, March 2005. Personal communication. Dearborn, Michigan.

[8] F. Cortès and M.J. Elejabarrieta. An approximate numerical method for the complex eigenproble in systems characterised by a structural damping matrix. *Journal of Sound and Vibration*, 296:166–182, 2006.

[9] Ph. Couderc, J. Callenaere, J. Der Hagopian, and G. Gerraris. Vehicle driveline dynamic behaviour: Experimentation and simulation. *Journal of Sound and Vibration*, 218(1):133–157, 1998.

[10] L. Cremer and M. Heckl. *Structure-Borne Sound.* Springer-Verlag, 1973. Translated and revised by E.E. Ungar.

[11] E.M. Daya and M. Potier-Ferry. A numerical method for nonlinear eigenvalue problems application to vibrations of viscoelastic structures. *Computers and Structures*, 79:533–541, 2001.

[12] Wim Dewulf and Guido De Roeck. The modal strain energy method critically revised. In *Proceedings of SPIE*, volume 3989 of *Smart Structures and Materials: Damping and Isolation*, pages 99–110, San Diego, 2000.

[13] Mark Donley, Wayne Stokes, Santosh Neriya, Vincent Minkaba, and Yuejun Li. Modeling of a driveline system using a building block approach. In *Proceedings of the 1999 Noise and Vibration Conference*, Traverse City, Michigan, May 1999. Society of Automotive Engineers. 1999-01-1762, P-342.

[14] Laëtitia Duigou, El Mostafa Daya, and Michel Potier-Ferry. Iterative algorithms for non-linear eigenvalue problems. application to vibrations of viscoelastic shells. *Computer methods in applied mechanics and engineering*, 192:1323–1335, 2003.

[15] A. Farshidianfar, M. Ebrahimi, H. Rahnejat, M.T. Menday, and M. Moavenian. Optimization of the high-frequency torsional vibration of vehicle driveline systems using genetic algorithms. *Proceedings of the Institution of Mechanical Engineers, Part K: Journal of Multi-body Dynamics*, 216:249–262, 2002.

[16] Foamex International Inc, 1000 Columbia Avenue, Linwood, PA 19061. *Foamex Technical Product Function Sheet: Acoustical Functions.*

[17] Foamex International Inc, 1000 Columbia Avenue, Linwood, PA 19061. *Sensus brochure.*

[18] Bryce L. Fowler, Eric M. Flint, and Steven E. Olson. Effectiveness and predictablility of particle damping. In *Smart Structures and Materials 2000: Damping and Isolation*, volume 3989, pages 356–367. SPIE, 2000.

[19] J. Robert Fricke. Lodengraf damping—an advanced vibration damping technology. *Sound and Vibration*, pages 22–27, July 2000.

[20] Lorna J. Gibson and Michael F. Ashby. *Cellular Solids: structure and properties.* Cambridge University Press, 1997.

[21] Gene H. Golub and Henk A. van der Vorst. Eigenvalue computation in the 20th century. *Journal of Computational and Applied Mathematics*, 123:35–265, 2000.

[22] Peter Göransson. Acoustic and vibrational damping in porous solids. *Philosophical Transactions of the Royal Society A*, 364:89–108, 2006.

[23] J.P. Den Hartog. *Mechanical Vibrations.* Dover Publications, New York, 1985.

[24] John R. House. Damping hollow tubular structures with 'lightweight' viscoelastic spheres. In *Proceedings of the ACS Division of Polymeric Materials: Science and Engineering*, volume 60, pages 734–738, Dallas, Texas, 1989.

[25] T.C. Huang. The effect of roatry inertia and of shear deformation on the frequency and normal mode equations of uniform beams with simple end conditions. *Journal of Applied Mechanics*, 28:579–584, December 1961.

[26] K. Hutter and K.R. Rajagopal. On flows of granular materials. *Continuum Mechanics and Thermodynamics*, 6(2):81–139, 1994. review article.

[27] R.R. James. Progress report no. 5, development of damping treatments for destroyer hulls. Technical report, Mare Island Naval Shipyard Rubber Laboratory, 1961. Report Number 94-30.

[28] L. Jaouen, B. Brouard, N. Atalla, and C. Langlois. A simplified numerical model for a plate backed by a thin foam layer in the low frequency range. *Journal of Sound and Vibration*, 280:681–698, 2005.

[29] Conor D. Johnson and David A. Kienholz. Finite element prediction of damping in structures with constrained viscoelastic layers. *AIAA Journal*, 20(9):1284–1290, 1982.

[30] Miguel C Junger and David Feit. *Sound, Structures, and their Interaction.* MIT Press, 1972.

[31] V. Kartick and D.R. Houser. Analytical predictions for the transmission error excitation in various multiple-mesh gear-trains. In *Proceedings of the ASME Design Engineering Technical Conference*, pages 515–524, 2003.

[32] Arthur W. Leissa. *Vibration of Shells.* National Aeronautics and Space Administration, Washington, D.C., 1973. NASA SP–288.

[33] A.Y.T. Leung. Subspace iteration for complex symmetric eigenproblems. *Journal of Sound and Vibration*, 184(4):627–637, 1995.

[34] Rongming Lin and Yong Xia. A new eigensolution of structures via dynamic condensation. *Journal of Sound and Vibration*, 266:93–106, 2003.

[35] W. Liu, G. R. Tomlinson, and J. A. Rongong. The dynamic characterisation of disk geometry particle dampers. *Journal of Sound and Vibration*, 280:849–861, February 2005.

[36] B.-A. Ma and J.-F. He. A finite element analysis of viscoelastically damped sandwich plates. *Journal of Sound and Vibration*, 152(1):107–123, 1992.

[37] E. Mallil, H. Lahmam, N. Damil, and M. Potier-Ferry. An iterative process based on homotopy and perturbation techniques. *Computer methods in applied mechanics and engineering*, 190:1845–1858, 2000.

[38] E.R. Marsh and L.C. Hale. Damping of flexural waves with embedded viscoelastic materials. *Journal of Vibration and Acoustics*, 120(1):188–193, January 1998.

[39] Yuma Miyauchi, Koji Fujii, Takayuki Nishino, Koichi Hatamura, and Toru Kurisu. Introduction of gear noise reduction ring by mechanism analysis including fem dynamic tuning ring. In *SAE World Congress, Transmission and Driveline Systems Symposium*, Detroit, March 2001. Society of Automotive Engineers.

[40] R.E. Morris. Rubber materials for damping vibration of metal structures. In *Proceedings of the Sixth Joint Army-Navy-Air Force Conference on Elastomer Research and Development*, volume 2, pages 443–466, Boston, 1960. U.S. Quartermaster Research and Engineering Command.

[41] S.A. Nayfeh, J.M. Verdirame, and K.K. Varanasi. Damping of flexural vibration by coupling to low-density granular materials. In G. Agnes, editor, *Smart Structures and Materials 2002: Damping and Isolation*, volume 4697, pages 158–167. SPIE, March 2002.

[42] Samir A. Nayfeh. *Design and Application of Damped Machine Elements.* PhD thesis, Massachusetts Institute of Tehcnology, Cambridge, MA, 1998.

[43] H. Oberst. *Kunststoffe*, 46, 1956.

[44] Daniel L. Palumbo and Junhong Park. Structural and acoustic damping characteristics of polyimide microspheres. In *AIAA/ASME/ASCE/AHS/ASC Structures, Sturctureal Dynamics, and Materials Conference*, Austin, Texas, April 2005.

[45] R.J. Pamley, J.R. House, and M.J. Brennan. Comparison of passive damping treatments for hollow structures. In Daniel J. Inman, editor, *Proceedings of SPIE*, volume 4331 of *Smart Structures and Materials: Damping and Isolation*, pages 455–467, 2001.

[46] H. V. Panossian. Structural damping enhancement via non-obstructive particle-damping technique. *Journal of Vibration and Acoustics*, 114(1):101–105, 1992.

[47] A. Papalou and S. Masri. Response of impact dampers with granular materials under random excitation. *Earthquake Engineering and Structural Dynamics*, 25:2530–67, 1996.

[48] A. Papalou and S. Masri. An experimental investigation of particle dampers under harmonic excitation. *Journal of Vibration and Control*, 4:361–379, 1998.

[49] Junhong Park. Measurements of the frame acoustic properties of porous and granular materials. *Journal of the Acoustical Society of America*, 118(6):3483–3490, December 2005.

[50] Junhong Park. Transfer function methods to measure dynamic mechanical properties of complex structures. *Journal of Sound and Vibration*, 288:57–79, 2006.

[51] PCB Piezotronics, 3425 Walden Avenue, Depew NY 14043. *Shock and Vibration Sensors Catalog.*

[52] Homer Rahnejat. *Multi-Body Dynamics: Vehicles, Machines, and Mechanisms.* Professional Engineering Publishing, London, 1998.

[53] D. Richards and D.J. Pines. Passive reduction of gear mesh vibration using a periodic drive shaft. *Journal of Sound and Vibration*, 264:317–342, 2003.

[54] E.J. Richards and A. Lenzi. On the prediction of impact noise, VII: the structural damping of machinery. *Journal of Sound and Vibration*, 97(4):549–586, 1984.

[55] J.A. Rongong and G.R. Tomlinson. Vibration damping using granular viscoelastic materials. In *Proceedings ISMA 27*, volume 27 of *Noise and Vibration Engineering Conference*, pages 431–440, Leuven, Belgium, 2002.

[56] J. Derek Smith. *Gear Noise and Vibration.* Marcel Dekker, New York, 2003.

[57] Spectral Dynamics, Inc., 1010 Timothy Dr., San Jose, CA 95133. *The STAR System Reference Manual.*

[58] N.G. Stephen. The second frequency spectrum of timoshenko beams. *Journal of Sound and Vibration*, 80(4):578–582, 1982.

[59] J.C. Sun, H.B. Sun, L.C. Chow, and E.J. Richards. Predictions of total loss factors of structures, Part II: Loss factors of sand-filled structure. *Journal of Sound and Vibration*, 104(2):243–257, 1986.

[60] Zhaouhui Sun, Glen C. Steyer, Glenn Meinhardt, and Mark Ranek. Nvh robustness design of axle systems. In *SAE Noise and Vibration Conference and Exposition*, Traverse City, Michigan, May 2003. Society of Automotive Engineers.

[61] S. Theodossiades, M. Gnanakumarr, H. Rahnejat, and M. Menday. Mode identification in impact-induced high-frequency vehicular driveline vibrations using an elasto-multi-body dynamics approach. *Proceedings of the Institution of Mechanical Engineers, Part K: Journal of Multi-body Dynamics*, 218:81–94, 2004.

[62] Eric E. Ungar and Jr. Edward M. Kerwin. Plate damping due to thickness deformations in attached viscoelastic layers. *Journal of the Acoustical Society of America*, 36(2):386–392, February 1964.

[63] S. Vafaei, M. Menday, and H. Rahnejat. Transient high-frequency elasto-acoustic response of a vehicular drivetrain to sudden throttle demand. *Proceedings of the Institution of Mechanical Engineers, Part K: Journal of Multibody Dynamics*, 215:35–52, 2001.

[64] Kripa K. Varanasi. *Vibration Damping using Low-Wave-Speed Media with Applicatiosn to Precision Machines.* PhD thesis, Massachusetts Institute of Tehcnology, Cambridge, MA, 2004.

[65] Kripa K. Varanasi and Samir A. Nayfeh. Damping of flexural vibration by coupling to low-density foams and granular materials. In *Proceedings of DETC 2003: 2003 ASME Design Engineering Techinal Conference*, Chicago, September 2003. ASME.

[66] Kripa K. Varanasi and Samir A. Nayfeh. Damping of flexural vibration using low-density, low-wave speed media. *Journal of Sound and Vibration*, 292(1–2):402–414, April 2006.

[67] T.E. Vigran, L. Kelders, W. Lauriks, M. Dhainaut, and T.F Johansen. Forced response of a sandwich plate with a flexible core described by a biot-model. *Acta Acustica*, 83(6):1024–1031, 1997.

[68] David A. Wagner, Yuksel Gur, Susan M. Ward, and Marsha A. Samus. Modeling foam damping materials in automotive structures. *Journal of Engineering Materials and Technology*, 119:279–283, July 1997.

[69] Gang Wang and Norman M. Wereley. Spectral finite element analysis of sandwich beams with passiv constrained layer damping. *Journal of Vibration and Acoustics*, 124:376–386, July 2002.

[70] Huan Wang, Keith Williams, and Wei Guan. A vibrational mode analysis of free finite-length thick cylinders using the finite element method. *Journal of Vibration and Acoustics*, 120:371–377, April 1998.

[71] Brian K. Wilson and Mark L. Clapper. A sound simulation technique used for the prediction of passenger compartment noise. In *SAE Noise and Vibration Conference and Exposition*, Traverse City, Michigan, May 1999. Society of Automotive Engineers.

[72] Zhiwei Xu, Michael Yu Wang, and Tianning Chen. Particle damping for passive vibration suppression: Numerical modelling and experimental investigation. *Journal of Sound and Vibration*, 279(3–5):1097–1120, 2005.

[73] T. Yanagida, A.J. Matchett, and J.M. Coulthard. Energy dissipation of binary powder mixtures subject to vibration. *Advanced Powder Technology*, 12(2):227–254, 2001.

[74] Simone L. Yaniv. Impedance tube measurement of propagation constant and characteristic impedance of porous acoustical material. *Journal of the Acoustical Society of America*, 54(5):1138–1142, 1973.

[75] J.A. Zapfe and G.A. Lesieutre. Broadband vibration damping in beams using distributed viscoelastic tuned mass absorbers. In *AIAA/ASME/ASCE/AHS/ASC Structures, Structural Dynamics and Materials Conference and Exhibit*, pages 2427–2436, April 1996.